UNIVERSIT`A DEGLI STUDI ROMA TRE

SCOULA DOTTORALE /DOTTORATO DI RICERCA IN INGEGNERIA MECHANICCA
CICLO DEL CORSO DI DOTTORATO- XXVIII

TITOLO DELLA TESI

(Noise and vibrations characteristics of a micro car diesel engine)

Docente Guida/Tutor:Prof.

Prof G.Chiatti

Nome e Cognome del dottorando

Sunny Narayan

Coordinatore:Prof

Prof E. Bemporad

A dissertation presented
to the Faculty of Engineering of
The University of Roma Tre

by

Sunny Narayan

in Partial Fulfillment of Requirements

for the Degree of

Doctor of Philosophy

The University of Roma Tre

May 2016

Dedication

To all mighty god

Acknowledgments

In course of this period, I have realized that I could never have done any of this work without encouragement and support of so many people. I am thankful to all who have supported me during course of my study of Phd study period at ′ The University of Roma Tre′. First and foremost, of all I would like to thank my advisors Prof. G. Chiatti and Prof. O. Chiavola who gave me this wonderful opportunity to study in their research group. Without their support and guidance, none of this work would have been possible. During my period of study, they supported and advised me by reviewing my work continuously. These years of study at ′ The University of Roma Tre′, have helped me to gain the requisite knowledge.

I am also grateful to Ing. F. Palmieri, PhD and Mr. Rashid Ali, PhD for their initial support and guidance. I would also like to express my gratitude to Ing. Erasmo Recco for his support to carry out various experimental activities and who spent hours to help me out in this work.

I thank all my family members who were constant source of support and inspiration for me. My sincere thanks goes to people in DOMUS SRL group including Mrs. Ellena and Mr. Trulli Carlo who were always there to provide me any logistic support.

It was a challenging period of my life and I have enjoyed it gaining the expertise to grow as a professional.

Rome, 3rd April 2016.

Sunny Narayan

Declaration

I, Sunny Narayan do hereby declare that this thesis titled " Noise and vibration characteristics of a micro car diesel engine " and the work involving it are results of my own research. I further confirm that:

a) The work has been done while in candidature for a research degree at this University.
b) No part of this work has been previously submitted for award of any degree /qualification at this University or any other university or institution.
c) Wherever I have quoted from the work of others, the source has been always given.
d) I have acknowledged all major sources of help.
e) Wherever the portions of work presented in this thesis was done by myself jointly with others, I have made clear exactly what was done by others and what I have contributed myself.

Signature:

Date :03/04/2016

Abstract

In cylinder pressure developed, noise emissions and vibrations signature of an engine structure are important parameters that provide information about its working conditions. Due to several drawbacks of various conventional techniques used, novel methods of condition monitoring are becoming the next hot topic of research for major automotive companies around the world.

Diesel engines have been widely used for a variety of industrial as well as domestic applications. Despite their advantages in terms of fuel economy (as compared to gasoline engines), these engines are often less popular due to their worst performance in terms of noise, vibration and harness (NVH) benchmarks. Hence it is important to develop a suitable scheme which is capable enough to detect faults by monitoring various signals acquired from these engines before actual breakdown takes place.

In this work, data was collected from a dual cylinder diesel engine installed in the laboratory of Internal combustion engine at ′University of Roma Tre′ by changing speed, load, amount and duration of fuel injected. The collected data was further processed using various MATLAB based processing tools. The presented work also discusses various numerical models based on mathematical analysis. The discussed research work has following major objectives:

Objective 1-To review different sources of noise in engines.
Objective 2-To study the effects of variations of different engine operational conditions on various signals acquired from transducers mounted on the test engine.
Objective 3- To show the applicability of various signal processing methods for effecting condition monitoring of engines.

Objective 4-To analyze combustion based noise using acquired data.
Objective 5-To develop various numerical models of piston lateral motion and validate them using experimental data.
Objective 6-On the background of presented work, provide a guideline for further research**.**

The presented work has been organized into six chapters. Basic principles of noise, vibration and harness (NVH) have been presented in the first two chapters. Chapter 1, analysis different sources of noise in an engine and briefly discusses various techniques used for effective separation of these sources. Chapter 2 discusses various signal processing methods adopted for diagnosis of different signals acquired. Chapter 3 focuses on various characteristic features of various sources of noise in an engine. Chapter 4 deals with combustion based noise and discusses use of in cylinder pressure, noise emissions and engine block vibration signals for its analysis. Chapter 5 is deals with noise emissions due to lateral motion of piston assembly. The dynamic equations of lateral motion of skirt were solved and effects of various parameters were analyzed. Chapter 6 presents a summary of various results and relates it to previous objectives presented. Further suggestions have also been made for future research work.

The novelty of methods discussed in the presented work lies in analysis of various combustion noise related indices which showed a good correlation with actual in cylinder pressure development. Further various mathematical models have been used for analysis of lateral motion of skirt and effects of various skirt design parameters on it.

As the output signals from various transducers mounted on the test engine are available at an early stage, various methods discussed in the presented work may become an attractive option for effective detection and localization of various faults and hence, form an important aspect of preventive maintenance of engines.

Keywords: Diesel engines, in cylinder pressure, noise, vibrations and harness.

Table of Contents

Chapter 4

Combustion based noise

Chapter 5

Piston Slapping Noise

Chapter 6

Conclusions and future work

List of publications

Appendix

List of Symbols

a- Dilation parameter
b- Translation parameter
A_r -Area of noise radiating surface
Ac- Proportionality coefficients
A-Cylinder surface area
A.T.S.-Anti thrust side
ATDC-After top dead center
a_p - Location of connecting rod from its top part of skirt
B-Cylinder bore
b (f)-Radiation rate
b_c -Distance of skirt center of mass from its top part
BEM-boundary element method
BTDC-Before top dead center
C-Speed of sound
C(t)-Output response
C_V(h)-The covariance of a given function x(h)
C˜(t)-Approximation of combustion noise
CWT (a, b)-Complex wavelet transform
$C_{p,a}$ (f)-Coherence function between in-cylinder pressure block vibration signals
CHRR- Cumulative heat release rate
C-Speed of sound
C(f)- Decay constant
C_θ- Torsion damping coefficient of skirt
C_c-Wave propagation speed
C_b-Dynamic damping coefficient of engine block
C_p-Dynamic damping coefficient of skirt
CI, Ƶ -Combustion Index
Cp, d_p-Pin offset distance
CN-Combustion noise levels
C-Crank case offset
c_a -Wave speed
dBA- A weighted sound pressure level
dB -Decibel level
D-Number of teeth
D-Piston diameter
D.I.-Direct injection
d_{COG} , Cg-Center of gravity offset
EVO-Exhaust valve opening
EVC-Exhaust valve closure
E_A-Impact energy
ECN-End of combustion noise
E(t)-Total noise emissions
E(f)- Available energy at engine surface
e_t –Top eccentricity
e_b -Bottom eccentricity
F(f) -Force applied at top of piston
f_s -Excitation frequency
f(ω)-Fourier transformation of a function f(t)
f – Frequency
f_g –Gas resonance frequency
f_r -Resonant frequency
f_c - Central frequency
f_b - Bandwidth
f_{mean}-The mean frequency of a signal
F_t ,F_x- Lateral force on liner
F_f - Frictional force between liner and skirt

F_g -Gas force
F_h -Oil reaction force
F_L-Force in connecting rod
F_f- Frictional force between liner and skirt
F_{fr}- Frictional force between liner and rings
FFT-Fast Fourier transformations
FEA-Finite element analysis
F_{IC} -Inertial force acting along X axis
$\bar{F}_{IC}$ -Inertial forces along Y axis
$\tilde{F}_{I,J}$ - average of local force
$\tilde{G}(t)$- Approximation of mechanical noise
$G_x(f)$-Input function spectrum
$G_y(f)$- Output function spectrum
$G_h(f)$-Transfer function spectrum
H_1- Transfer function of combustion noise
h-Oil film thickness
$\underline{h}(t-\tau)$ - Window function
$\bar{h}$ - Dimension less oil film thickness
H(t)- Impulse response
HCCI-Homogenous charge compression ignition
IVC-Inlet valve closure
IVO-Inlet valve opening
I_O -Overall intensity of noise
I(f) -The intensity of radiated noise
I- Intensity of combustion noise
IFFT-Inverse Fast Fourier transformations
J, I_{piston} -Piston skirt having moment of inertia
K_b-Dynamic stiffness of engine block
K_p-Dynamic stiffness of skirt
K_θ-Torsion stiffness coefficient of skirt
L_w[A]-A weighted sound power level of engine
L-Axial length
L_x-Horizontal offset of center of gravity from pin position
L_y-Vertical offset of center of gravity from pin position
L-Skirt length
l – Connecting rod length
LPP-Location of peak pressure rate
LMA -Least value of filtered accelerometer signals
MA -Modal analysis
M_z-Total Moment about the wrist-pin
M_f -Moment of F_f about the wrist-pin
M_{IC} -Rotatory moment about wrist pin
m_b-Dynamic Mass of engine block
M_b-Dynamic mass of engine block
m_{piston} -Skirt mass
m_{sl}-Small end connecting rod mass
m_t -Total mass of pin, skirt and small end of connecting rod
M_h -Moment of oil force about piston pin
m_{piston} -Mass of skirt
m_{pin} -Piston pin mass
MN-Mechanical noise levels
MBF50 - Crank angles locations at which 50% of fuel is burnt
MBF100-Crank angles locations at which 100% of fuel is burnt
MPRR-Peak pressure rise rate
M(t)- Corrupted component/Mechanical noise
M_p-Dynamic mass of skirt
M_z-Moment about piston pin

NI-Noise Index
N -Engine RPM
N_{ideal} -Ideal engine speed
NVH- Noise, vibration and harness
ON-Overall noise levels
$(\frac{dP}{dt})_{pilot}$ - Maximum pressure gradient during pilot injection period

$(\frac{dP}{dt})_{main}$ -Maximum pressure gradient during main injection
$((\frac{dP}{dt})_{motored}$ -Maximum pressure gradient in motored pressure signal
$P_{injection}$ -Injection pressure
P_{max} -Maximum pressure value
$P_{residual}$-Residual pressure levels
$P_{Motored}$ -Motored pressure levels
PCCI-Pre-mixed charge compression ignition
$p(x, \theta)$ −Non linear oil pressure distribution
P_a -Acoustic power available at surface
P-Oil pressure distribution
$P(f_k)$- k^{th} sample of power spectrum and w is signal frequency band
p(f)-Pressure spectrum
p-In cylinder pressure
P_H-Pitch
$P_{p,a}$ -Cross PSD function between in-cylinder pressure block vibration signals
$P_{p,P}$ -Auto PSD function of in-cylinder pressure
$P_{a,a}$ -Auto PSD function of block vibration signals
P_v- Impact power
P_v- Impact force
$(\frac{dP}{dt})_{max}$ -Maximum rate of pressure rise
$\underline{P}(t)$ –Input response
$\bar{p}$ - Dimension less oil pressure
$(\frac{dP}{d\theta})$ -Rate of pressure rise (PRR)
$(\frac{dQ}{d\theta})$ -Rate of heat release (ROHR)
Q- Amount of heat released(J)
Q_{pre} -Amount of fuel injected in pre-injection period
Q_{pre} -Amount of fuel injected main-injection period
$q_{m,n}$ -Modes of resonance frequency
r, r_p-Crank radius
S-Radiated surface area
S-Stroke length
SEA-statistical energy analysis
SCN- Start of combustion noise
SPL-Sound pressure levels
$S_{PP}(f)$ - Auto spectrum of P(t)
$S_{PD}(f)$ -Cross spectrum of P(t) and E(t)
SOI_{pre}-Start of pre-injection period
SOI_{main}- Start of main-injection period
$\underline{STFT}$ (τ, f)-The short time frequency analysis
$\bar{t}$ - Dimension less time
T_p-Rotation torque about piston pin
T_f -Frictional torque
T_G -Gas torque
TDC-Top dead center
T.S.-Thrust Side
TPA- Transfer path analysis
u- Surface velocity

U-Skirt velocity along X axis
v(f) -Average mean square root velocity of engine block
$(\frac{dV}{d\theta})$ -Rate of volume change
V - In cylinder volume
V-Skirt velocity along Y axis
v_r -Surface velocity
V_v -Impact velocity
$W_{I,J}$-Energy transferred to each grid point
W- Velocity along Z axis
Wc -Combustion impact power
Wn -Combustion noise power
W(t)-Spectro filter response
W_A -Impact speed of roller
W-Radiated acoustic power
X_m-Discrete function
x(t) - Input signal
x^(h)-Hilbert transformation of function x(h)
$\underline{x}^{+'}$ -Complex conjugate of x^+
$\bar{x}$ -Dimension less X coordinate
X_c, C- Nominal skirt-liner gap
X_p -Lateral displacement of skirt
X_b-Displacement of engine block
X'_p -Lateral velocity of skirt
X'_b- Velocity of engine block
X_p"-Skirt acceleration along X axis
X''_p -Lateral acceleration of skirt
X''_b- Acceleration of engine block
X_{ob}-Bore offset
x^(h)-Hilbert transformation of function x(h)
$\underline{x}^{+'}$ -Complex conjugate of x^+
$\bar{x}$ -Dimension less X coordinate
X_c, C- Nominal skirt-liner gap
X_p -Lateral displacement of skirt
X_b-Displacement of engine block
X'_p -Lateral velocity of skirt
X'_b- Velocity of engine block
X''_p -Lateral acceleration of skirt
X''_b- Acceleration of engine block
X_{ob}-Bore offset
Y_p" -Skirt acceleration along Y axis
y_h- Y_s- Location of skirt-liner contact point
$\bar{y}$ - Dimensionless Y coordinate
Z-Axial displacement of piston along liner
Z(f) -Mechanical impedance
Z-Impedance
Z- Number of sprocket teeth
$\bar{z}$ - Dimensionless Z coordinate
ρ-Density of air
σ-Radiation efficiency
ρC- Acoustic impedance
Ψ^2-Power density function (PSD)
ψ(t) -Mother Wavelet function
ʌ -Pressure angle
υ-Linear density of chain
γ - Specific heat ratio
η(f)-Transmission rate coefficient

η, μ-Dynamic viscosity of oil
ξ - Piston liner center eccentricity
£- Convergence limit
ρ_{0}- Oil Density at mean liner temperature
ρ_a -Density of air
η_t .Overall transmission efficiency
β, θ-Tilting angle of piston
Φ, φ -Tilting angle of connecting rod
ψ_G-Dimensionless gas forces
ψ_{PY} - Dimensionless inertial force on piston skirt
ψ_{SY} - Dimensionless inertial force on connecting rod
ω-Angular velocity
τ -Shear force in oil film
ω_a-First resonant frequency

List of Figures

List of Tables

Chapter 1 Introduction

1.1 Background

Diesel engines constitute major sources of power for various ships, buses, trains as well as road machinery. About one fifth of the total energy consumption in U.S.A. goes towards operating such engines [1], and hence demand for these engines is growing fast as compared to gasoline engines [2]. Sales of vehicles using diesel engines reached peak during the decade of 1980′s in U.S.A. due to major oil crises as depicted in figure no 1.1 [1].

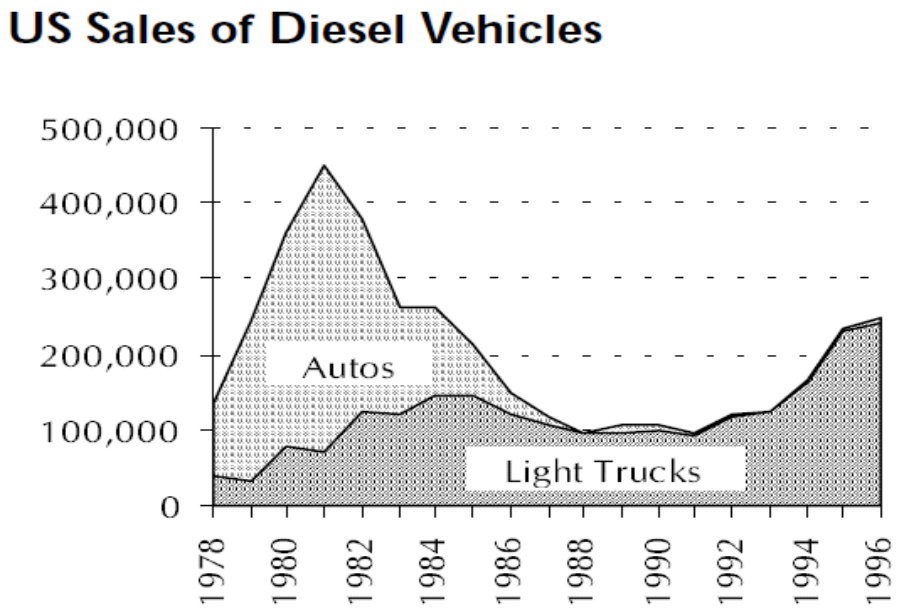

Figure no 1.1-Trends in sales of various diesel engines based automobiles in U.S.A. [1]

Various projections at that time had predicted that an increase of about 20% in sales would be achieved at the end of decade [3]. However, due to variations in the fuel costs, falling prices of petrol and various problems associated with operations of diesel engines led to fall in their overall sales [4, 5].

Gasoline engines use spark ignition system for initiation of fuel reaction as compared to diesel engines (which are based on the compression ignition of fuel-air mixture). Diesel engines operate at higher compression ratios, thus allowing more useful work output during course of their operation. Combustion in these type of engines can be made to take place away from chamber walls, thus helping in reduction of overall heat release rate. In addition, there are various throttling as well as pumping losses associated with operation of gasoline engines. These are some of the major reasons for their lesser cyclic efficiency when compared with diesel engines. Overall fuel efficiency of a diesel engine may pass over 40% in case of medium sized engines and 50% for larger ones (which are generally used in marine propulsions) [6].

The above discussed factors have hence led to renewal of interest of various automotive companies towards development of diesel engines. Data about sales of various automobiles in Europe have indicated that about a quarter of new automobiles were powered using diesel engines [7, 8]. In France, diesel engines accounted for almost half of total engine sales [9]. Sales of diesel engine based cars in Japan have almost tripled in past [10]. Several commercial vehicle suppliers have now started to manufacture their own diesel engines. Table no 1.1 shows the market share of diesel engines supplied by various automotive manufacturers in U.S.A [11].

Automotive Make	Engine Make	Market Share
Hino	Hino	100%
Freightliner	Cummins	62.3%
	Detroit Diesel	37.0%
	Mercedes Benz	0.7%
International	Cummins	7.2%
	Navistar	92.8%
Volvo	Cummins	13.6%
	Volvo	86.4%
Western Star	Cummins	21.2%
	Detroit Diesel	78.8%
Mack	Cummins	6.0%
	Mack	94.0%
Peterbilt	Cummins	65.2%
	PACCAR	34.8%

Table no 1.1- Supply of diesel engines by various manufacturer, Year-2013 [11]

Recently several key technologies like direct injection (D.I.) systems, recirculation of exhaust gas (EGR) as well as turbocharging are being introduced for further development of diesel engines [12]. Other methods include use of pre-mixed (PCCI) and homogenous charge (HCCI) compression ignitions systems [13-15]. However, higher periods of pre-mixed combustion in these methods may lead to higher noise emissions from engines. Hence various merits of using diesel engines may be lost over their poor performance on various noise, vibration and harness (NVH) benchmarks.

1.2 Summary of various sources of noise in combustion engines

Vehicle noise and vibrations can have bad effects on overall performance of automobiles. These aspects also form important benchmarks for perception of customers while choosing a vehicle as parameters of comfort levels and vehicle reliability. The collective term of noise, vibration and harness (NVH) is used to indicate the unwanted sounds and vibrations [16]. NVH is a term commonly used for the branch of engineering related to vehicle refinement in terms of sound and vibration performance as experienced by its occupants.

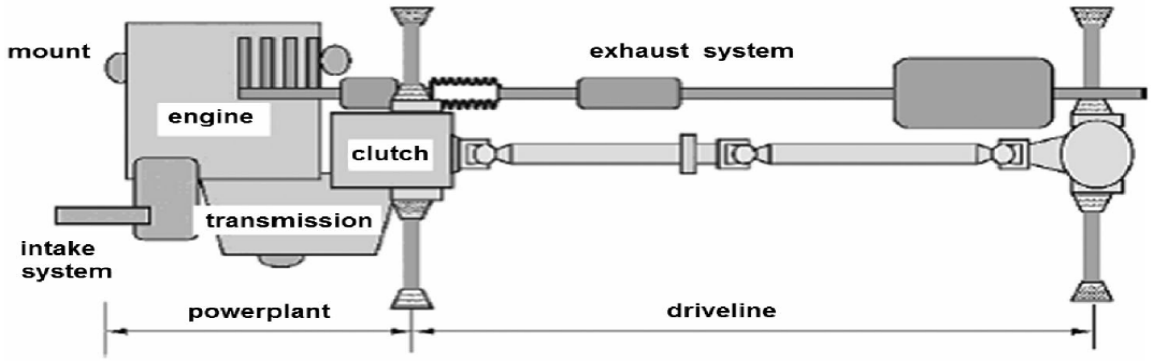

Figure no 1.2–Powertrain system [17]

Figure no 1.2 shows general layout of engine powertrain system showing engine block, transmission systems, clutch, driving systems as well as intake and exhaust systems [17]. The powertrain constitutes core part of any vehicle. The chassis includes frame, tires and isolators etc. As most individual systems, subsystems, and components of a vehicle form either sources or transmitters, the generation of noise and vibrations depends on systems as well as their constituent components [18].

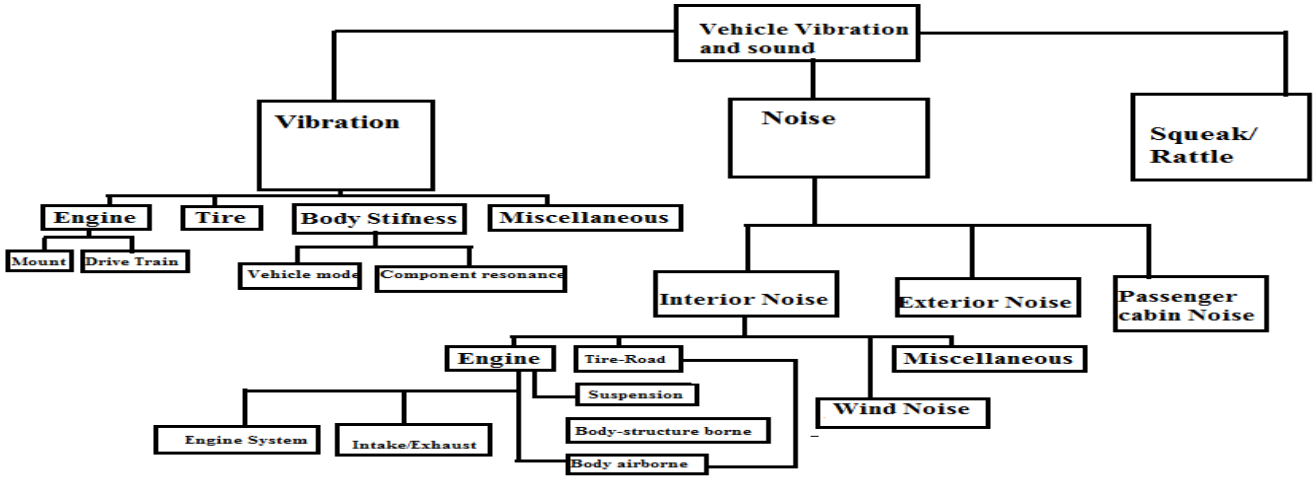

Figure no 1.3 –Noise and vibration sources in an engine [17]

Various sources of vibrations in an automobile may be further classified as external or internal ones as depicted in figure no 1.3. The internal sources are due to variable pressure acting on piston head as well as inertia of various moving parts. The external ones refer to vibrations due to unbalanced moments and variable engine torque. Further various sources of noise in an engine may be classified as mechanical noise, combustion based noise and aerodynamic noise etc. as shown in figure no 1.4.

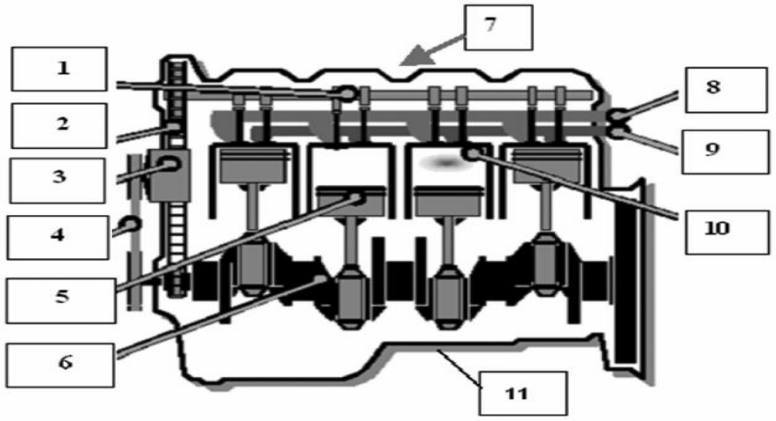

Figure no 1.4 -Schematic representation of various sources of noise (1: valve train, 2: chain drive, 3-4: accessory belt noise, 5: piston slap,6: bearing noise,7: cover noise, 8: intake noise, 9: exhaust noise, 10: combustion noise,11: oil pan noise) [17]

Combustion based noise can be analyzed by monitoring the speed of combustion process taking place inside combustion chambers, crank angle positions corresponding to 50% mass fraction burnt (CA50), 100% mass fraction burnt (CA100), locations and amplitudes of maximum in cylinder pressure developed (P_{max}) and maximum values of its derivative $[(\frac{dP}{d\phi})_{max}]$.

Combustion based noise is generated as an impulsive pressure wave due to combustion process which impacts the walls of liner and piston head [19]. The intensity of this noise is proportional to the square of in cylinder pressure developed [20]. This noise may be further classified as direct or indirect type [20]. Direct one is related to the development of in cylinder pressure, whereas the indirect part refers to portion that is transferred to structure from the combustion chamber.

Motion based noise which is proportional to operational speed of engine arises due to relative motion of parts or various inertial forces which results in various impacts. This type of noise includes contributions due to piston primary and lateral motions, bearing noise, cam noise, oil pump noise, timing belt and chain noise as well as structural noise of cover [21]. This noise may be estimated by running engine under motored condition assuming that other components such as flow based noise are neglected.

Aerodynamic noise includes contributions due to intake noise, exhaust noise and noise due to motion of fan. Various vibrations due to transmissions and driveline also contribute separately. There are also other noise sources which includes squeak and rattle of engine body system. Noise levels experienced by passengers inside the vehicle are not only dependent on various sources, but also on engine structure and acoustic transfer functions. Various sources have typical frequency ranges as shown in table no 1.2 [22]. Ranges of these frequencies not only depend on operational conditions, but also on various configurations of engines. Hence identification and estimation of specific frequency range must be done by proper testing procedure [23].

Noise source	Approximate frequency ranges	Effecting factor
Combustion Noise	500-8000Hz	In cylinder pressure
Piston Slap	2000-8000Hz	Speed, piston design
Valve Operation	500-2000Hz	Valve type, Engine speed
Fan Noise	200-2000Hz	Speed, number of blades
Intake flow noise	50-5000Hz	Turbulence
Exhaust flow noise	50-5000Hz	Turbulence
Injection Pump Operation	2000Hz	Pump features
Gear noise	4000Hz	Speed, number of teeth
Accessory Belt-chain noise	3000Hz	Engine speed, misalignment, number of teeth

Table no 1.2–Frequency ranges of various noise sources [17]

1.3 Quantification of noise emissions from engines

During the decade of 1970's, introduction of more stringent noise control regulations led to more attention being paid towards the acoustic performance of engines. Priede analyzed a relationship between development of in cylinder pressure and subsequent noise emissions from engines [23]. Kamal focused his work on finite element analysis (FEA) of individual engine components for the dynamic analysis of engines [24]. Later on the basis of various noise transfer paths, main bearing of connecting rod was found to be a major transmission path for the indirect component of combustion based noise [25].

In modern days, various multidisciplinary approaches are being utilized for evaluation of NVH performance of engines. Some of these methods include modal analysis (MA), finite element techniques (FEA), boundary element method (BEM), statistical energy analysis (SEA), lumped mass approach as well as transfer path analysis (TPA).

Each of these methods have specific frequency ranges over which they are most reliable e.g. FEA is more suited in low frequency ranges, whereas TPA is more suitable for medium frequency ranges. SEA gives more accurate results in higher ranges. Evaluation of acoustic performance of engines can be done both objectively as well as subjectively using these techniques [26].

Figure no 1.5 shows plots of in cylinder pressure spectra for two different types of engines [27]. A difference of about 20dB is seen at 1kHz frequency.

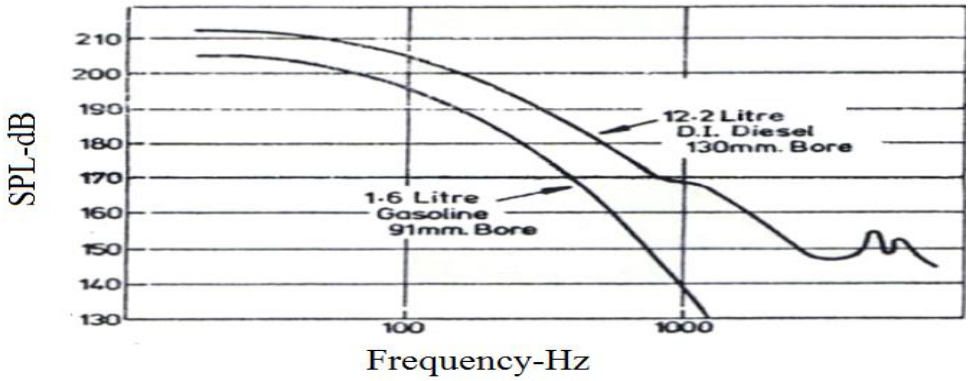

Figure no 1.5 -In cylinder pressure spectrum [17]

Based on various mathematical relationships, Anderton developed models to quantify the combustion based noise according to type of engine [28]. It involved calculation of mechanical impedance Z(f) between the force applied at top of piston F(f) and resulting velocity v(f) of engine block. i.e.

$Z(f) = \frac{V(f)}{F(f)}$ (1.1)

The average surface velocity V(f) may be expressed in terms of in cylinder pressure (p) and cylinder bore (B) as:

$V(f) = \frac{Z(f)\pi B^2}{4} P$ (1.2)

Further the relationship of radiated acoustic power (W) from a surface may be written as:

$W(f) = \rho C S V^2(f) \sigma = \frac{p^2}{\rho C}$ (1.3)

Where σ is radiation efficiency and S is radiated surface area.

Combining the above relationships, we have:

$W(f) = \sigma S \rho C [\frac{Z(f)\pi B^2 P}{4}]^2$ (1.4)

The intensity of radiated noise I(f) is given by:

$I(f) = \sigma \rho C [\frac{Z(f)\pi B^2 P}{4}]^2$ (1.5)

In order to minimize the dependence of engine speed, various in cylinder pressure spectra have been analyzed [29]. Variations in these plots were observed like a straight line in frequency ranges 0.8kHz –3kHz. The slope of pressure spectrum in this range was defined as combustion noise index (Ƶ) [29].

Using further analysis, it was shown that in cylinder pressure spectrum p(f) may be expressed as [28]:

$p^2(f) \sim (\frac{N}{f})^{Ƶ}$ Antilog(3N) (1.6)

Where N is engine RPM

From the above relationships we have:

$I(f) \sim (\frac{N}{f})^{Ƶ}$ Antilog(3N) $\sigma \rho C [\frac{Z(f)\pi B^2}{4}]^2$ (1.7)

Or

$I(f) \sim (\frac{N}{f})^{Ƶ} \sigma \frac{B^4 Z(f)^2}{4}$ (1.8)

Overall Intensity I_O can be expressed by integration over a given frequency range [f_1, f_2] as:

$$I_O \sim N^2 B^4 \int_{f_1}^{f_2} \frac{\sigma}{f^2} Z(f)^2 \quad (1.9)$$

Various empirical relationships have been developed at ISVR, University of Southampton for prediction of noise emissions in terms of sound pressure levels (S.P.L.) for different types of engines. Some of these are as follows [29]:

$$SPL_{\text{N.A. Direct Injection Diesel engines}} = 30*\log(N) + 50*\log(B) + 106 \quad (1.10)$$

$$SPL_{\text{Turbocharged Diesel engines}} = 40*\log(N) + 50*\log(B) - 135 \quad (1.11)$$

$$SPL_{\text{Indirect injection Diesel engines}} = 43*\log(N) + 60*\log(B) - 176 \quad (1.12)$$

$$SPL_{\text{Petrol engines}} = 50*\log(N) + 60*\log(B) - 203 \quad (1.13)$$

As compared to diesel engines, a gasoline engine operates at higher operational speeds has smaller bore and reciprocating mass. Consequently, such an engine has lower in cylinder pressure and hence lower sound pressure levels (SPL) of radiated noise as seen from figure no 1.6.

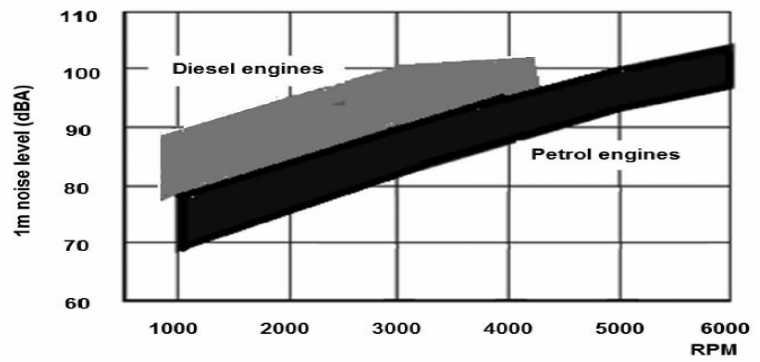

Figure no 1.6 –Variations of sound pressure levels with engine speed [17]

The diesel engine knocking refers to noise mainly in 500Hz-6000Hz range and is dominant under low speed idle operational conditions. Various moving parts in diesel engines are designed heavier and stronger as compared to gasoline engines in order to meet durability requirements under high operational pressures. Hence the mechanical impacts in case of a diesel engine are stronger when compared to gasoline engines. There are additional sources of noise due to turbochargers and operation of fuel injection pumps in case of a diesel engine. However, there are some sources of noise exclusively associated with operation of a gasoline engine which includes piston pin tickling noise under low speed conditions, clatter noise under cold operational conditions and slip stick piston noise originating from crank shaft [31-33].

1.4 Methods for quantification of noise emissions

There are several techniques that have been used to quantify various sources of noise in engines [34]. Some of these includes selective shielding of parts, surface vibration method as well as acoustic intensity technique. Of these methods, the selective covering by lead is the most expensive as well as time consuming one. These techniques have been discussed further in the next portion of this work.

a) **Selective lead covering method** -It is one of most reliable methods of source identification in field of engine acoustics. This method consists of measurement of noise emissions from engine using selective covering of engine parts with lead (which is a high transmission loss material). The increase in radiated noise is then noted by removing lead cover from the component. This procedure is repeated one by one for all major parts. Figure no 1.7 shows results of such a test that was performed on a 6 cylinder naturally aspirated diesel engine [34].

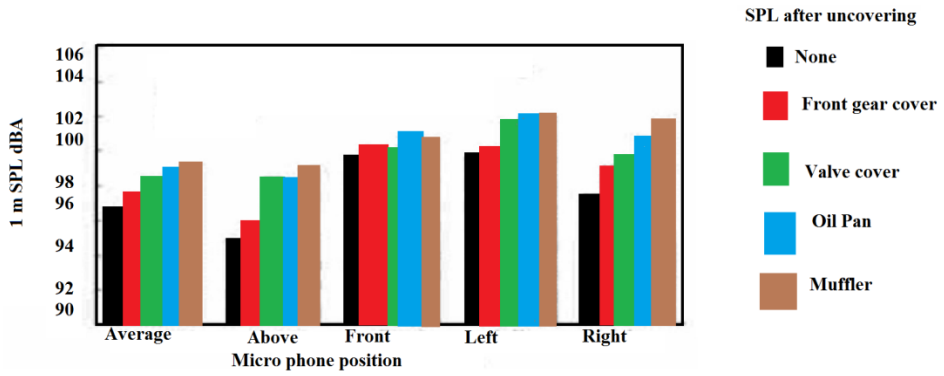

Figure no 1.7-Noise analysis using lead cover method [34]

Total sound power level (SPL) emitted from this engine was found to be around 114 dBA with valve cover, muffler, front gear cover and oil pan contributing about 21%, 10%, 8% and 7% respectively.

b) Surface vibration method-The A weighted sound power level of engine (L_w[A]) can be expressed in terms of acoustic impedance (ρc), surface velocity (u), radiation efficiency (σ) and surface area (S) by following relationship [34]:

$$L_w[A]= 10*\log(\rho c)+10*\log(S)+10*\log(\sigma)+10*\log(u) \qquad (1.14)$$

The radiation efficiency is ability of surface vibrations to get converted to air borne noise. The radiation efficiency can be estimated by considering engine as a radiating rigid sphere. The radiation efficiency of component is also related to its critical frequency which may be defined as the frequency at which wavelengths of vibrations from a given structure matches with those of natural wavelengths. At frequencies lower than the critical ones, the radiation efficiency is less than unity and vice versa.

The dominant range of critical frequency for various components of a typical diesel engine lies in range of 400Hz-800Hz. The radiation efficiency was seen to rise at an approximate rate of 40dB/decade in these ranges. The value of critical frequency occurs when $kr \approx 4$, where k is wave number and r is radius of an arbitrary sphere that has same volume as that of engine under consideration

Measurement of surface vibrations can be best done by mounting accelerometers on engine block. Positioning of accelerometers must be carefully done, as surface vibrations vary with wall thickness. Hence proper balancing between less and strong sensitive measurement points is necessary. The surface velocity can be calculated by using Fourier transformations (FT) to first convert acceleration data into frequency domain and then carrying out integration.

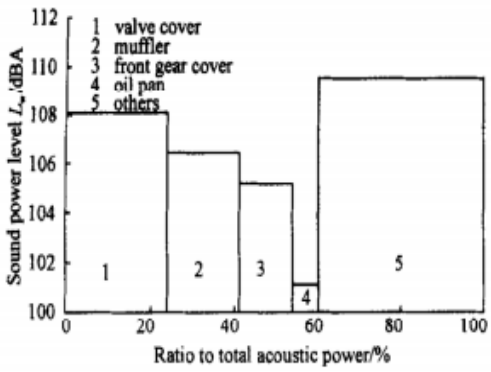

Figure no 1.8-Noise analysis using vibrational analysis method [37]

Figure no 1.8 shows the results of contributions of various components as obtained by surface velocity method [37]. It can be seen that larger contributions take place from valve cover, muffler shell, gear cover and oil pan cover.

c) Use of Spectro- filters [35]

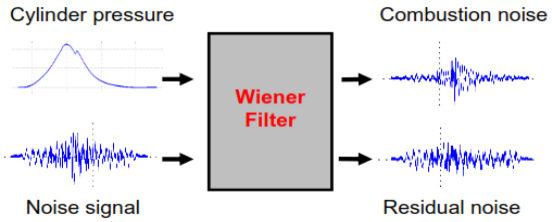

Figure no 1.9-Application of Wiener filter for estimation of combustion noise [35]

Noise emissions from diesel engines has several contributing sources of which combustion based noise and motion based noise are major ones. If the in cylinder pressure signal is known, these two sources can be separated using suitable Wiener Spectro-filters. These types of filters extract noise sources that are coherent with in cylinder pressure signals, hence providing an estimation of combustion based noise. Wiener filter has a single input response P(t) giving a single output response C(t) as seen from figure no 1.9. The impulse response function has been denoted by H(t). The system is corrupted by external component M(t). This model can be represented by following relationships [35]:

$C(t)=P(t)*H(t)$ (1.15)

$G(t)=M(t)+C(t)$ (1.16)

The Spectro-filter H(t) can be estimated from following equations:

$W(f) = \frac{S_{PD}(f)}{S_{PP}(f)}$ (1.17)

$W(t)=IFFT[W(f)]$ (1.18)

In these equations $S_{PP}(f)$ denotes the auto spectrum of P(t), whereas $S_{PD}(f)$ denotes the cross spectrum of P(t) and M(t). Convolution of input P(t) with W(t) gives an estimate of C(t) i.e.

$\tilde{C}(t)=P(t)*W(t)$ (1.19)

$\tilde{G}(t)=E(t)- \tilde{C}(t)$ (1.20)

In case of a mono cylinder engine C(t) denotes the combustion noise, P(t) denotes in cylinder pressure developed, M(t) denotes the mechanical based noise, E(t) denotes total noise emissions and H(t) denotes the relationship function between in cylinder pressure and noise emissions as shown in figure no 1.10.

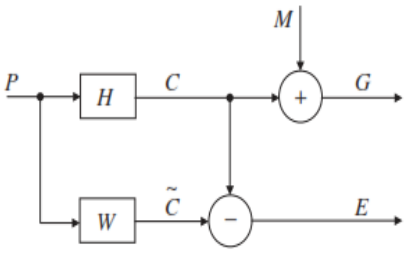

Figure no 1.10-Engine noise model (single cylinder) [35]

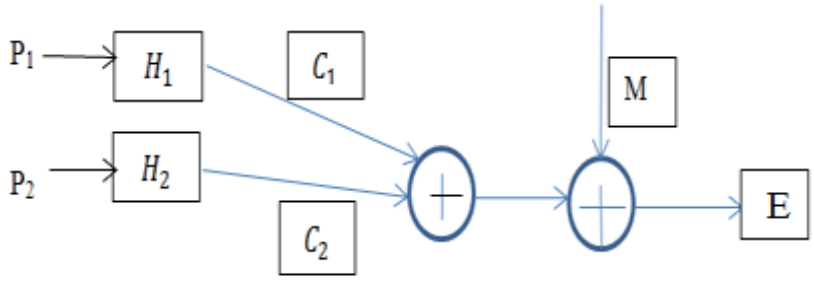

Figure no 1.11-Engine noise model (dual cylinder)

In case of a dual cylinder engine, figure no 1.11 shows the noise model. This is a multiple inputs and a single output (MISO) system. The combustion noise C(t) can now be considered as sum of the individual components produced by each cylinder i.e.

$C(t)=C_1(t)+C_2(t)$ (1.21)

The above discussed filtering technique was applied to noise emission data from a single cylinder for testing cases presented in table no 1.4. Specifications of test engine and various transducers mounted on it are enlisted in appendix portion of work. Various cyclo-stationary signals computed by subtraction of average values from original signals were used for effective source separation. The average values of signals have very higher levels of energy in frequency ranges above 500Hz. As a result, accuracy of Wiener filter is high above this frequency range [35]. It is evident from figure no 1.12, 1.13 that mechanical noise dominated at higher speed conditions.

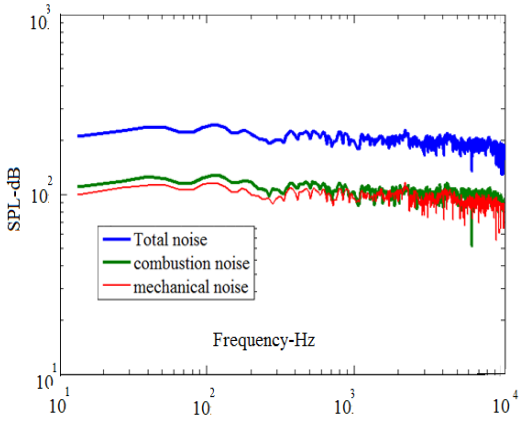

Figure no 1.12-Noise separation by Spectro -filters (1600RPM, full load)

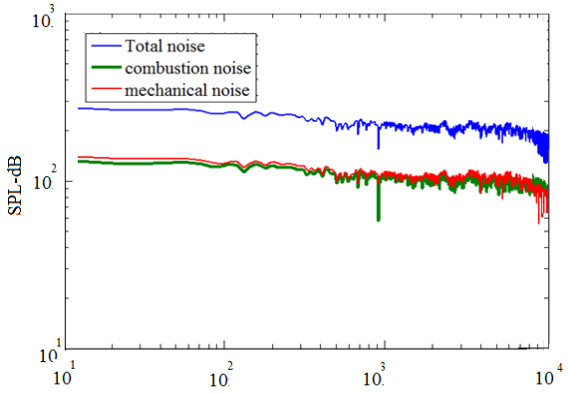

Figure no 1.13-Noise separation by Spectro -filters (2000RPM, full load)

Load	RPM	SOI $_{main}$ (Degrees BTDC)	SOI $_{pre}$ (Degrees BTDC)	Q $_{main}$ (mm^3/stroke)	Q $_{pre}$ (mm^3/stroke)	P $_{Rail}$ (Bar)
100%	1600	6.29°	14.6°	13	1	714
100%	2000	6.29°	14.5°	13	1	710

Table no 1.3-Spectro- filter analysis cases

1.5 Summary

Automotive industry had an annual turnover of about 1 Trillion U.S.$ with a growth rate of about 6% [32]. Attributes such as durability and serviceability requires a vehicle to be in service for certain period of time. Costs of vibration and noise control are usually very high, e.g. the yearly costs of warranty for brake noise was about 1 Billion U.S.$. during the year 2005 [35-41]. So it is necessary to analyze various NVH aspects of combustion engines. The presented research work has following major motivations:

Objective 1-To review different sources of noise in engines.

Objective 2-To study the effects of variations of different engine operational conditions on various signals acquired from transducers mounted on test engine.

Objective 3- To show the applicability of various signal processing methods.

Objective 4-To analyze combustion based noise using acquired data.

Objective 5-To develop various numerical models of piston lateral motion and validate them using experimental data.

Objective 6-On the background of presented work, provide a guideline for further research**.**

In this work, results from various experiments conducted on a LDW442CRS type Lombardini make diesel engine are discussed. The test engine is a common rail, dual cylinder and water cooled one. The collected data from engine was processed using various MATLAB based signal processing tools. The discussed methodology can be helpful for early fault detection and hence form an important aspect of condition monitoring of an engine.

1.6 References

[1]Davis,S.C.,1998,"Transportation Energy Data Book",18th edition, Report No. ORNL-6941, Last accessed on January 28, 2016.

[2]De Cicco, J., and Mark,J.,1998, "Meeting the energy and climate challenge for transportation in the United States", Energy Policy,Vol.26,no.5,pp. 395-412.

[3]John, A.,1991,Department of Transportation (DOT) Briefing Book on the United States Motor Vehicle Industry and Market,Version 1,Volpe National Transportation Systems Center, Cambridge, Last accessed on January 28, 2016.

[4]Sperling, D.,1989,"New Transportation Fuels: A strategic approach to technological change", Energy Policy, Vol. 18, no.8,pp.787-789.

[5]Cronk, S.,1995,"Building the E-Motive Industry: Essays and conversations about strategies for creating and electric vehicle industry", SAE International, Warrendale,Pennsylvania,USA,ISBN-13: 978-1560915607.

[6]Evangelo, and Rakopoulos,2011,"Experimental study of combustion noise radiation during transient turbocharged diesel engine operation", Energy,Vol.36,no. 8,pp.495-499.

[7]Walsh,Michael, P.,1997,"Global trends in diesel emissions control-A 1998 Update", SAE Technical Paper 980186.

[8]Krieger,R.,Siewert,R.,Pinson,J.,Gallopoulos,N.,1997,"Diesel Engines: One option to power future personal transportation vehicles",SAE Technical Paper 972683.

[9]Wang,M.,Stork,K.,Vyas,A.,Mintz,M.,Singh,M.,and Johnson,L.,1997,"Assessment of PNGV fuels infrastructure. Phase 1 report: Additional capital needs and fuel-cycle energy and emissions impacts", UNT Digital Library, http://digital.library.unt.edu/ark:/67531/metadc696284/, Last accessed on January 28, 2016.

[10]Walsh,Michael,P.,1998,"Global trends in diesel emissions control-A 1997 Update", SAE Technical Paper 970179.

[11]Sonya,G.,Labelle,A.,2014, Special report TD Economics, U.S. auto sales basking in their comeback glow, Last accessed on January 28, 2016.

[12]Kondo,M.,Kimura,S.,Hirano,I.,Uraki,Y.,Maeda, R.,2001,"Development of noise reduction technologies for a small direct-injection diesel engine",JSAE Review,Vol.21,no.3,pp.327-333.

[13]Torregrosa,AJ.,Broatch,A.,Novella, R.,Monico, LF.,2011," Suitability analysis of advanced diesel combustion concepts for emissions and noise control", Energy,Vol.36,no.2,pp.825–838.
[14]Shi,Y.,Qiao,X.,Ni,J.,Zheng,Y.,Ye,N.,2010,"Study on the combustion and emission characteristics of a diesel engine with multi-injection modes based on experimental investigation and computational fluid dynamics modelling", Proceedings of intuition of Mechanical Engineers,Part D-Journal of Automobile Engineering,Vol.224,pp.971–986.
[15]Mohamad,S.,Qatu,Mohamed,Abdelhamid,K.,Pang,J.,Sheng,G.,2009,"Overview of automotive noise and vibration", International Journal of Vehicle Noise and Vibration,Vol.5,no.1/2,pp.1-35.
[16]Genuit, K.,2004,"The sound quality of vehicle interior noise-a challenge for NVH engineers", International Journal of Vehicle Noise and Vibration,Vol.1,no.1/ 2,pp.58-68.
[17] Sheng, G.,2012, "Vehicle Noise Sound Vibration and Sound Quality", SAE international, Warrendale, Pennsylvania, USA,ISBN of 978-0-7680-3484-4.
[18]Carlucci, P.,Ficarrela, A.,Laforgia, D.,2001," Study of the influence of the injection parameters on combustion noise in a common-rail diesel engine using ANOVA and neural networks", SAE Technical Paper 2001-01-2011.
[19]Priede,T.,1979, "Problems and developments in automotive engine noise research", SAE Technical Paper 790205.
[20]Russell,M.,Haworth,R.,1985,"Combustion noise from high speed direct injection diesel engines", SAE Technical Paper 850973.
[21]Payri, F.,2000, " Injection diagnosis through common-rail pressure measurement", Proceedings of the Institution of Mechanical Engineers, Part D: Journal of Automobile Engineering, Vol 220,no3,pp. 347-357.
[23] Priede,T.,Grover,E., Anderton,D.,1968, "Combustion induced noise in diesel engines", Proceedings of diesel engines users association congress, London.
[24]Hickling, R., Kamal, M.,1982, "Engine Noise - Excitation, vibration and radiation", Plenum Press, New York, ISBN-978-1-4899-4988-2.
[25] Offner, G.,Priebsch, H H.,Ma, M T.,Karlsson, U.,Wikstrom, A.,and Loibnegger,B.,2004, " Quality and validation of crank train vibration predictions – effect of hydrodynamic journal bearing models ", Multi-Body Dynamics: Monitoring and Simulation Techniques-III, pp. 255–271.
[26]Russell, M.F.,1972, " Reduction of noise emissions from diesel engine surfaces", SAE Technical Paper 720135.
[27]Ochiai, K.,and Yokota, K.,1982, " Light-weight, quiet automotive DI diesel engine oriented design method", SAE Technical Paper 820434.
[28]Anderton,D.,2003, "Noise source identification techniques", ISVR course notes.
[29] Grover., Lalor,1973,"A review of low noise diesel engine design at I.S.V.R.", Journal of Sound and Vibration, Vol 28, no 3, pp. 429-431.
[30]Warring, R.H.,1972, "Handbook of noise and vibration control", Modern Trade and Technical press, Surry, U.K.,ISBN - 0854610359.
[31]Werkmann, M.,Tunsch,M.,and Kuenzel, R., 2005, "Piston pin related noise – quantification procedure and influence of pin bore geometry", SAE Technical Paper 2005-01-3967.
[32]Pollack,M.,Govindswamy, K., and Hartwig,M.,2005, "Cold start engine clatter noise evaluations", SAE Technical Paper 2005-01-2455.
[33] Beardmore, J., 1982, "Piston stick slip noise generation mechanism", SAE Technical Paper 820753.
[34]Yuehui, Liu.,2002,"Engine noise source identification with different methods", Transactions of Tianjin University ,Vol 8,no 3,pp. 174-177.
[35]Pruvost,L.,Leclere,Q.,Parizet,E.,2009,"Diesel engine combustion and mechanical noise operation using an improved specto-filters", Mechanical Systems and signal processing, Vol 23,no7,pp.2072-2087.
[36]Pischinger, F.,Schmillen,K.,Leipold,FW.,1979,"A new measuring method for the direct determination of diesel engine combustion noise", SAE Technical Paper 790267.
[37]http://www.fev.com/fileadmin/user_upload/Media/Spectrum/en/spectrum21.pdf,Last Accessed on May 01, 2016.
[38] http://luis.lemoyne.free.fr/Indicating_Product%20Overview_2009.pdf, Last Accessed on January 8, 2016.

[39] Crocker,M.J.,2007, "Handbook of noise and vibration control", John Wiley & Sons Inc., New York NY, USA,ISBN- 978-0-471-39599-7.
[40]Norton, M.P., and Karczub,D.,2007, "Fundamentals of noise and vibration analysis for engineers ", Second Edition, Cambridge University Press, U.K., ISBN -978-0-521-49913-2.
[41]Beranek,2007, " Noise and vibration control engineering: principles and applications", John Wiley & Sons Inc., New York NY, USA , ISBN-9780470172568.

Chapter 2

Methodology for condition monitoring in engines

2.1 Introduction

Various diagnosis methodologies have ability to detect various faults earlier before any actual damage can take place to a machine. The early detection of faults has advantages both in terms of cost as well as time. These methodologies allow the downtime of maintenance to be rescheduled, thus preventing sudden shutdown of machines or risks of any potential injury to its operators. In cylinder pressure, vibrations and noise emissions data provide a rich source of information about physical conditions and operational parameters of engines [1]. The present section provides details about various diagnosis methodologies adopted in case of diesel engines for their condition monitoring. Some of these include:

A. Vibration monitoring -It is most commonly used methodology, but effective location of transducer is a big challenge as mixing of signals may occur due to different transmission paths. Vibration signals can be analyzed by frequency spectrum, peak or RMS values. These can be used to monitor various imbalances, bearing damage or shaft misalignments [1].
B. In cylinder pressure monitoring- Data about cylinder pressure development provides information about injector faults, wear, valve operational problems, incorrect injection timings and hence overall combustion efficiency of engines. However, higher temperatures conditions make various pressure sensors expensive with short life span time [2].
C. Noise emissions - Noise levels are perceived by the humans as air pressure oscillations reaching ears which lead to motion of the ear drums. Various sound features can be analyzed by means of sound pressure levels (SPL). In order to obtain the levels that bear a closer relationship to loudness judgment, three different networks of frequency weighting (A, B, and C) filters have been incorporated into various sound level meters with the A-weighting most closely matching the hearing capacity of human ears [3].

Due to higher compression ratios, diesel engines are known to produce higher noise emissions as compared to gasoline engines [4,5]. Higher compression ratio increases various forces acting on piston assembly at the ignition timings which results in increase of vibrations from engine structure. Overall, this leads to increase in noise emissions from engine. Due to large number of external effects, the acceleration and noise emissions data may become contaminated leading to several complexities. Hence various signal processing methods can reveal information about various events which have fixed time of occurrence depending on the crank mechanism of engine. These methods include Short Time Fourier Transformations (STFT), Wavelet Transformation (WT), Bilinear Time-frequency Distribution (BTFD) [6]. Winger –Ville distribution (WVD), Born –Jordan distribution (BJD) and Choi-Williams distribution (CWD) are commonly used BTFD methods [7]. When these BTFD methods are applied to a transient signal, large ripples are produced on the envelopes which may lead to loss of information [8]. However, these methods have better frequency as well as time resolutions when compared to conventional Fourier transformations. In this part of work some of the commonly used signal processing techniques have been discussed. Various important properties of these methods have been presented, and finally their performance was evaluated by application on the data acquired from engine.

2.2 Signal processing tools

A. Power spectral density function

This function (Ψ^2) which denotes a random process, provides the frequency composition of data in terms of its mean square values [9]. The mean square values of a time sample in frequency range [ω, ω+ Δ ω] can be obtained by passing sample through a band pass filter with sharp cutoff frequency features and then computing the average of squared output from filter. The average square values approach mean square values as T→∞.i.e.

$$\Psi^2(\omega, \Delta\omega) = \text{Lim}_{\Delta x \to \infty} \frac{\int_0^T x^2(t)dt}{T} \qquad (2.1)$$

B. Time frequency analysis

The Fourier transformation of a function f(t) in frequency domain can be represented as:

$$f(\omega) = \int_0^t f(t)e^{-j\omega t}dt \qquad (2.2)$$

This analysis is useful as long as frequency content of signals do not vary with time. Hence time-frequency analysis or wavelet analysis are more suitable for analysis of transient signals [10]. In the time-frequency analysis, the signal is windowed into small intervals and then Fourier transformation is taken for each interval [11]. Length of window can be used to change the resolution of the output signal. A shorter window has higher resolution in time domain, but a poor resolution in frequency domain and vice versa. The short time-frequency analysis (STFT) of signal may be represented as:

$$\text{STFT}(\tau, f) = \int_0^T x(t)\, h^*(t-\tau)e^{-j\omega t}dt \qquad (2.3)$$

Where x(t) is input signal & h(t-τ) is window function. Wigner Ville function that has following quadratic time-frequency distribution is represented by [9]:

$$\text{STFT}(\tau, f) = \int_0^T x\left(t-\frac{\tau}{2}\right) x^*(t+\frac{\tau}{2})e^{-j\omega t}dt \qquad (2.4)$$

C. Wavelet Analysis

Wavelet analysis maps a signal on joint time -frequency plane and is sensitive towards the transient nature of signals. One of the major drawbacks of various time-frequency processing methods is that they produce ripples, hence making it difficult extract valuable information [12]. During wavelet analysis, the frequency resolution is better at low frequencies whereas the time resolution is better at higher ones. Hence Wavelet analysis results are more accurate as compared with other methods [13]. Using wavelet analysis, a signal is transformed onto a family of zero mean functions which are known as wavelets. These have high time resolution and have no cross-term interference.

The squared wavelet transform is called Scalogram. A single Scalogram can easily cover audible frequency range with a time resolution of approximately 0.1 m-s for the high-frequency components [14]. This makes Scalogram more suitable for such various signals like squeak and rattle noise for which wider ranges of frequency analysis are needed. Mathematically for a function f(t), a complex wavelet transform is defined by [15] :

$$\text{CWT}(a, b) = \int_{-\infty}^{+\infty} f(t)\frac{1}{\sqrt{a}}\Psi * [\frac{(t-b)}{a}]dt \qquad (2.5)$$

Where

Ψ*(t): Complex Mother Wavelet
f(t): Analyzed signal a: Scaling factor
b: Shifting factor CWT (a, b) : Wavelet coefficients

Mother Wavelet function ψ(t) must satisfy following conditions:

a) This function has zero average and decays exponentially to zero. i.e.

$$\int_{-\infty}^{+\infty} \psi(t)dt = 0 \qquad (2.6)$$

b) Function and its Fourier transformation must satisfy admissibility condition i.e.

$$\int_{-\infty}^{+\infty} \frac{\psi*(t)^2}{|f|} \leq 0 \qquad (2.7)$$

Both dilation as well as translation parameters in CWT are subjected to variations that makes its use more complex. Discretization of signals can help to reduce this problem to certain extent. The CWT of a signal discrete signal X_m is defined in terms of its sampling time Δt and sample data points m, n as:

$$\text{CWT} = \sum_{m=0}^{N-1} X_m \psi^* \left[\frac{(m-n)\Delta t}{X_j}\right] \qquad (2.8)$$

Where t = m Δt, b = n Δt, m &n varies from 0,1,2…N-1,N

Time -frequency analysis is suitable for analysis of signals having slow frequency changes such as those generated during engine ramp down, whereas wavelet analysis is more suited for fast frequency changes such as those generated during rattle [16]. Higher time resolution at higher frequencies makes it possible to resolve short consecutive events using wavelet transformation.

2.3 Experiments

Several experiments were conducted on the test engine that is commonly used in case of small commercial vehicles. The fuel injection methodology used is a dual injection type having pre and main injection periods before piston reaches top dead center position during compression stroke. The amount of fuel injected during pre-injection period is denoted as Q_{pre}, whereas the amount injected during main injection period is represented by Q_{Main}. Instants at which these injections start were defined by crank angle positions denoted by SOI_{pre} & SOI_{main} respectively. Fuel is injected inside cylinders through a common rail system at injection pressure P_{rail} that is expressed in Bars. Tests were conducted at motored as well as full load conditions by varying various crank angle positions at which fuel is injected as shown in table no 2.1. The main aim of present activity was to analyze noise emissions from engine at different locations by changing the positioning of microphone.

2.4 Results and discussions

Diesel engine acoustics emissions contains rich information about working conditions of engine [17]. In order to analyze noise emissions at various locations, a grid was built around the test engine to change the location of microphone. Particular attention was focused on three positions marked A, B, C as depicted in figure no 2.1. Figure no 2.2,2.3 shows recorded noise emissions at three chosen locations under full load conditions. It can be observed that all traces have low frequency oscillations related to firing frequency of engine. Position C is characterized by high frequency oscillations around 360°crank angle position due to onset of combustion events. Such a trend was not visible in signals acquired at position A and B.

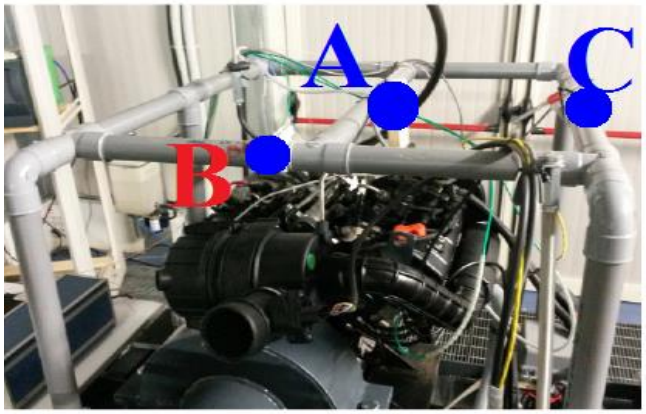

Figure no 2.1-Three positions to acquire noise emissions

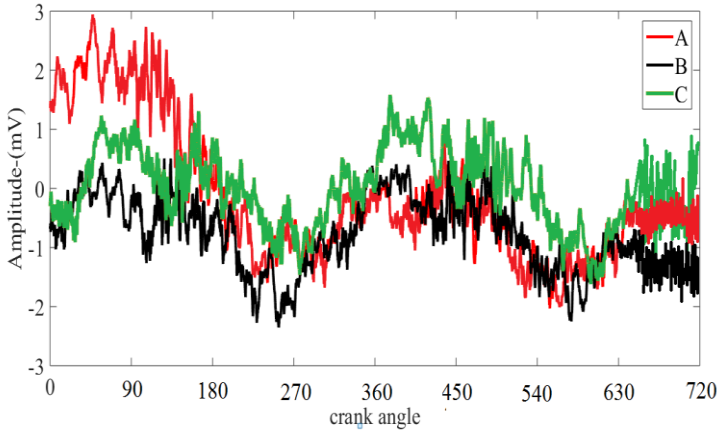

Figure no 2.2-Noise emissions at 1600 RPM,100% load

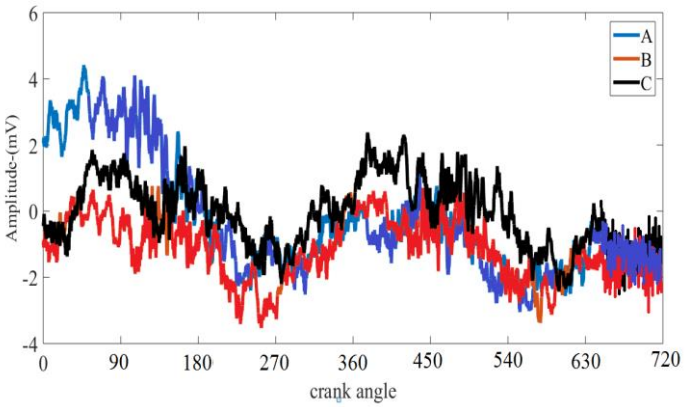

Figure no 2.3-Noise emissions at 2000 RPM,100% load

Position B was next investigated to see if any information could be extracted regarding intake flow noise. Figure no 2.4, 2.5 shows plot of intake pressures acquired at this positon. Absence of any noticeable changes in signals acquired shows that acoustic signals were least affected by load values.

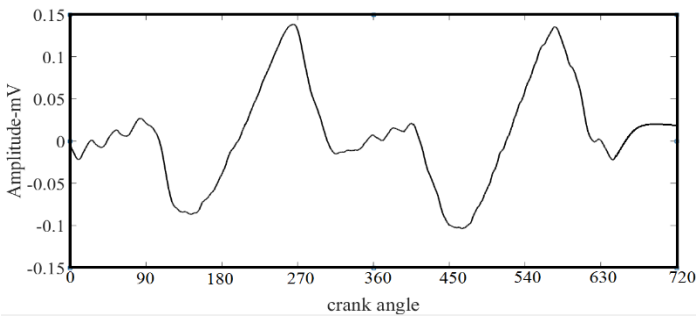

Figure no 2.4 -Intake pressure at 1600 RPM,80% load

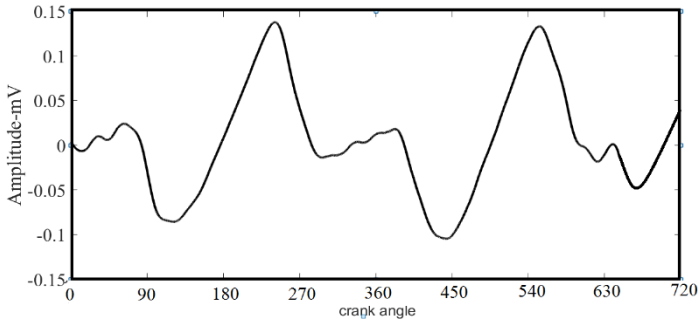

Figure no 2.5-Intake pressure at 1600 RPM,100% load

Further coherence function was used for analysis of signals. This function which is denoted as a normalized function that may be defined as the ratio between the square of cross power spectral densities of input and output signals to the product of the power spectral density (PSD) of individual signals. The value of this function varies from zero to unity.

Figure no 2.6, 2.7 shows plot of coherence functions between intake pressure and noise radiated from engine at location B were computed using a Hanning window of length 1/6th of engine cycle. It may be observed that a close relationship exists between the two signals in frequency range [50Hz-400Hz] irrespective of load values. Such a band in which intake pressure signals are closely correlated with noise emissions is dependent on engine speed. In this frequency band, gas exchange process may be considered as a major contributor towards overall noise emissions.

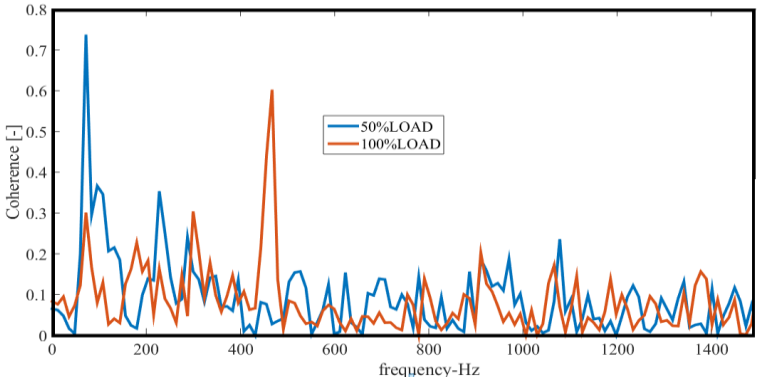

Figure no 2.6 -Coherence between cylinder pressure and intake pressure signals (1600RPM)

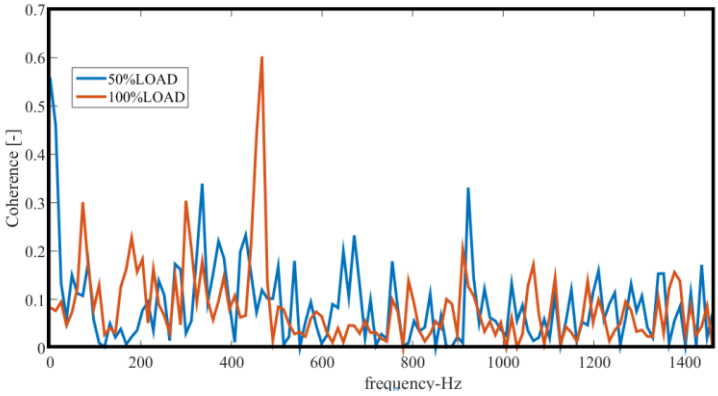

Figure no 2.7-Coherence between cylinder pressure and intake pressure signals (2000RPM)

The noise emissions at location C were filtered in the above mentioned frequency range and compared with those of unfiltered noise emissions at location B as shown in figure no 2.8, 2.9. A close correlation between two signals shows the selected frequency band was properly chosen.

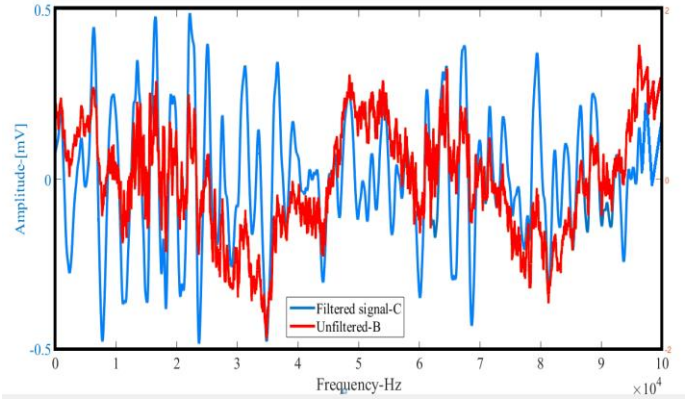

Figure no 2.8-Comparison between signals (1600RPM-100%load)

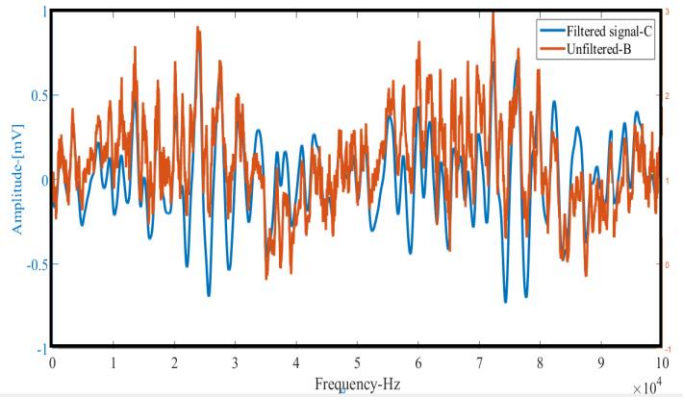

Figure no 2.9-Comparison between signals (2000 RPM-100%load)

Case	RPM	Load	SOI $_{main}$ (Degree Before TDC)	SOI $_{pre}$ (Degree Before TDC)	Q $_{main}$ (mm^3/stroke)	Q $_{pre}$ (mm^3/stroke)	P $_{Rail}$ (Bar)
B1	1600	100%	6.29°	14.6°	13	1	714
B2	1600	Motored	-	-	-	-	-
B3	2000	100%	6.29°	16.5°	13.8	1	710
B4	2000	Motored	-	-	-	-	-

Table no 2.1– Fuel injection parameters

Further tests were done in order to investigate signals at various marked locations as reported in table no 2.1. Figure no 2.10, 2.11 shows the in cylinder pressure spectrum plots for given testing conditions acquired at location C using FFT function. The contribution of combustion process towards in cylinder pressure development is clearly visible from these graphs. In order to minimize the presence of cyclic variations, all signals were averaged on basis of 30 cycles. These plots show the energy distribution among frequency harmonics associated with pressure evolution. The differences in the energy levels of motored and fired conditions is clearly noted. Comparisons between various traces show low energy distribution in mid frequency ranges during motored conditions when compared to firing conditions. In low frequency ranges, the spectrum of cylinder pressure plots depends upon peak pressure and integral of pressure curve. In middle ranges it depends on pressure rise rate, whereas in higher ranges peaks are observed due to rapid pressure rise.

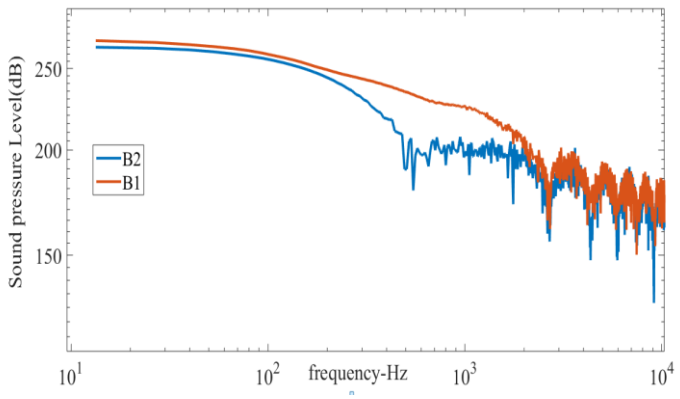

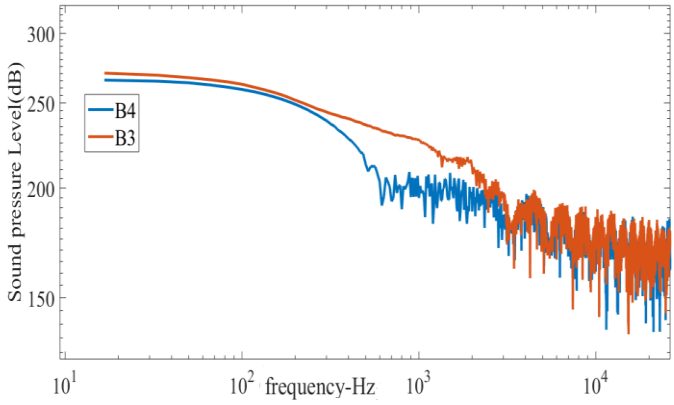

Figure no 2.10- In cylinder Pressure Spectrum (1600RPM) Figure no 2.11-In cylinder Pressure Spectrum(2000RPM)

Further PSD plots of various signals were analyzed using Pwelch function. Peaks were found in PSD plots of in cylinder pressure at frequencies which were integral multiples of fundamental firing frequency of engine. These plots highlight that main changes due to firing of fuel inside cylinder occurs at 300Hz frequency (fig no 2.12, fig no 2.13). Hence all combustion related events must be considered above this frequency.

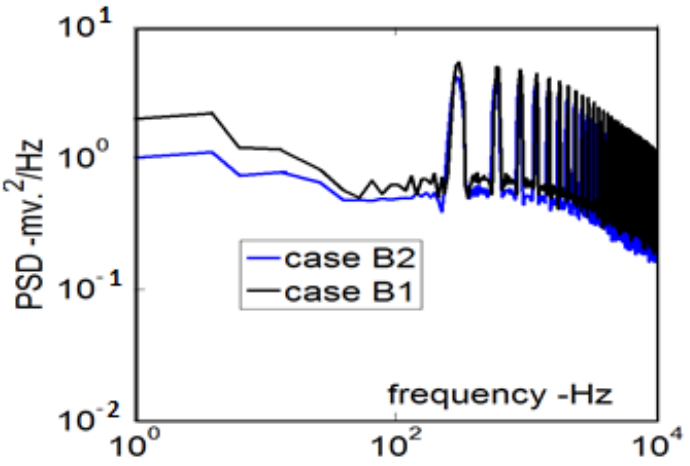

Figure no 2.12- PSD plots for Cylinder Pressure Signals(1600RPM)

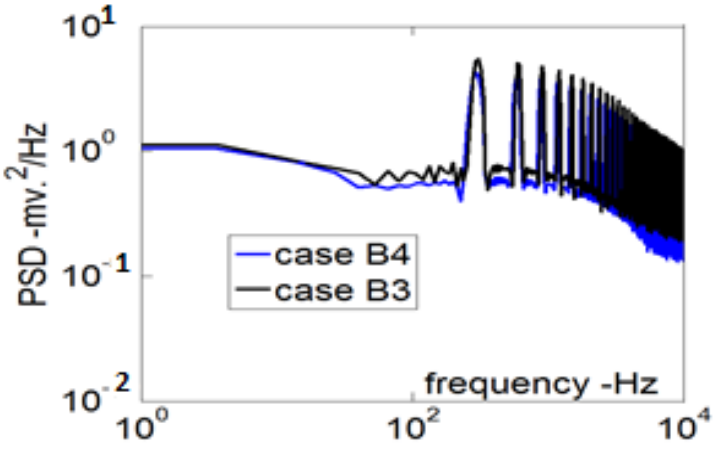

Figure no 2.13- PSD plots for Cylinder Pressure Signals(2000RPM)

Since the acoustic power radiated from engine also depends upon the block velocity, the velocity of in cylinder pressure evolution also represents an important term in study of combustion source. PSD plots of this parameter for given testing conditions were plotted as seen from figure no 2.14,2.15. It is clear that the region 2 corresponding to medium frequency ranges of combustion noise (discussed in chapter 4) begins after 1kHz.

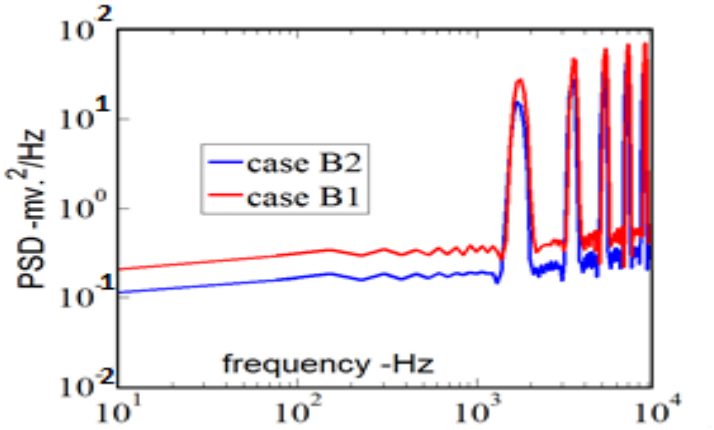

Figure no 2.14-PSD plots for Cylinder Pressure Derivative Signals(1600RPM)

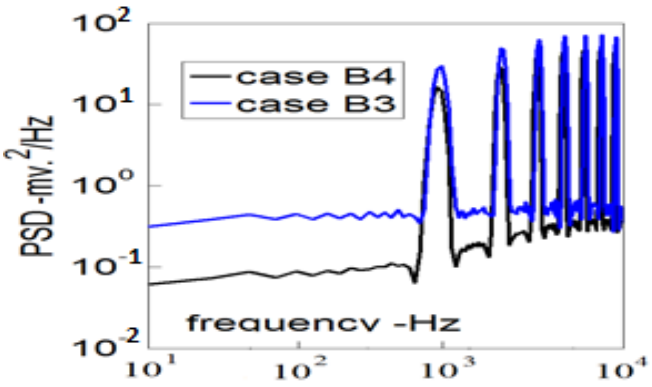

Figure no 2.15 -PSD plots for Cylinder Pressure Derivative Signals(2000RPM)

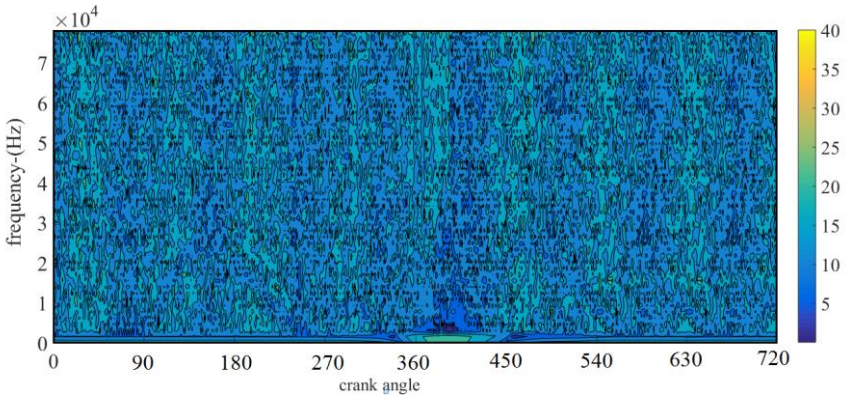

Figure no 2.16-Cylinder Pressure spectrogram at 1600RPM,100%load

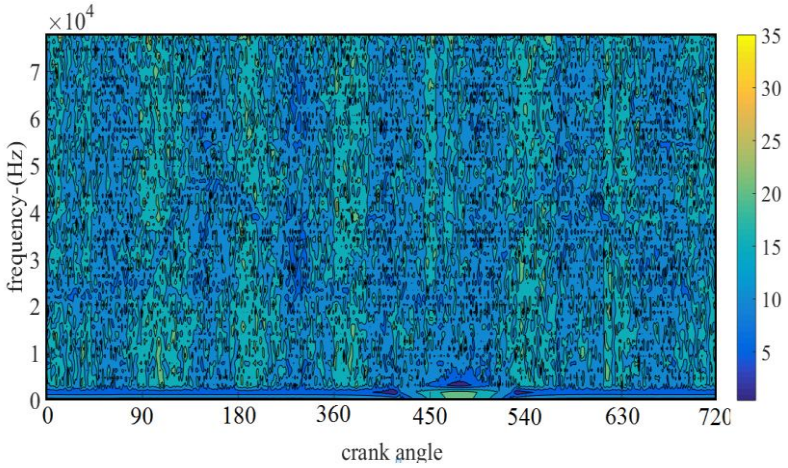

Figure no 2.17-Cylinder Pressure spectrogram at 1600RPM, Motored

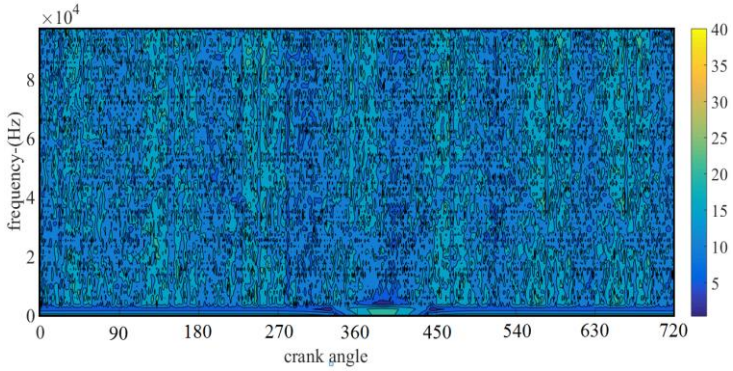

Figure no 2.18-Cylinder Pressure Spectrogram at 2000RPM,100%load

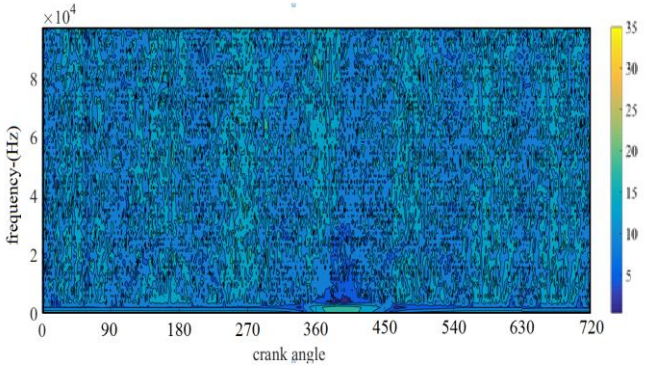

Figure no 2.19-Cylinder Pressure spectrogram at 2000RPM, Motored

Further in cylinder pressure signals acquired at location C were studied using time-frequency spectrogram analysis as seen from figures 2.16-2.19. The frequency contents of signals were calculated by means of discrete Fourier transformation that were computed using FFT of overlapped windowed segments of signals. The color bars in these figures denotes the amplitude of components. Dark colors denote higher energy bands, whereas the lighter ones displays lower energy bands. From these plots, contributions of combustion events are clearly visible due to broadening of frequency bands near 360°TDC position under full load conditions as compared to motored conditions. High frequency components were found in frequency range 500Hz -40kHz owing to rapid increase in cylinder pressure after pre- injection period a few degrees before TDC position.

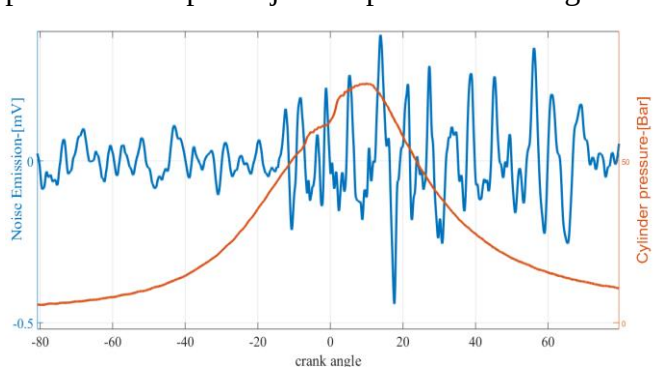

Figure no 2.20-Comparison of cylinder pressure [------], Filtered noise signals[------](1600RPM)

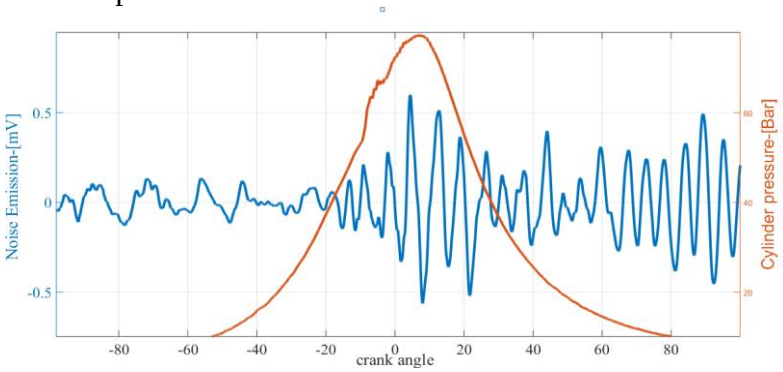

Figure no 2.21- Comparison of cylinder pressure [------], Filtered noise signals[------]((2000RPM)

As position C was found to be sensitive towards combustion process, noise signals acquired at this position were filtered in relevant frequency band defined previously by time-frequency analysis and compared with in cylinder pressure as seen in figure no 2.20,2.21. The contributions of combustion process towards noise signals is clearly visible. Once various frequency ranges were characterized, the radiated noise signals were investigated in order to understand relationship between various signals. Figure no 2.22,2.23 shows the PSD plots for noise signals acquired both at motored as well as fired conditions using microphone located at position marked as A. It can be seen that contributions of combustion process towards noise emissions occurs at wider frequency bands when compared with cylinder pressure PSD plots. This may be due to several non–linear paths of noise propagation through engine as discussed in [16]. Noise PSD plots were characterized by high frequency components that may be due to several other contributing sources.

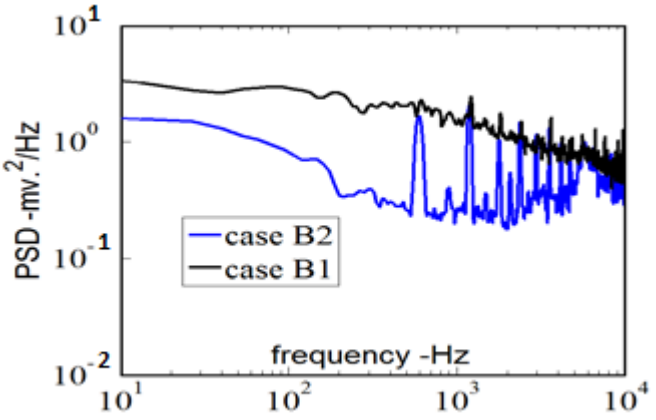

Figure no 2.22 -PSD plots for Noise Signals(1600RPM)

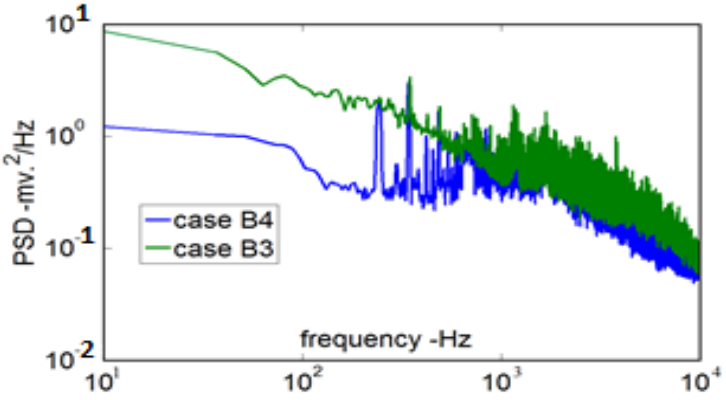

Figure no 2.23-PSD plots for Noise Signals(2000RPM)

Once signals were analyzed, time frequency wavelet analysis of noise emissions acquired at location A was done using wavelet analysis, in order to investigate the spectral distribution of energy among various events taking place in an engine cycle as seen in figure no 2.24,2.25 with operations under full load conditions. These plots show periodicity of various contributing sources clearly characterized by high frequency components below 1kHz range. These closely correlate with that of actual occurrence of events shown in Table no E. Index 1 indicates various events for case cylinder having pressure transducer mounted on it, whereas index 2 indicates events for other non-instrumented one.

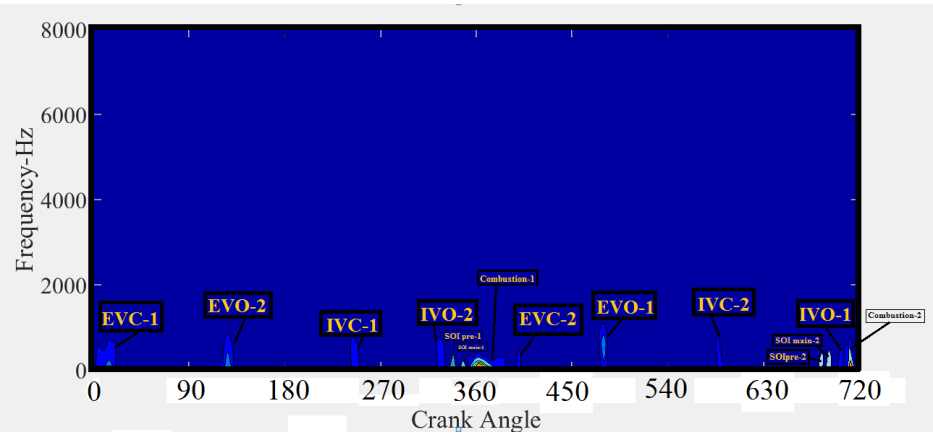

Figure no 2.24 -Time frequency analysis of noise signals(1600RPM)

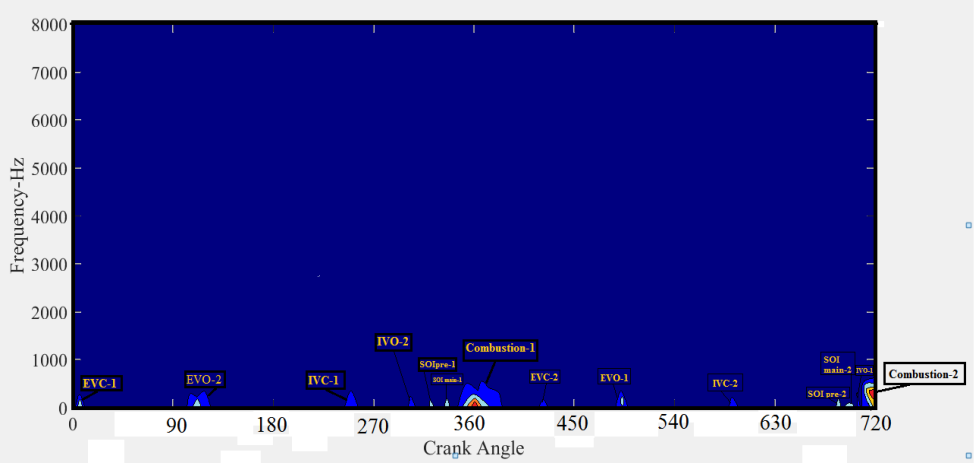

Figure no 2.25-Time frequency analysis of noise signals(2000RPM)

The combustion process is responsible for high frequency components in spectrogram and is well represented below 2kHz range. Analysis of noise spectrogram plots show no significant modification due to variations in engine load or speed conditions.

The above discussed spectral trends in cylinder pressure have highlighted distribution of energy among frequency harmonics. An increase in speed of engine causes a translation towards higher values, but amplitude of various components does not show significant variations with changes in engine load. Hence another method which is based on study of variations of mean frequency trends was used for analysis of signals [18,19, 20].

The mean frequency of a signal is given by [20]:

$$f_{mean} = \frac{\sum_{k=0}^{W} f_k P(f_k)}{\sum_{k=0}^{W} P(f_k)} \qquad (2.9)$$

Where $P(f_k)$ is k^{th} sample of power spectrum and w is frequency band of signal.

The covariance of a given function x(h) can be computed as follows:

$$Cv(h) = \frac{1}{2N+1} \sum_{k=-N}^{k=+N} x^{+}(h) x^{+'}(h+k) \qquad (2.10)$$

Where $x^{+}(h) = x(h) + j\, x\hat{}(h)$ is analytical signal of input x(h) calculated using its Hilbert transformation x^(h). $x^{+'}$ is complex conjugate of x^{+}. The relationship between mean frequency and covariance function of signal can be represented as:

$$f_{mean} = \frac{1}{2\pi h} Tan^{-1}\left[\frac{Imag[C_v(h)]}{Real[C_v(h)}\right] \qquad (2.11)$$

The analysis of mean frequency trends reveals time variations in frequency composition of signals which is based on the analysis of the mean value of the spectrum of the samples in a window sliding on the signal. This method analyses samples in a sliding window and evaluates the mean frequency trends using the complex covariance function.

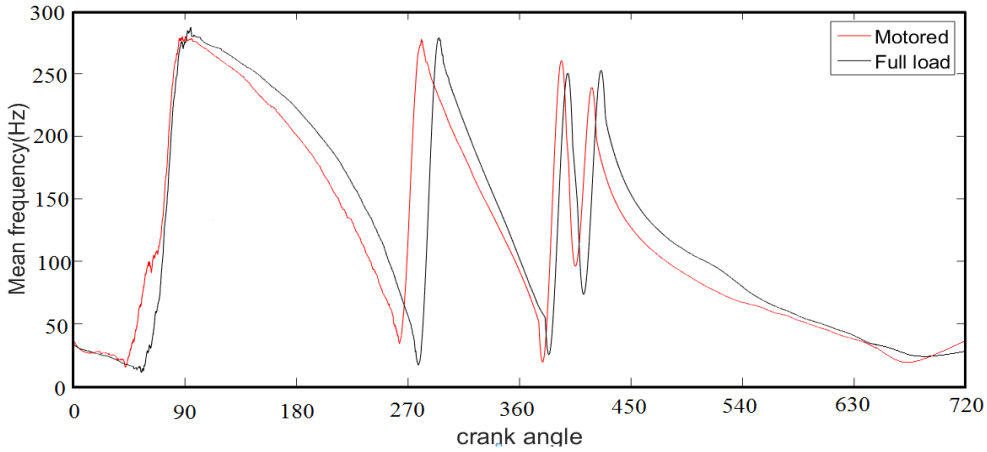

Figure no 2.26 -Mean frequency trends of cylinder pressure at 1600 RPM

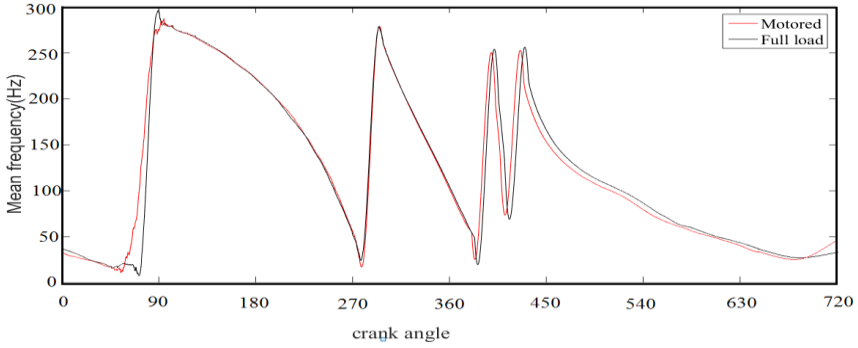

Figure no 2.27 -Mean frequency trends of cylinder pressure at 2000 RPM

Figure no 2.26, 2.27 shows variations in the mean frequency trends for in cylinder pressure signals acquired at location A under full load. All trends show excitation of sources in terms of their frequency contents, their amplitude and locations of crank angles at which they appear.

During the intake process, a smooth development of cylinder pressure is responsible for lower values of initial mean frequency trends. Once compression starts, an increase in rate of pressure causes increase in mean values of frequencies after 270˚ position. Then in the vicinity of TDC position, (360°CAD) a reduction in trends denotes start of combustion process.

During power stroke, the rapid increase in combustion chamber pressure is responsible for rise in trends until peak values are achieved. During exhaust process smooth development of in cylinder pressure is again cause of lower values of mean frequencies. Various trends were found to be same irrespective of load variations. Motored case was observed to reach peak values before full load condition.

2.5 Summary

This part of work analyzed the effects of changes in various injection parameters on development of combustion pressure and noise emissions from engines. Scope of using non-intrusive diagnosis technique has been analyzed by changing various locations of microphone around the test engine. For this purpose, three positions were chosen denoted by A, B and C. Position C was seen as being most sensitive towards combustion process, position B was found to be sensitive towards intake process and finally position A was seen to have contribution of all other sources towards noise emissions.

Various characteristic frequency ranges of contributing sources were identified. Time–Frequency analysis showed the onset of various cyclic events associated with working of engine. Based on the identification of various frequency bands, it is possible to device suitable filters in order to extract more information about combustion and motion based noise which has been done in later part of this work.

2.6 References

[1] Moore,D.J.,2013, "Condition monitoring of diesel engines", Phd Thesis, University of Manchester.
[2] El-Ghamry,M., Steel,J.,Reuben,R., and Fog,T., 2005, "Indirect measurement of cylinder pressure from diesel engines using acoustic emissions", Mechanical Systems and Signal Processing, Vol 4,no19,pp.751-765.
[3] Ball,A.,F.,Gu, and Li, W.,2000, "The condition monitoring of diesel engines using acoustic measurements part 2 fault detection and diagnosis", SAE Technical Paper 2000-01-0368.
[4]Albarbar, A., Gu, F., Ball, A. and Starr, A., 2010, "Diesel engine fuel injection monitoring using acoustic measurements and independent component analysis", Journal of Measurement, Vol 43,no.10,pp.1376-1386.
[5]Albarbar, A., Gu, F., Ball, A. and Starr, A., 2010, "Acoustic monitoring of engine fuel injection based on adaptive filtering techniques", Applied Acoustics, Vol 71, no 17, pp.1132–1141.
[6] Albarbar, A., Gu, F., Ball, A. and Starr, A., 2007, "Internal combustion engine lubricating oil condition monitoring based on vibro-acoustic measurements ", Journal of Non-Destructive Testing, Vol 49, no 7, pp.715-718.
[7] Chiollaz, M., and Faver, B., 1993, "Engine noise characterization with Wigner-Ville time-frequency analysis", Journal of Mechanical Systems and Signal Processing, Vol 75, pp.375-400.
[8]Albarbar, A., Gu, F., Ball, A., Starr, A., 2008, "On acoustic measurement based internal combustion engines", Advances in Applied Acoustics (AIAAS) ,Vol 50, no.1,pp.30-33.
[9]Sheng, G.,2012, "Vehicle noise sound vibration and sound quality", SAE international, Warrendale, Pennsylvania, USA, ISBN- 978-0-7680-3484-4.
[10] Cohen, L.,1989, "Time-frequency distributions – A Review", Proceeding of the IEEE, Vol.77, no.7.
[11]Ball, A., Gu, F., Weidong, L., 2000, "The condition monitoring of diesel engines using acoustic measurements, part 1: Fault detection and diagnosis", SAE Technical Paper 2000-01-0730.
[12]Chiollaz, M., and Faver, B., 1993, "Engine noise characterization with Wigner-Ville Time-Frequency analysis", Journal of Mechanical Systems and Signal Processing Vol 75,pp.375-400.
[13]Chiatti ,G.,Chiavola, O., Fulvio, P. and Andrea,P.,2015," Diagnostic methodology for internal combustion diesel engines via noise radiation", Energy Conversion and Management, Vol 89,pp.34-42.
[14]Chiatti ,G., and Chiavola, O., 2004 , "Combustion induced noise in single cylinder diesel engines", Small Engine Technology Conference, paper no.2004-32-0071.
[15]Chiatti, G., Chiavola, O., 2003,"Experimental analysis of combustion noise in spark ignition engine", NVC conference, paper no. 2003-01-1442.
[16]Daubechies, I., 1992,Ten lectures on wavelets, Society for industrial and applied mathematics, Philadelphia.
[17]Wu, J., Chen, J.,2006, "Continuous wavelet transform technique for fault signal diagnosis of internal combustion engines", NDT International Vol 39,pp.304–31.

[18]Wang, J., McFadden, P., 1996, " Application of wavelet to gearbox vibration signals for fault detection", Journal of Sound and Vibration Vol 192, no 5,pp. 927-939.
[19]Lin, J., Zuo, M., 2003, "Gearbox fault diagnosis using adaptive wavelet filter", Mechanical Systems and Signal Processing", Vol 17, no 6,pp.1259–69.
[20]Smith, T., 2000, "The application of the wavelet transform to the processing of aeromagnetic data", PhD Thesis, The University of Western Australia.

Chapter 3

Features of various sources of noise in engines

3.1 Introduction

Evaluation of NVH performance of an engine is an important aspect from point of view of overall design and planning of automotive systems using these engines. This procedure includes repeated testing of engines using various fuel injections strategies, as well as study of engine-to-engine variations [1, 2, 3]. Vehicle noise may be broadly classified as structure borne noise and air borne noise. The type of noise entering air via acoustic path is known as air borne noise, whereas sound entering the air via structural path with vibrational energy as its main exciting source is known as structure borne noise. The structure borne noise has low frequency ranges of 500Hz-1000Hz, whereas the air borne noise is dominant in higher ranges. The experimental and analytical investigations in engine acoustics includes major focus on following aspects:

A. Overall sound pressure level measurements under various speed and load conditions.
B. Identification and ranking of various contributing sources.
C. Study of various noise transfer paths and mechanisms.
D. Subjective as well as objective assessments.

Some of the major works related to current thesis are enlisted in table no 3.1.

Author	Engine used	Aim	Method used
Jung, I., Jin, J., So, H., Nam, C.[4]	4 Cylinder diesel engine	Development of various combustion noise related indices	Variations in fuel injection
Ingemar Andersson ,Tomas McKelvey, Martin Larsson[5]	6 Cylinder diesel engine	Estimating combustion phasing parameters	Vibrational energy
Zhenpeng He,Weisong Xie , Guichang Zhang , Zhenyu Hong, Junhong Zhang[6]	4 Cylinder diesel engine	Observe the effects of geometrical parameters of skirt on piston lateral motion	Simulation of lateral motion of skirt
N.Dolatabadi,B.Littlefair,M.DelaCruz,S.Theodossiades ,S.J.Rothberg, H. Rahnejat[7]	1Cylinder gasoline engine	Identification of locations of various slapping events	Analysis of engine block accelerations
Yeow-Chong Tan, Zaidi Mohd Ripin[8]	4 Cylinder diesel engine	Simulation of resulting block vibrations	Lumped mass approach

Table no 3.1- Summary of related research works

In order to carry out detailed acoustic analysis of engines, it is necessary to focus on individual contributing sources. The present portion of work discusses characteristic features of various sources of noise in an engine.

3.2 Combustion noise

Combustion is an important phenomenon that needs to be taken into account while designing and performance calibration of system, and hence forms a primary source of noise which is particularly dominant in case of a direct injection diesel engine. There are three important modes of transfer of this noise to surroundings. These include from cylinder top, liner walls and connecting rod assembly. This noise is mainly related to rate of pressure rise inside cylinders. Tung and Crocker have studied combustion noise in a turbocharged diesel engine [9]. Structural attenuation also effects the noise radiated from engine which may be defined as the difference between in cylinder pressure spectrum and radiated noise from engine surface. High structural stiffness of cylinder bore leads to higher values of resonant frequencies. Higher values of resonant frequencies can help to the attenuate high frequency contents in combustion noise.

Combustion noise can be reduced either by increasing the structural attenuation of engine or by reducing the in cylinder pressure developed. Reduction in the delay period during ignition leads to lower values of in cylinder pressures and hence resulting combustion noise. Other factors which may help to reduce the combustion noise includes higher values of compression ratios, increase in the intake air pressure, use of higher exhaust gas recirculation rates and increased structural attenuation of various engine parts [10].

Previously methods to quantify this noise includes use of AVL combustion noise meter [11] or wavelet based noise meters [12]. However, decomposition of cylinder pressure has proved to be more effective than other techniques [13]. Effects of variations in cetane number on noise combustion noise have been observed by Machado and Thiele [14, 15]. Further CFD modeling of combustion noise was conducted by Blunsdon [16] and Luckhchoura [17].

3.3 Piston assembly noise

There are three types of noises that are generally seen in piston assembly. These include pin tickling noise, piston slap and piston rattling noise. Piston slapping noise has a major contribution among these. This is caused due to lateral motion of piston assembly between skirt and liner bore. There may be several events of skirt-liner lateral contact in an engine cycle as shown in figure no 3.1 [18], with most prominent ones occurring just after TDC firing position.

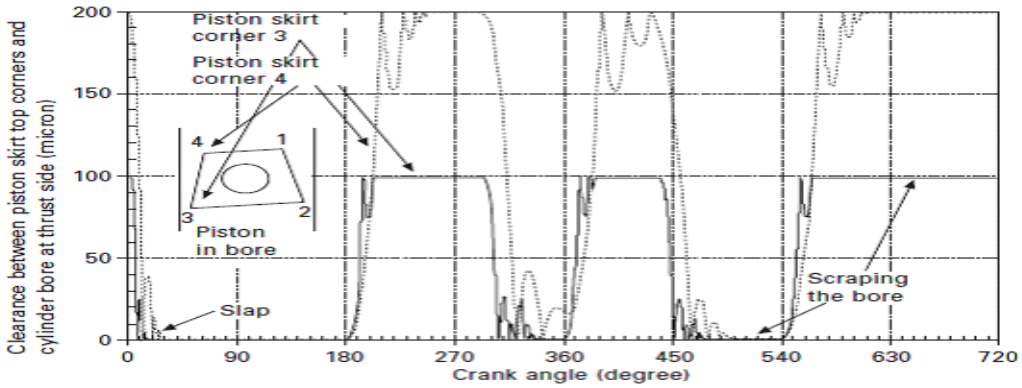

Figure no 3.1-Simulation of piston secondary motion [18]

The slap noise is more dominant under idle cold starting conditions as well as high load-low speeds operations.

Proper design of skirt is a key aspect to control this noise. Major factors that influence the secondary motion of piston include:

A) Piston side thrust force-lower values of engine speeds, lower piston assembly masses and higher values of crank radius to connecting rod length ratio can help to reduce the side thrust force and hence resulting piston slapping noise [19].
B) Moments about piston pin- lower inertia of skirt assembly, optimum values of piston pin and crankshaft offsets, proper supply of the lubricant can also help to control the pin frictional forces and moments [20].
C)Allowable distance of travel before hitting liner wall- smaller gap between piston skirt-to-bore can help to reduce the lateral motion at the expense of increased shear frictional force.
D)Oil damping force -sufficient supply of oil around skirt can help to reduce slapping noise significantly. Lower ring tensions, longer skirt length and increased area of contact in the piston rings are some of other effective ways to increase the oil film thickness and hence piston slap noise [21].
E) Controlling the damping and stiffness–impacts of softer piston skirt causes lesser noise emissions due to larger deformations. Hence it is crucial to increase the gap between top part of land and bore in order to avoid the contact which otherwise would produce sharp rattling noise.

3.4 Valve train noise

This type of high frequency noise includes following three major excitation sources:

A) Cam acceleration-At higher speeds, the opening and closure of cam excites high frequency vibrations due to inertial forces.

B) Valve train impacts -These include impulsive impacts during opening of valve (between cam and follower), during valve closure (between valve seat and valve) as well as bouncing noise observed at higher speeds.

C) Frictional vibrations-This noise is dominant over lower speed ranges as the asperity contact occurs between cam and follower near the nose of cam when the velocity of lubricant almost becomes zero.

Identification of valve train noise has been done by analysis of acceleration–cam angle graph [22]. Anderton and Zheng found that the valve train vibrations had major contributions towards total noise in higher engine speeds of above 2000RPM–3300RPM range in case of a six-cylinder gasoline engine [23]. Savage and Matterazzo have done experiments on a 3.3 L gasoline engine to investigate the effects of various factors like as jerks in cam, tension in valve spring, tappet-bore gap, valve-stem gap, surface finish, clearance at rocker arm bearing, overlap timings and damping coefficients of cylinder head [24]. Use of high precision manufacturing of cam profile, greater oil film thickness, higher valve train stiffness and smaller tappet-to-bore clearance are very important for reduction of valve train noise [25, 26].

3.5 Gear train noise

The rattle noise during transmissions in the drive trains has been a primary cause of concern in NVH development. Transmission of non-uniform torque from crank train to drive train causes rattle noise in gears. Clearances are often provided among the meshing tooth of gears to account for thermal expansions and tolerances. At lower engine speeds, with oscillating torque when gears are lightly loaded, there is a high probability of separation of meshing teeth which results in vibrational impacts. Other type of gear noise includes whining noise which is due to tooth deflection. Gear train noise is dependent on the number of meshing teeth, size of gear train, magnitude of torsional inputs and location of gear train. Detailed investigation of gear train noise was done by Spessert and Ponsa [27] as well as Zhao and Reinhart [28].

3.6 Crank train and engine Block vibrations

Torsional vibrations in the crank shaft and thin sections of engine block are important sources of noise and vibrations. Detailed analysis of crankcase and engine block vibrations was done by Russell [29], Ochiai [30] and Maetani [31]. Several commercial Softwares like ENGDYN are now available to record the response of the crank train and engine block system taking into account lubrication effects of oil [32].

3.7 Aerodynamic noise

Low frequency intake noise is due to turbulent fluctuations in flow of air at inlet ducts which also depends on intake valve area and engine speed. Design of intake ducts has been done previously which was based on gas dynamics [33]. Exhaust noise occurs due to pressure variations in the exhaust duct as periodic charging and discharging occurs. The noise due to mechanical vibrations in exhaust pipe is known as shell noise [34]. Turbocharging noise also forms an important part of aerodynamic noise.

3.8 Bearing noise

Bearings present in the crankshaft as well as connecting rod have clearances that are likely to generate noise under action of external excitation forces as seen in figure no 3.2 [35]. One of the major sources of noise due to bearing effect is the rumbling noise which is due to engine torsional and bending resonance induced by clearances [36].

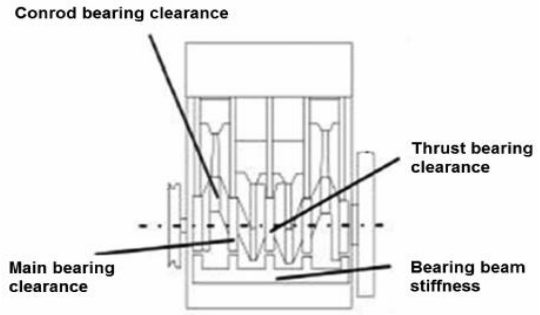

Figure no 3.2-Various bearing parameters effecting engine noise [35]

Methods to control bearing noise include optimization of clearances, application of optimal crank shaft damper and application of flexible flywheel design.

3.9 Timing belt and chain noise

Major factor effecting timing chain noise include meshing impact and polygon effect [37]. The meshing frequency of this noise depends on engine speed and number of meshing teeth as shown in figure no 3.3[35].

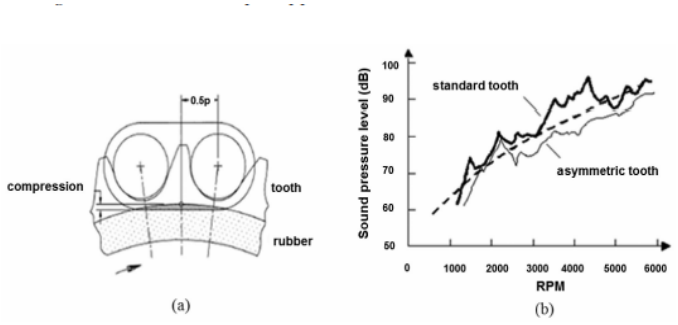

Figure no 3.3-Schematic representation of Timing chain and its noise spectra [35]

The polygon effect causes elevation and drop of chain element and leading to transverse and torsional vibrations of chain. The impacting speed of roller (W_A) and chain sprocket can be estimated in terms of its pitch (P_H), number of teeth (D), pressure angle (Λ) and number of sprocket teeth (Z) as [35]:

$$W_A=\frac{\pi N P_H}{3600} Sin(\frac{360}{Z}+\Lambda) \qquad (3.1)$$

The impact energy E_A can be estimated by linear density of chain (υ):

$$E_A= \frac{W_A{}^2 \upsilon P_H}{2000} \qquad (3.2)$$

Use of rubber rings in chain sprocket can help to reduce noise as depicted in figure no 3.3(a). Combustion engines also have transmission belts systems (figure no 3.4) which can exhibit number of modes of vibrations as seen from figure no 3.5.

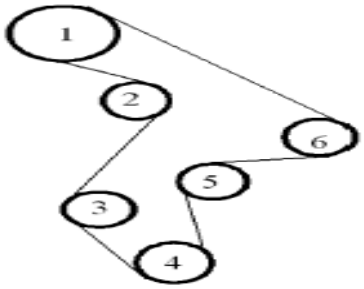

Figure no 3.4-Timing belt Transmission system (1: Sprocket,2: Tensioner,3: Fuel pump sprocket,4: Crankshaft sprocket,5: Idler sprocket,6: Water pump sprocket) [35]

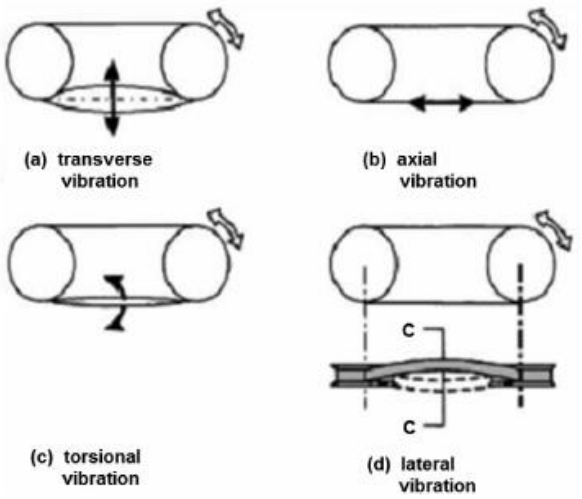

Figure no 3.5-Timing belt vibration sources [35]

Due to differences in the pitch of tooth belt and sprocket of timing belt, the meshing belt creates an impact which is a periodic excitation having frequency (f_s) given by:

$$f_S= \frac{ZD}{60} \qquad (3.3)$$

Typical spectrum of belt noise is seen from figure no 3.6 with dominance at lower and medium frequencies [38].

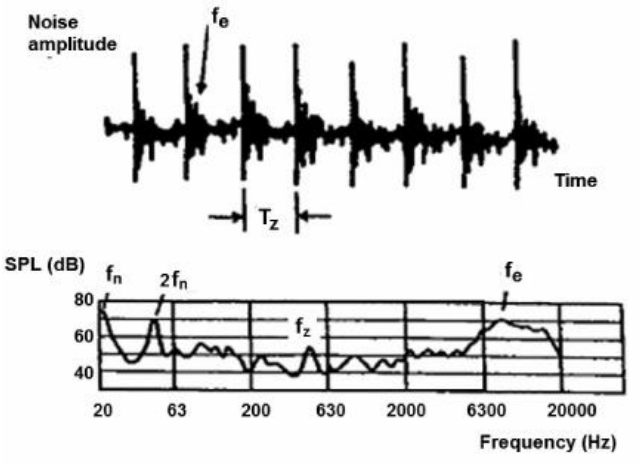

Figure no 3.6-Timing belt noise spectra [35]

3.10 Summary

Figure no 3.7 depicts generation mechanism for various sources of noise in an engine with plots of estimated contributions recorded at a distance of 1m from engine in an anechoic chamber featured in figure no 3.8.

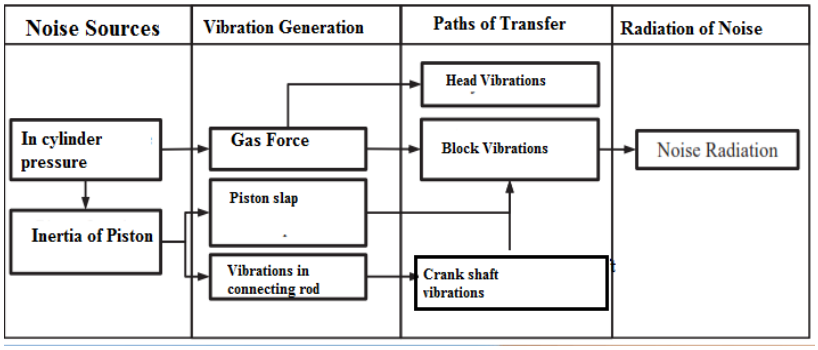

Figure no 3.7-Mechanism of noise generation [39]

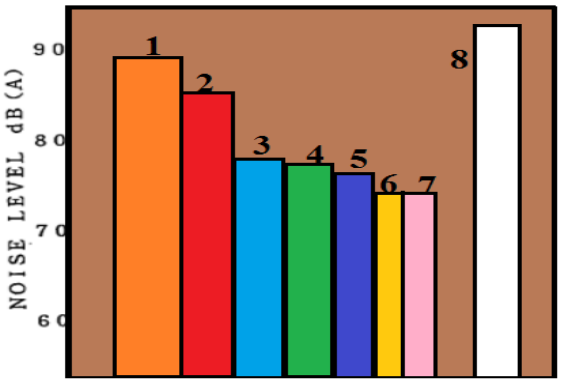

Figure no 3.8- The total noise contribution (8) can be decomposed into contributions due to combustion noise (1), contribution due to piston slap noise (2), contribution due to fan noise (3), contribution to gear operation noise (4), contribution due to pump operations (5), valve noise (6) and other sources (7) [26]

As evident from the above figures the combustion based noise and piston slapping noise have major contributing portions (about 80%), hence it is necessary to focus on these aspects of engine acoustics. These two features have been discussed in details in further parts of this work.

3.11. References

[1] Reinhart, T E., 1987, "An evaluation of the Lucas combustion noise meter on Cummins B series engines", SAE Technical Paper 870952.
[2] Reyes,M.,Melgar,A.,Perez,A., and Gimenez,B.,2015,"Study of the cycle-to-cycle variations of an internal combustion engine fuelled with natural gas/hydrogen blends from the diagnosis of combustion pressure", International Journal of Hydrogen Energy, Vol 38, no 35,pp.15477–15487.
[3]Han,Bin,S.,1997, " A study of cycle-to-cycle variations with dwell angle in spark ignition engines",Transactions of the Korean Society of Mechanical Engineers B, Vol 21, no 12,pp.1701-1709.
[4] Jung, I., Jin, J., So, H., and Nam, C., 2013,"An advanced method for developing combustion noise through the analysis of diesel combustion," SAE Technical Paper 2013-01-1901.
[5] Andersson,I.,McKelvey,T., Larsson,M.,2009, "Combustion parameters estimation and control using vibration signal : application to the diesel HCCI engine", Proceedings of the IEEE conference on decision and control.
[6] He, Z., Xie,W.,Zhang,G.,Hong,Z.,Zhang,J.,2014, "Piston dynamic characteristics analyses based on FEM method Part I: effected by piston skirt parameters ", Advances in Engineering Software, Vol 75,pp. 68–85.
[7] Dolatabadi et al,2015, "On identification of piston slap events in internal combustion engines using tribo dynamic analysis", Mechanical Systems and signal processing, Vol 58-59, pp 308-324.
[8] Mohd Ripin, Z., and Chong Tan,Y.,2013, "Analysis of piston secondary motion", Journal of Sound and Vibration, Vol 332,pp.5162–5176.
[9]Tung,V., and Crocker, M J., 1982, "Diesel engine noise and relationship to cylinder pressure", SAE Technical Paper 820237.
[10]Shu, G., Wei ,H., and Han, R., 2005, 'The transfer function of combustion noise in DI-diesel engine", SAE Technical Paper 2005-01-2486.
[11] AVL450 combustion noise meter, AVL manual, August 2000.
[12] Christen,U., Vantine,K., Chevalier,A.,Moraal,P.,and Scholl,D.,2006, "A wavelet based combustion noise meter , Proceedings of the 2006 IEEE International conference on control applications.
[13]Torregrosa, A J.,Broatch, A.,Martin, J., and Monelletta, L., 2007, "Combustion noise level assessment in direct injection diesel engines by means of in-cylinder pressure components", Measurement Science and Technology, Vol 18, no2,pp.2131–2142.
[14]Machado,G B., and De Melo, T C C ,2005, "Diesel cetane number versus noise emission ",SAE Technical Paper 2005-01-2150.
[15] Alt, N.,Sonntag,H., Heuer, S., and Thiele, R.,2005, "Diesel engine cold start noise improvement ", SAE Technical Paper 2005-01-2490.
[16]Blunsdon, C A.,Dent, J., and Das, S.,1995, "Modelling the origins of combustion noise in the indirect injection diesel engine ", SAE Technical Paper 952432.
[17] Luckhchoura, V.,Won, H.,Sharma, A.,Paczko, G.,and Peters, N.,2008, "Investigation of combustion noise development with variation in start of injection using 3-dimensional simulations by applying representative interactive flamelet (RIF) model ", SAE Technical Paper 2008-01-0950.
[18] Xin, Q.,2011, "Diesel engine system design", Cambridge university press, U.K., ISBN: 978-1-84569-715-0.
[19] Oetting, H.,Pundt, D.,and Ebbinghaus, W.,1984, "Friction in the piston group and new ideas for piston design", SAE Technical Paper 841299.
[20]Munro, R.,and Parker, A.,1975, "Transverse movement analysis and its influence on diesel piston design", SAE Technical Paper 750800.
[21]Ryan, J P.,Wong, V W.,Lyon, R H., Hoult, D P.,Sekiya, Y.,Kobayashi, Y.,and Aoyama, S.,1994, " Engine experiments on the effects of design and operational parameters on piston secondary motion and piston slap", SAE Technical Paper 940695.
[22] Suh, I-S., and Lyon ,R H., 1999, "An investigation of valve train noise for the sound quality of IC engines ",SAE Technical Paper 1999-01-1711.

[23] Anderton,D.,and Zheng, J H.,1993, "A new measurement method for separating airborne and structure borne sound from an IC engine's valve train mechanism ",SAE Technical Paper 931335.
[24] Savage,J.,and Matterazzo, J.,1993, "Application of design of experiments to determine the leading contributors to engine valve train noise", SAE Technical Paper 930884.
[25] Hanaoka,M., and Fukumura, S.,1973, "A study of valve train noises and a method of cam design to reduce the noises", SAE Technical Paper 730247.
[26]H.Kanda,M.Okubo,T.Yonezawa,1990, "Analysis of noise sources and their transfer paths in diesel engines ",SAE Technical Paper 900014.
[27] Spessert, B.,and Ponsa, R.,1990, "Investigation in the noise from main running gear, timing gears and injection pump of DI diesel engines ", SAE Technical Paper 900012.
[28]Zhao, H., and Reinhart, T E., 1999, " The influence of diesel engine architecture on noise levels ", SAE Technical Paper 1999-01-1747.
[29]Russell, M.F.,1972, " Reduction of noise emissions from diesel engine surfaces ", SAE Technical Paper 720135.
[30]Ochiai, K.,and Yokota, K.,1982, " Light-weight, quiet automotive DI diesel engine oriented design method ", SAE Technical Paper 820434
[31]Maetani, Y.,Niikura, T.,Suzuki, S.,Arai, S., and Okamura, H.,1993, " Analysis and reduction of engine front noise induced by the vibration of the crankshaft system", SAE Technical Paper 931336.
[32]Offner, G.,Priebsch, H H.,Ma, M T.,Karlsson, U.,Wikstrom, A.,and Loibnegger,B.,2004, "Quality and validation of crank train vibration predictions – effect of hydrodynamic journal bearing models ", Multi-Body Dynamics: Monitoring and Simulation Techniques-III, pp. 255–271.
[33]Silvestri, J., Morel, T., and Costello, M.,1994, " Study of intake system wave dynamics and acoustics by simulation and experiment ", SAE Technical Paper 940206.
[34]Pang ,J.,Kurrle, P.,Qatu, M.,Rebandt, R.,and Malkowski, R.,2003, "Attribute analysis and criteria for automotive exhaust systems ", SAE Technical Paper 2003-01-0221.
[35] Sheng, G.,2012, "Vehicle Noise Sound Vibration and Sound Quality", SAE international, Warrendale, Pennsylvania, USA,ISBN of 978-0-7680-3484-4.
[36] Qatu, M. S., Abdelhamid, M. K., Pang, J., and Sheng, G., 2009, " Overview of automotive noise and vibration", International Journal of Vehicle Noise and Vibrations, Vol. 5, no. 1/2, pp.1-35.
[37] Young, J. D., Marshek, K. M., Poiret C., and Chevee P.,2003, " Camshaft roller chain drive with reduced meshing impact noise levels ",SAE Technical Paper 2003-01-1666.
[38]Sheng, G., et al., 2006, "A new mechanism of belt slip dynamic instability and noise in automotive accessory belt drive systems ",International Journal of Vehicle Noise and Vibration, Vol 2, pp.30-33.
[39]Dolatabadi,N.,Littlefair,B.,DelaCruz,M.,Theodossiades,S.,Rothberg,S.,Rahnejat, H., 2015," A transient tribodynamic approach for the calculation of internal combustion engine piston slap noise", Journal of Sound and Vibration, Vol.352,pp.192–209.

Chapter 4
Combustion based noise

4.1 Introduction

Combustion noise generated mainly depends upon the rate of in cylinder pressure developed during ignition delay period. Overall design of combustion chamber as well as variations in various fuel injection parameters e.g. injection pressure, amount of fuel injected and its timings also play a crucial role in contributions of combustion noise emissions from engines [1]. Depending upon the type of engine as well as various operational parameters, overall noise emissions from a typical diesel engine may be in range 80dBA-110dBA [2, 3]. Split injection using electronic control unit (E.C.U.) may help to shorten the period of premixed phase of combustion and hence help to reduce the overall noise emissions by about 5dBA-8dBA [4]. Head and Wakes have shown that during transient operational conditions, overall noise levels are about 4-7dBA higher as compared to steady state operations [5]. Cold starting conditions may lead to higher ignition delay period which in turn causes increase in the premixed period of combustion [6]. Quality of fuel injected inside combustion chamber also affects the magnitude of combustion noise. It has been observed that a reduction of Cetane number of fuel from 50 to 40 causes a rise of up to 3 dBA in combustion based noise emissions [7]. For a naturally aspirated engine, the combustion based noise depends upon the quantity of fuel that mixes with air charge during the course of delay period and hence the compression ratio of engines also plays a vital role [7]. In case of gasoline engines, the delay period is longer due to lower compression ratio which may lead to lower temperature of charge and hence more noise emissions [7].

4.2 Background of combustion process in diesel engines

Diesel engines may be further classified into following two major types:

1. Direct injection (D.I.) engines
2. Indirect injection (I.D.I.) engines

In case of D.I. engines, the fuel is directly injected inside combustion chamber and as a consequence of it, lesser time is available for formation of fuel and air mixture. Hence a heterogeneous mixture consisting of both rich as well as lean parts is formed inside the chamber.

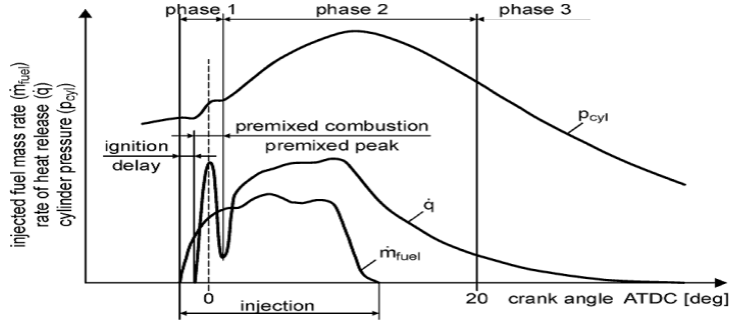

Figure no 4.1- Various phases of Diesel engine combustion [8]

Figure no 4.1 shows various phases of combustion as observed during course of operation of a typical diesel engine. The injection of fuel inside combustion chamber begins a few degrees before TDC position depending on the various injection conditions of engine. As soon as the cold jet of fuel penetrates the chamber, it mixes up with hot compressed air already present inside. The droplets thus formed vaporize, forming layers of fuel-air mixture around the periphery of jet. As the temperature rises to about 750K, the first break down of Cetane fuel takes place. Further propagation of various chemical reactions produces C_2H_2, C_3H_3, C_2H_4, CO_2 as well as water vapors [9].

Resulting rise in temperatures causes a complete combustion of fuel-air mixture formed. This sudden period of combustion further leads to rise in the heat release rate as well as high pressure gradient($\frac{dP}{d\theta}$). This further enhances temperatures in the pre-mixed zone leading to conditions favourable for production of NO_x. As, the premixed phase consumes all mixture formed, oxygen available for combustion is consumed around the inner regions wherein the temperatures in ranges of 1600-1700K are reached [8]. Now various partial burnt particles diffuse towards outer layers and begin to burn within a thin region of reaction formed around the periphery of spray which leads to formation of a diffusion flame.

This phase of combustion is known as diffusion controlled combustion and is depicted by region 2 and 3 in figure no 4.1. High temperatures along with lack of oxygen provides an ideal condition for the formation of soot.

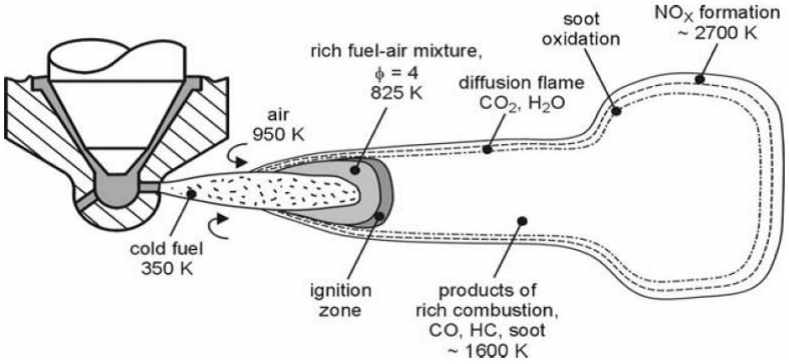

Figure no 4.2-Conventional diesel engine spray formation [8]

The diffusion flame thus formed then uses rest of oxygen available from surrounding environment resulting in high temperatures of order 2700K which consumes all the soot formed. At outer zone of flame there is enough oxygen content for formation of NO_x as shown in figure no 4.2.

Figure no 4.3 shows the rate of soot formation as a function of crank angle. Most of soot that is formed during earlier stages is later consumed and hence final exhaust emissions may have only a fraction of initial soot emissions. As seen from figure no 4.1, the diffusion controlled combustion can be divided into further three phases. During the second phase, the burning rate is dependent on rate of mixing of fuel fragments formed and air, and hence rate of reaction is faster. During the third phase, oxidation of remaining unburnt particles and soot takes place, however due to decreased temperature of end gas formed during the expansion stroke as well as lesser oxygen content available, slower reaction rates are observed.

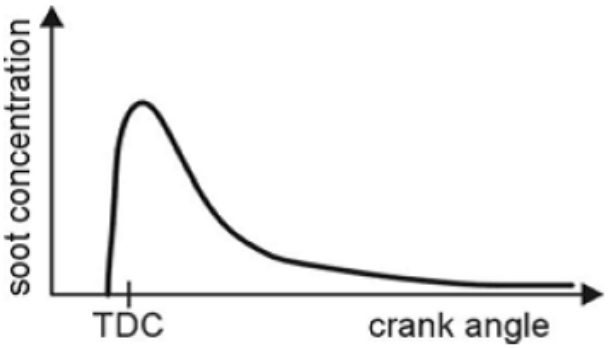

Figure no 4.3-Rate of soot formation [8]

Process of NO_X and soot formation in combustion engines shows an opposite trend as shown in figure no 4.4. In order to reduce the NO_x formation rate, it is necessary that local temperatures must not rise beyond 2000K [8]. A possible way to do so is to inject fuel late inside combustion chamber which further shifts the combustion phase towards expansion phase resulting in significant reduction of chamber temperatures. However, rate of consumption of fuel and soot formation increases due to late combustion.

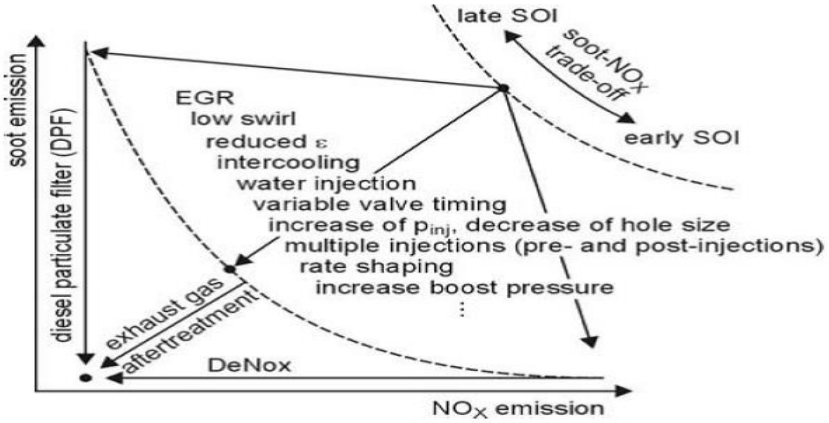

Figure no 4.4-Soot & NOx trade off [8]

Hence modern systems utilize multiple injection strategies in order to control both NO_x as well as soot formation rate [8, 9, 10, 11].

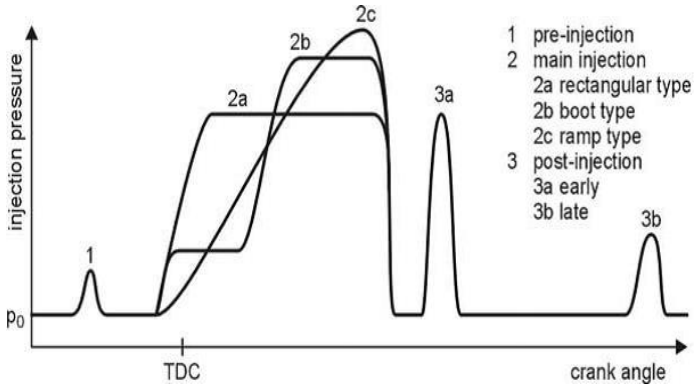

Figure no 4.5-Multiple injection process adopted for modern diesel engines [8]

There injection of fuel is carried out in three phases, namely pre-injection period, main-injection period & post injection period. There is a delay period between instant at which fuel is injected inside the combustion chamber and actual start of ignition process. Greater this delay period, more is the temperature achieved during course of combustion and hence better conditions exist for NOx formation. In order to shorten this delay period, a small amount of fuel is pre-injected before main injection takes place during the phase of pre-mixed combustion. It is advantageous to vary the injected fuel mass with time in order to reduce the specific consumption of fuel. This is achieved by rate shaping as seen in figure no 4.5. Rate shaping curve may be rectangular, step or boot type in shape. Torque and power produced in engine mainly depends on the duration of main injection period. Post-injection of fuel is done in order to reduce the soot emissions and in some cases may be useful for exhaust gas recirculation treatment [12]. It has been reported that post injection may reduce the rate of soot formation by about 70% without increasing the fuel consumption [13].

4.3 Combustion phase analysis

A) Introduction

Combustion process monitoring and analysis is an important aspect in NVH analysis of diesel engines, as a major portion of noise is attributed due to combustion process. Previous works have shown that engine block vibrations are also sensitive towards changes in fuel injection parameters [14]. Block accelerometer signals have been able to locate various important features of combustion process in diesel engines [14, 15]. Data from microphones located at a suitable distance from engine also provides an important information about performance of engines, however there is a major risk of contamination of these signals [16-19].

The main aim of present part of work is to investigate relationship between in cylinder pressure development and subsequent engine block vibrations. For this purpose, the test engine was operated under speeds of 2000RPM & 3000 RPM under 80% &100% load conditions with an aim to cover complete range of various operational conditions. The data was recorded during each test under steady state conditions as presented in Table no 4.1, 4.2.

B) Results and discussions

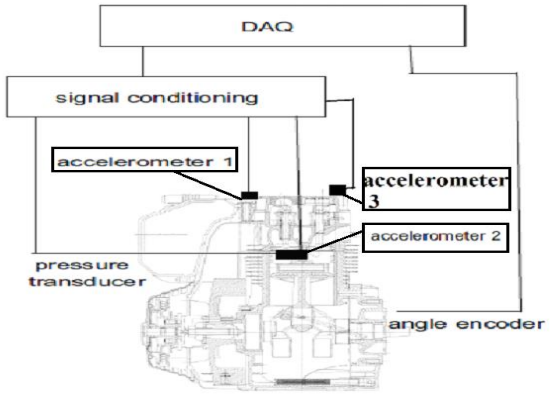

Figure no 4.6-Arrangement of various transducers

During the first step of activity, accelerometers were mounted on the test engine at three different locations (marked as accelerometer 1, accelerometer 2 and accelerometer 3) with an aim to select a suitable location which can best diagnose the combustion process as shown in figure no 4.6. The aim was to select a location that was most sensitive towards combustion process and least sensitive towards other sources of noise like valve operational noise, flow noise, pump noise etc. [11]. More detailed analysis has been discussed in [12, 13].

Case	P_{rail} (Bar)	Load	RPM
1	716	80%	2000
2	692	100%	2000
3	-	Motored	3000
4	814	80%	3000
5	612	100%	3000

Table no 4.1-Testing conditions

Case	SOI $_{main}$ (°BTDC)	SOI $_{pre}$ (°BTDC)	Q $_{main}$ (mm^3/stroke)	Q $_{pre}$ (mm^3/stroke)
1	6.2°	19.3°	15.4	1
2	8°	20°	16.7	1
3	-	-	-	-
4	9°	18.4°	17.8	1
5	5.5°	22.2°	14.6	1

Table no 4.2-Fuel injection specifications

Further, frequency analysis of signals was done with an aim to explore existence of common features between in cylinder pressure development and resulting block vibration signals as depicted in figures 4.7-4.11. The low frequency contents of in cylinder spectrum are related to compression curve, whereas the higher order harmonics are due to rate of in cylinder pressure rise during combustion process. The motored spectrum of vibration serves as a baseline for evaluation of combustion process for other signals as it constitutes contributions only due to mechanical events.

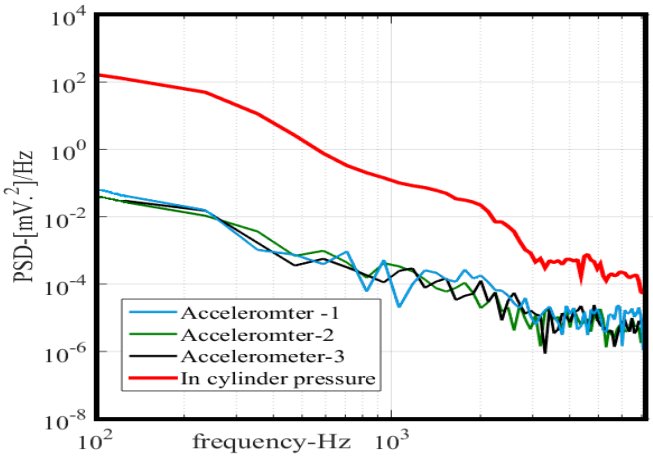

Figure no 4.7- PSD plots-(Case1)

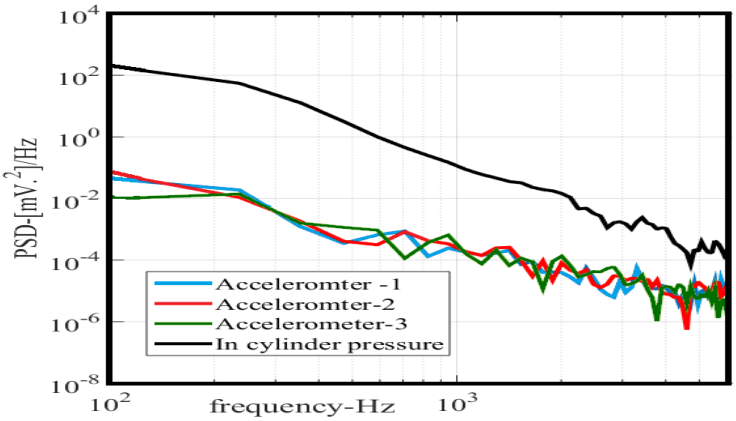

Figure no 4.8- PSD plots-(Case 2)

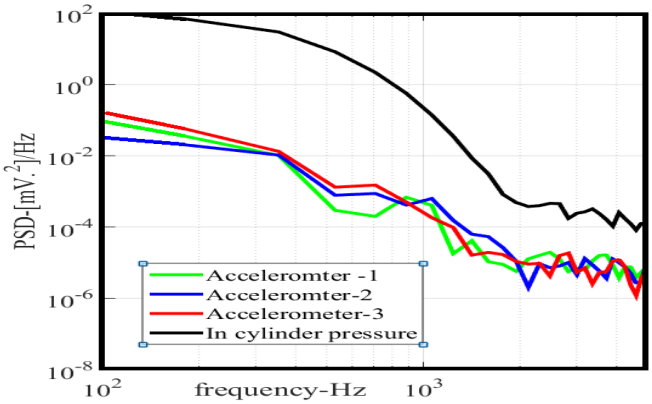

Figure no -4.9 PSD plots-(Case 3)

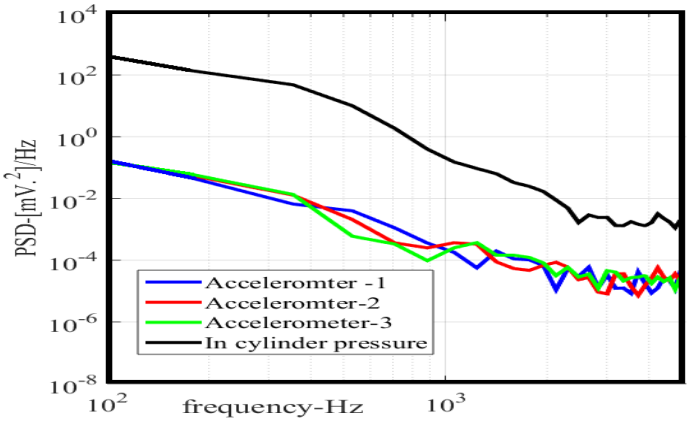

Figure no -4.10 PSD plots-(Case 4)

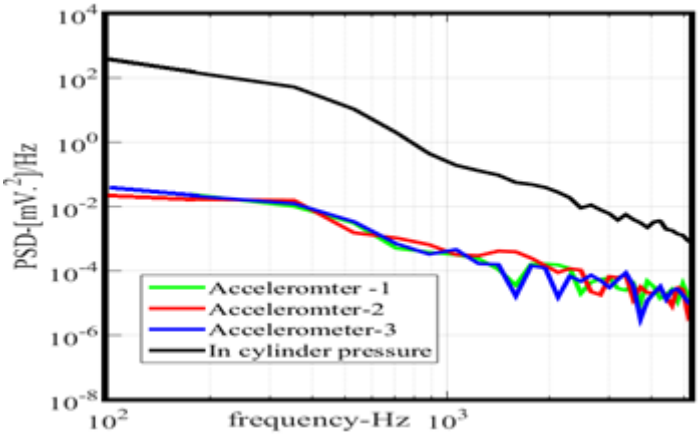

Figure no 4.11- PSD plots-(Case 5)

The cylinder pressure signals showed peak values in 100Hz-1.3kHz range which are may be attributed to combustion process. The engine block attenuation curves have high values at low frequencies which decays to minima and then rise again. Hence, energy levels of block vibrations have lower values. It can be seen that no significant difference in plots occurred as far as load variations were considered.

Further, coherence functions $C_{p,a}(f)$ between accelerometer data and in cylinder pressure development were plotted in order to investigate relationship as shown in figure no 4.12-4.16. This function is defined as ratio of cross PSD between in-cylinder pressure block vibration signals ($P_{p,\ a}$) to product of auto PSD of in cylinder pressure developed ($P_{p,\ p}$) and auto PSD of block vibration signals ($P_{a,\ a}$). The coherence functions were obtained by considering the accelerometer in vertical position (as depicted by accelerometer at position no 2) and horizontal positions (as depicted by accelerometer at position no 1, 3). This function was computed on basis of 30 cycles averaging with an aim to get accurate ranges in which the random data was attenuated using a Hamming window of length $1/6^{th}$ of an engine cycle. The plots show that the accelerometer signals acquired in horizontal positions were less coherent towards in cylinder pressure development as compared with those acquired at vertical position. This may be due to corruption of horizontal signals by other sources of noise like piston slap.

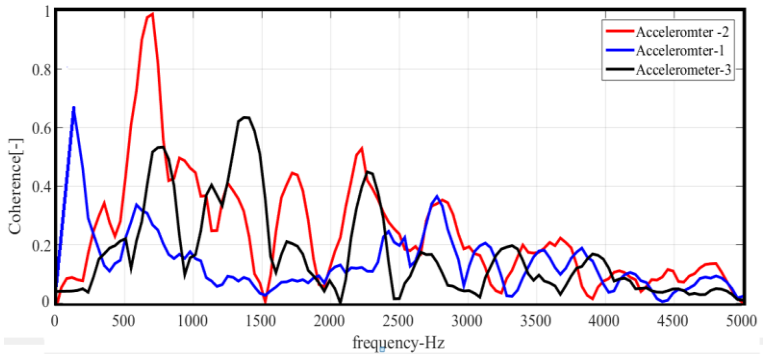

Figure no 4.12 -Coherence plots-(Case 1)

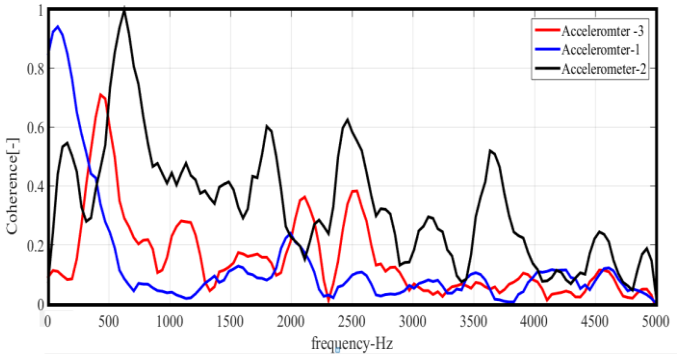

Figure no 4.13- Coherence plots-(Case 2)

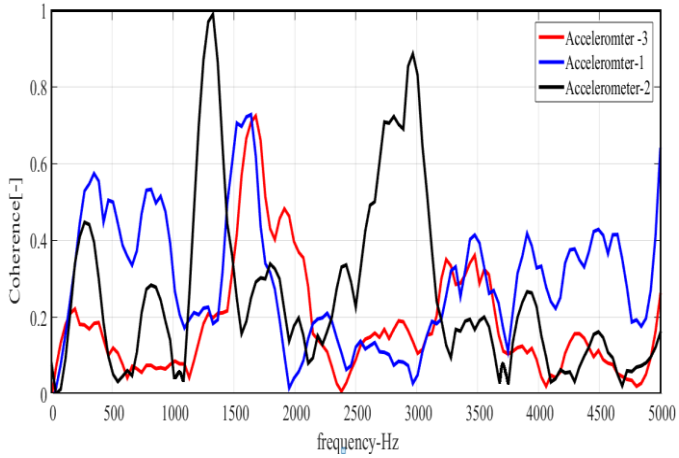

Figure no 4.14- Coherence plots-(Case 3)

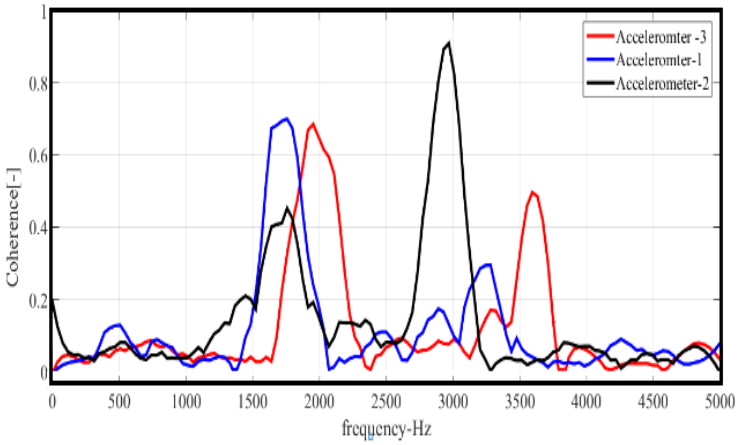

Figure no 4.15- Coherence plots-(Case 4)

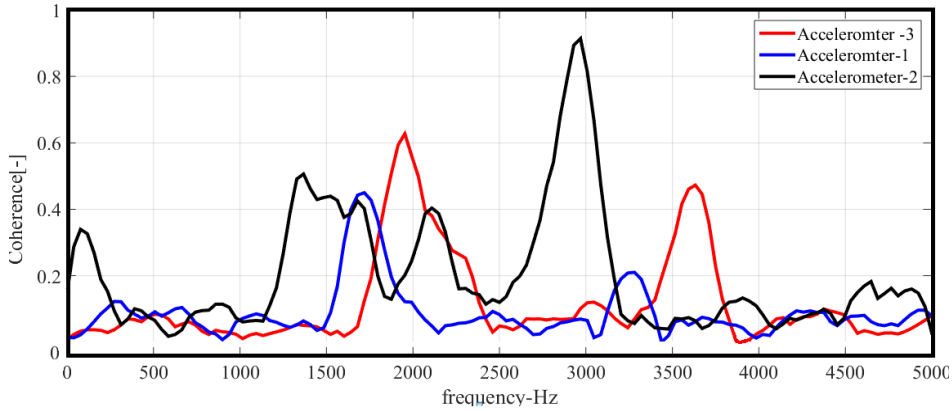

Figure no 4.16-Coherence plots-(Case 5)

From the plots it is clear that engine fundamental firing frequency and its integral multiples show a high values of coherence close to unity. This implies that harmonics of this frequency propagate through engine block and were recorded by accelerometers in both orientations. Regardless of locations of accelerometers and other operational conditions, higher values of coherence function were observed in a common frequency range of 0.5kHz-3.8kHz. This indicates that a strong relationship between the spectral components of in cylinder pressure and resulting block vibrations in this range. Table no 4.3 shows various values of coherence function in the above mentioned frequency range.

Case	Accelerometer position	Minima	Maxima
1	1	0.05	0.65
	2	0.001	0.98
	3	0.001	0.64
2	1	0.07	0.9
	2	0.19	0.99
	3	0.01	0.98
3	1	0.045	0.76
	2	0.050	0.99
	3	0.003	0.78
4	1	0.025	0.7
	2	0.04	0.89
	3	0.03	0.7
5	1	0.05	0.45
	2	0.065	0.89
	3	0.05	0.63

Table no 4.3-Coherence values

However, higher values of Coherence function do not mean that selected frequency band is dominated by combustion process. Hence, analysis was carried out by filtering the vertical accelerometer signals in frequency range dominated by combustion process so as to isolate various harmonic components useful for identification of various combustion parameters. Figures no 4.17-4.21 shows plots related to combustion pressure for various testing conditions in case of a single cylinder of engine and filtered vertical accelerometer signals. Higher pressure rise rate due to initial mixing of fuel and air contributes towards engine block vibrations. The accelerometer signals were found to be sensitive towards initial rapid rise of pressure gradient irrespective of fuel injection parameters. Contributions of motion based towards the vibration signature was less visible due to development of combustion process.

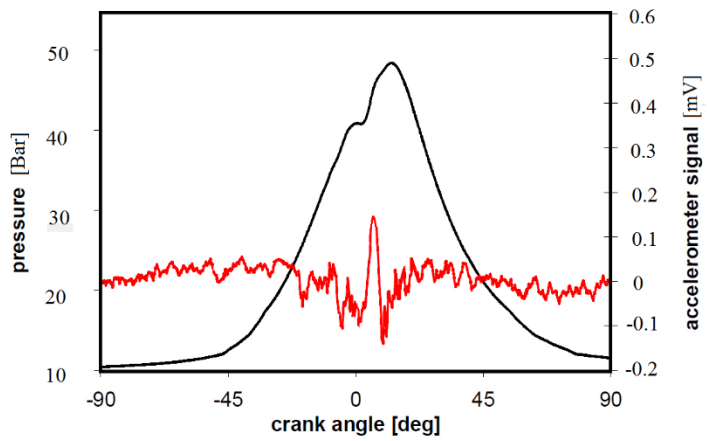

Figure no 4.17 -In cylinder pressure [----] and accelerometer signals[--------]-(Case1)

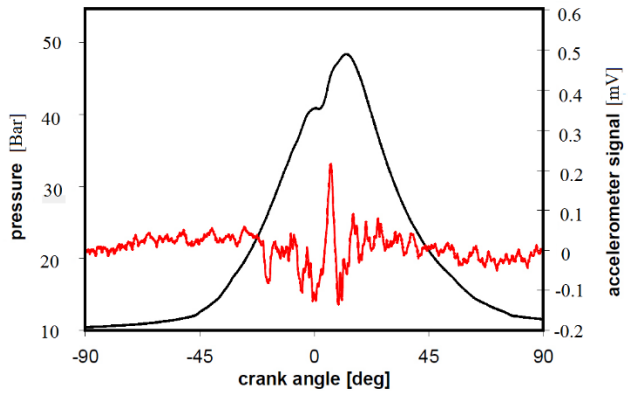

Figure no 4.18-In cylinder pressure [----] and accelerometer signals[--------]-(Case2)

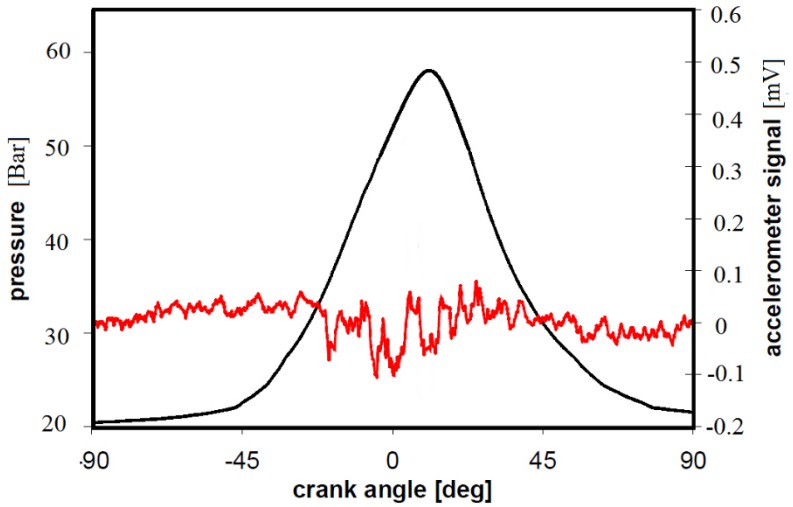

Figure no 4.19 -In cylinder pressure [----] and accelerometer signals[--------]-(Case3)

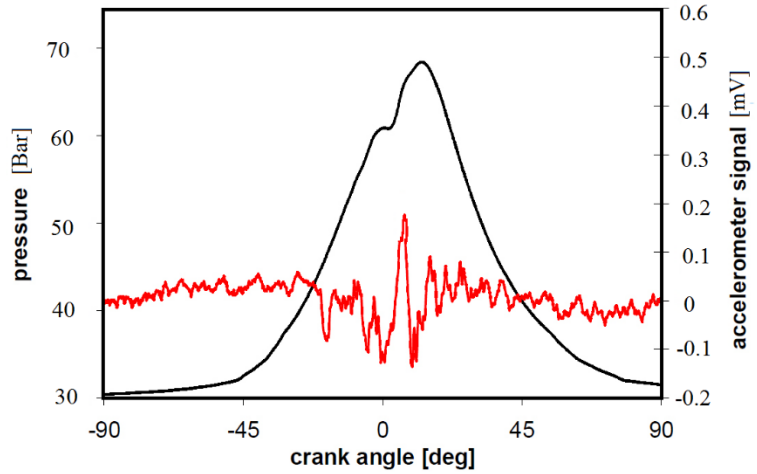

Figure no 4.20 -In cylinder pressure [----] and accelerometer signals[-------]-(Case4)

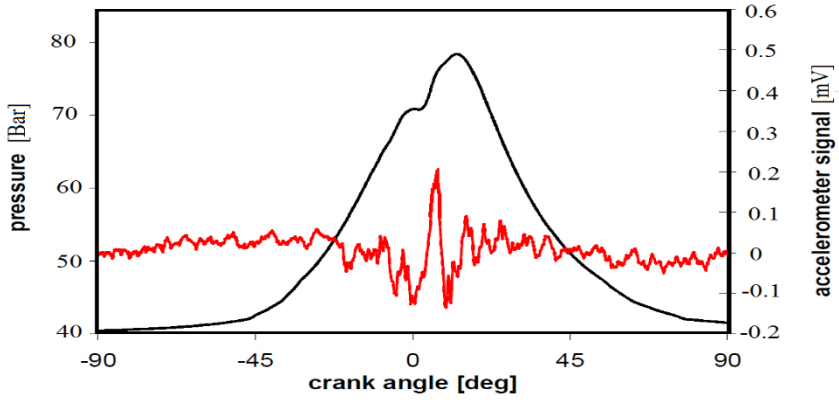

Figure no 4.21 -In cylinder pressure [----] and accelerometer signals[-------]-(Case5)

Aimed at further analysis the normalized values of filtered accelerometer signals were superimposed with corresponding non filtered in-cylinder pressure curves as depicted in figure no 4.22-4.26 in order to detect the crank angles in which premixed and diffusion phases of combustion were predominant. Normalization was done by division with corresponding maximum values.

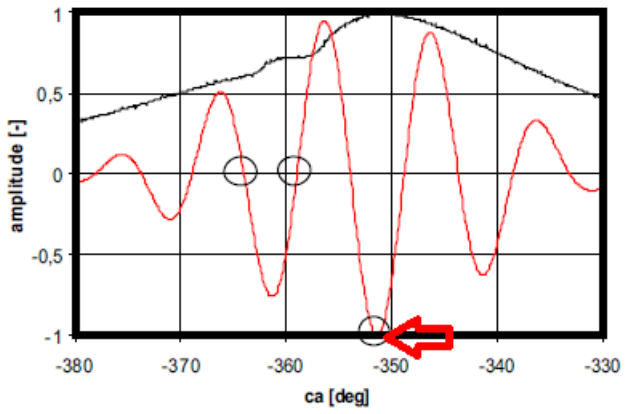

Figure no 4.22- In cylinder pressure plots [------], Filtered Accelerometer 2 signal[-----]-(Case1)

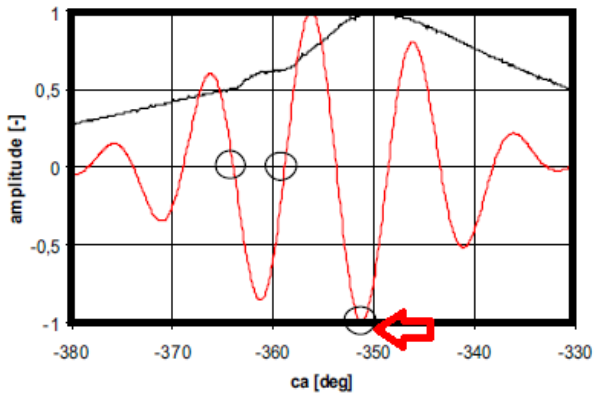

Figure no 4.23- In cylinder pressure plots [-------], Filtered Accelerometer 2 signal[-----]-(Case2)

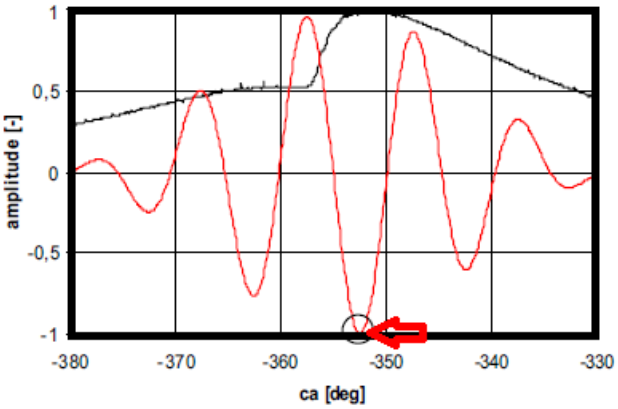

Figure no 4.24- In cylinder pressure plots [-------], Filtered Accelerometer 2 signal[-----]-(Case3)

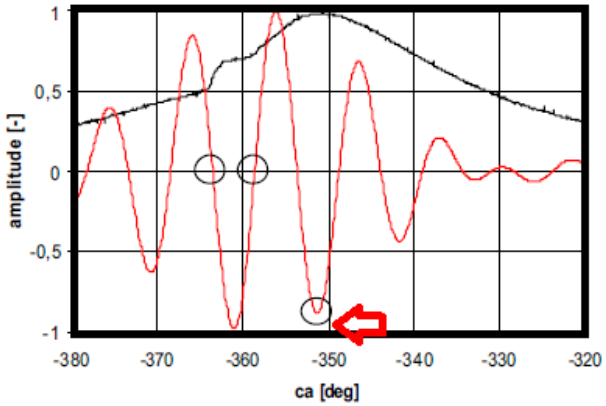

Figure no 4.25 -In cylinder pressure plots [---------], Filtered Accelerometer 2 signal[-----]- (Case 4)

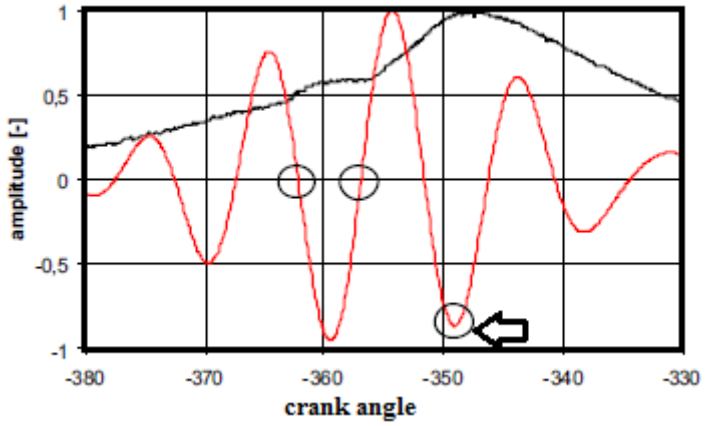

Figure no 4.26- In Cylinder Pressure plots [---------], Filtered accelerometer 2 signal [-----] -(Case 5)

It has been previously demonstrated that accelerometer data was able to locate the start of the combustion process [17]. Moreover, the vibration traces allow to detect the crank angles in which the diffusive phase dominates over the pre-mixed one. In the above figures circles have been used to indicate in vibration data the crank angles where onset of various phases of combustion takes place. The first one which is marked by vibration curve crossing zero value with a simultaneous sudden rise of in cylinder pressure denoting the start of pre-mixed phase of combustion [11]. The diffusive phase of combustion begins with the end of the negative oscillations in the vibration data corresponding to vibration values crossing the next zero markings [16]. Further circled arrows were used to indicate in filtered accelerometer data the crank angle positions corresponding to minimum value following the maximum one [17]. Regarding motored case when no fuel injection takes place ,only crank angle corresponding to minimum value of filtered acceleration signal has been marked. The results showed minimum sensitivity towards variations in fuel injection timings and amount of fuel injected. The crank angles corresponding to the minima of filtered vibration data (as denoted by circled arrows) and maxima of in cylinder pressure data were thus calculated. A coefficient of proportionality which is defined by the ratio of these values is seen in table no 4.4.

Case	Proportionality coefficient
1	0.985
2	0.99
3	0.99
4	0.99
5	0.98

Table no 4.4-Values of coefficient of proportionality

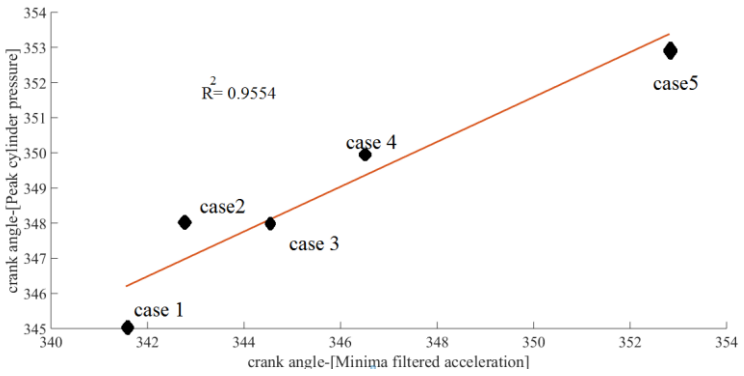

Figures 4.27-Correlation between normalized values, ------Interpolation line

Further nearly a straight line of interpolation between the above mentioned for crank angle positions shown in figure no 4.27 represents an almost linear correlation and is also indicative of higher values of coefficients of proportionality. This is due to frequency analysis of signals, which retains the components in the accelerometer signal mainly dominated by the combustion process [16]. More information can be extracted if further analysis of in cylinder pressure derivatives is done. Hence values of pressure derivatives were compared with that of filtered vertical block vibration signals as seen from figures 4.28-4.32. Similarity between these signals can be explained by assuming that vibrations that move through engine block are due to impulsive forces caused due to pressure gradient. So it can be concluded that these signals are sensitive towards variations in pressure gradient.

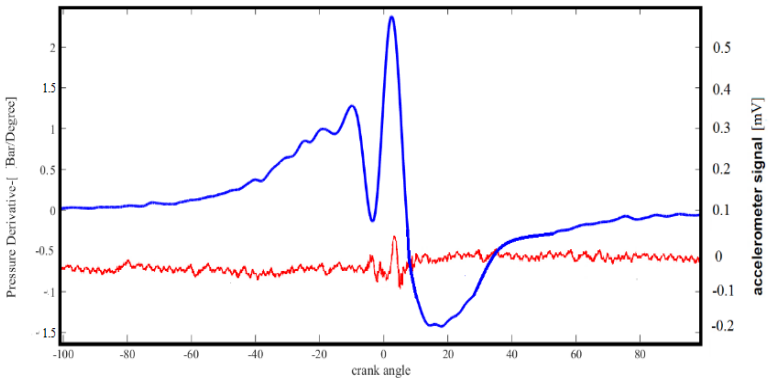

Figure no 4.28 - Pressure derivative **[----]**, Filtered accelerometer [----]- Case 1

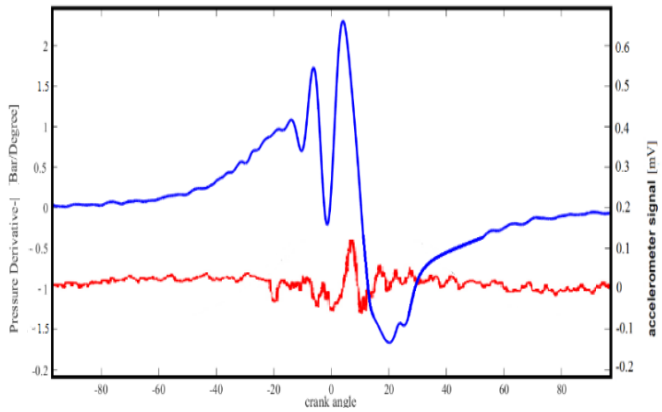

Figure no 4.28 - Pressure derivative **[----]** , Filtered accelerometer [----]- Case 2

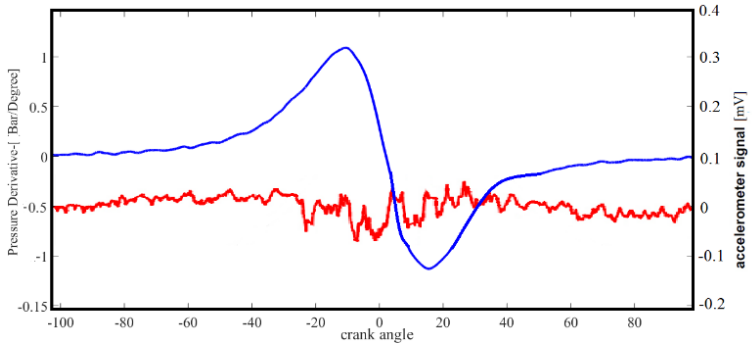

Figure no 4.30- Figure no 4.28 - Pressure derivative [----] , Filtered accelerometer [----]- Case 3

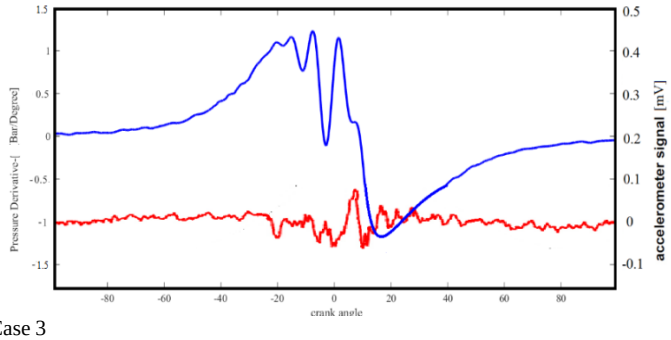

Figure no 4.31- Figure no 4.28 - Pressure derivative [----] , Filtered accelerometer [----]- Case 4

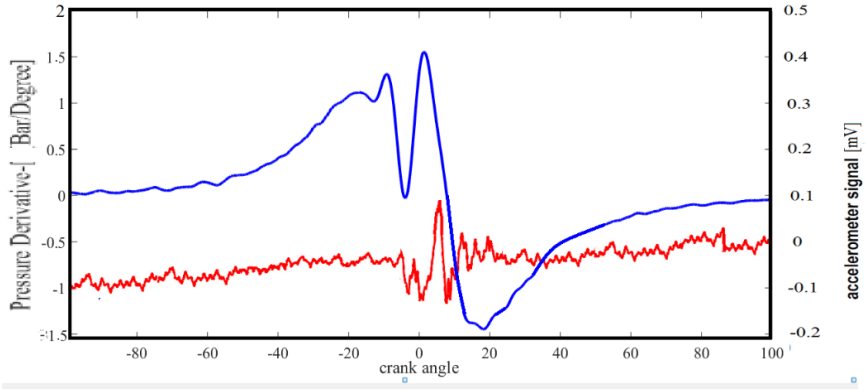

Figure no 4.32- Figure no 4.28 - Pressure derivative [----], Filtered accelerometer [----]- Case 5

It can be observed that there is a time delay between two curves crossing zero mark due to propagation time of vibration signals through the engine block. This delay can be compensated by retarding the injection period. Once in cylinder pressure data was analyzed, further analysis of rate of heat release rate (ROHR) was done which is given by [16]:

$$\frac{dQ}{d\theta}(ROHR) = V\frac{1}{\gamma - 1}\frac{dP}{d\theta} + P\frac{\gamma}{\gamma - 1}\frac{dV}{d\theta} \qquad (4.1)$$

Where V denotes the in cylinder volume, P represents the cylinder pressure and γ is specific heat ratio.

The cumulative heat release rate (CHRR) is given by integration of equation no 4.2. Normalized values of filtered accelerometer in vertical position were superimposed with CHRR curves to observe any possible relationship for full load conditions. It can be seen from figure no 4.33-4.34 that the marked circles correspond to initial and main combustion period of engine cycle. The marked arrow which denotes the minimum value of filtered acceleration signals (which is related to peak in cylinder pressure) does not correspond to peak CHHR in crank angle domain. This point in accelerometer curve is of interest in the combustion process monitoring, as it is related to crank angle position at which about half of injected fuel is burnt (MFB50) [17].

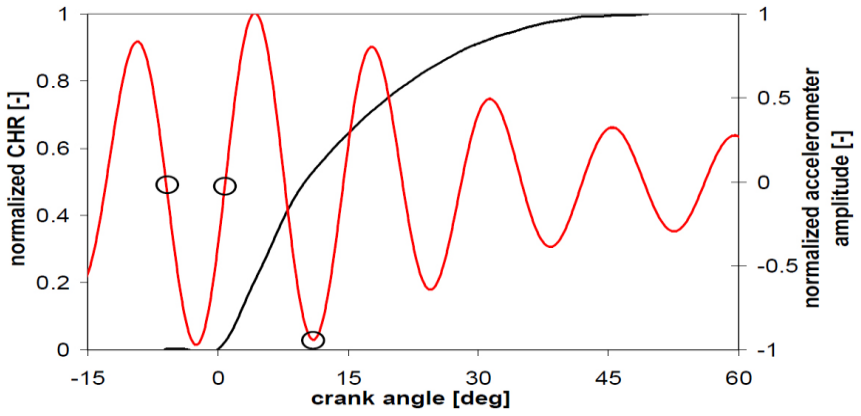

Figure no 4.33-CHHR [----] and Filtered accelerometer curve [----] -(Case2)

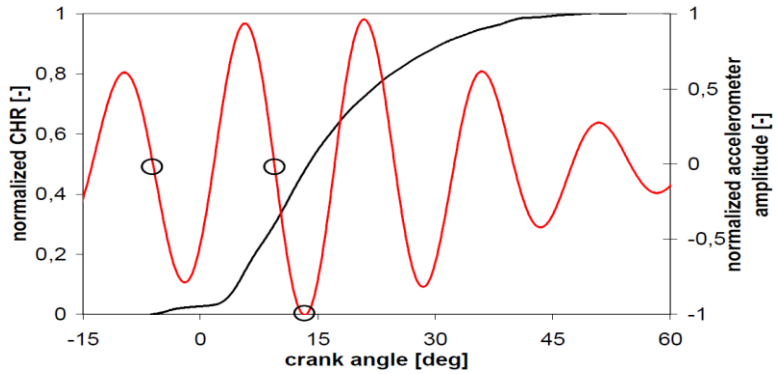

Figure no 4.34- Figure no 4.33-CHHR [----] and Filtered accelerometer curve [----]- (Case5)

Once a relevant frequency range was established, further time- frequency spectrogram analysis was performed in order to relate instantaneous frequencies with energies of in cylinder pressure and hence prove that the above mentioned frequency band was most sensitive towards combustion process development. Figure no 4.35-4.39 shows the time-frequency plots of in cylinder pressure signals in 3D surface (frequency, time, signal amplitude) as viewed from an angle which allows 2D display with third dimension in form of colored plots.

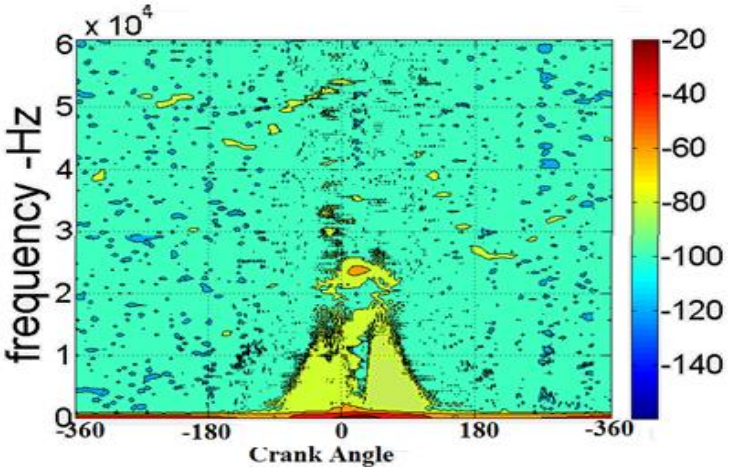

Figure no 4.35- In cylinder pressure time-frequency plots-(Case 1)

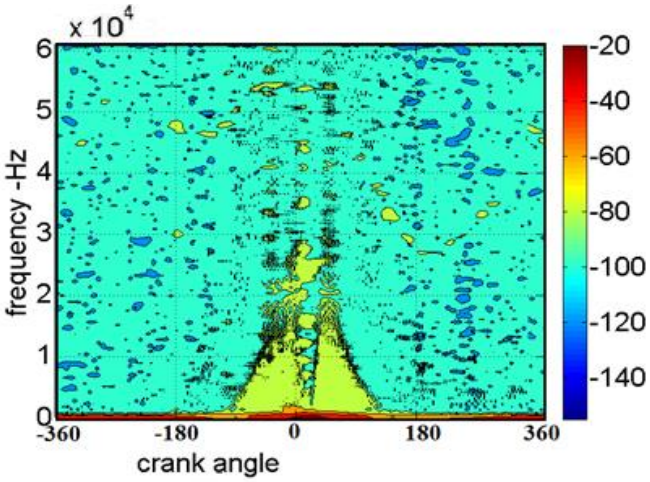

Figure no 4.36-In cylinder pressure time-frequency plots-(Case 2)

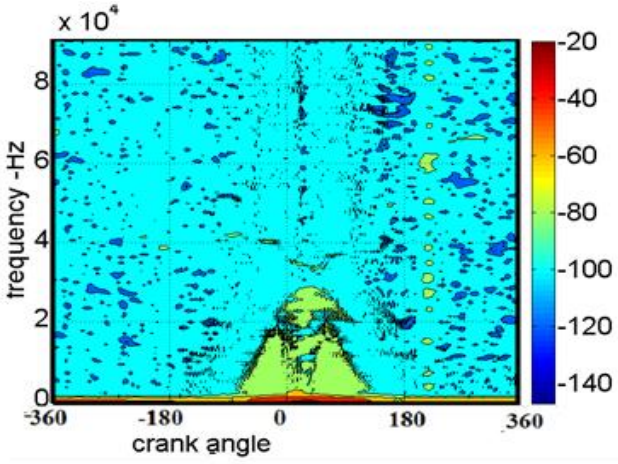

Figure no 4.37 -In cylinder pressure time-frequency plots-(Case 3)

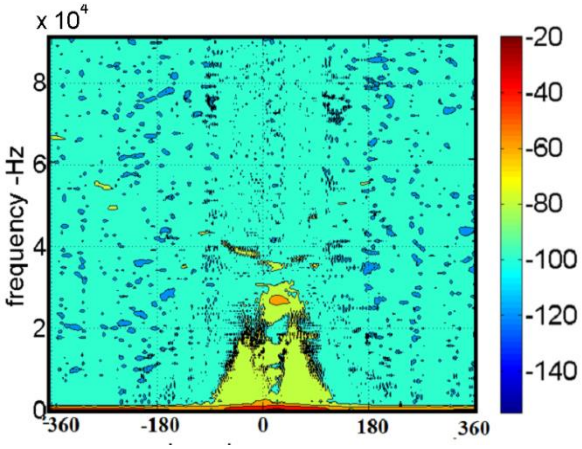

Figure no 4.38 -In cylinder pressure time-frequency plots-(Case 4)

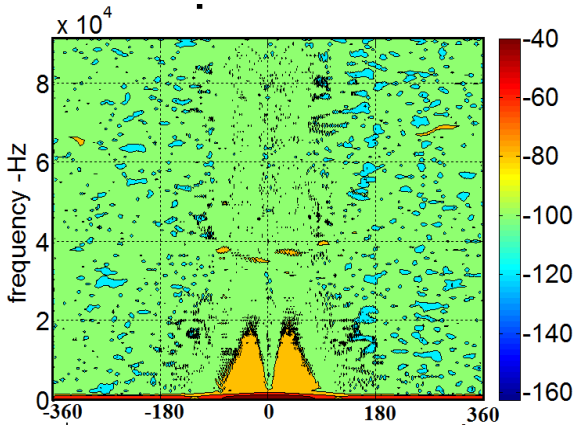

Figure no- 4.39 In cylinder pressure time-frequency plots-(Case 5)

These plots show frequency components belonging to the above mentioned range are characterized by higher amplitudes as combustion takes place. Further wavelet analysis of accelerometer signals mounted in vertical orientation was done as seen in figure no 4.40-4.44.

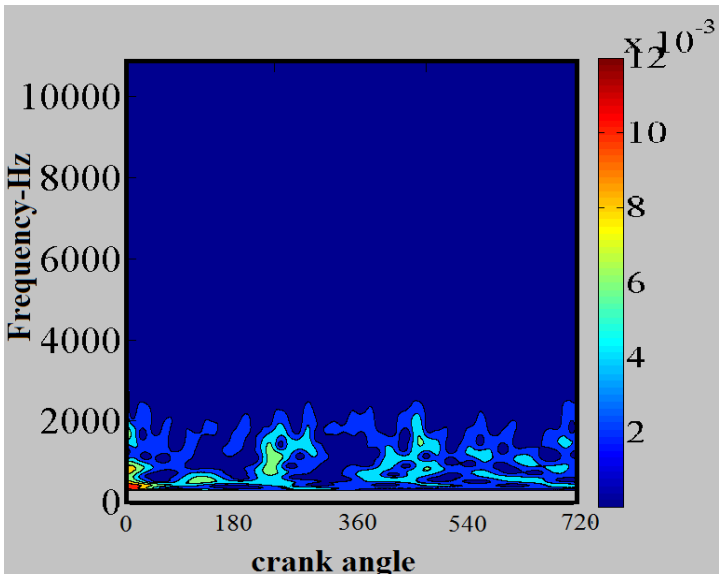

Figure no 4.40 -Time-frequency plots -Accelerometer 2 (Case1)

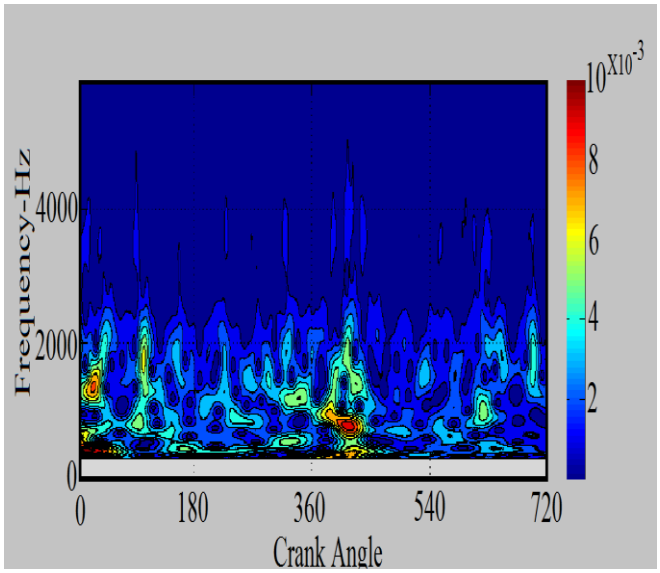

Figure no 4.41 -Time-frequency plots -Accelerometer 2(Case2)

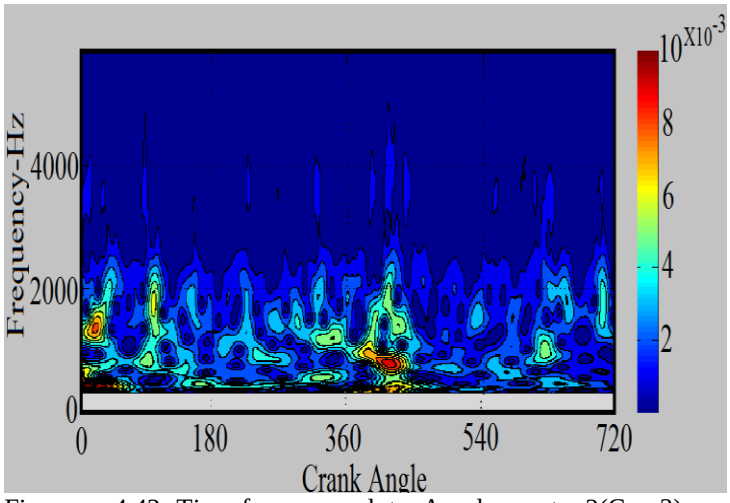

Figure no 4.42 -Time-frequency plots -Accelerometer 2(Case3)

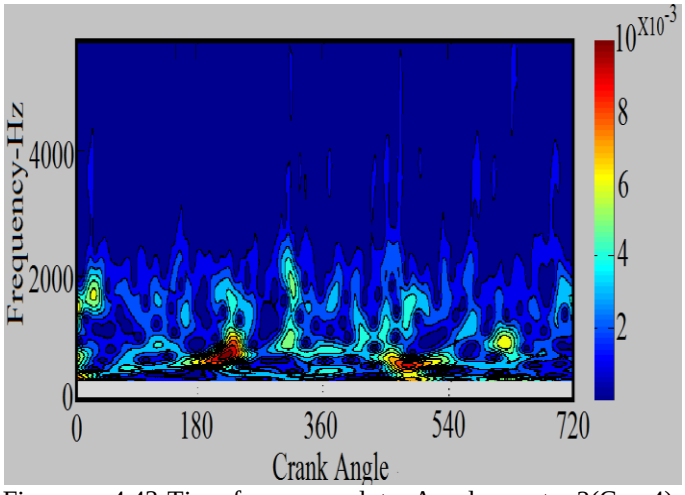

Figure no 4.43-Time-frequency plots -Accelerometer 2(Case4)

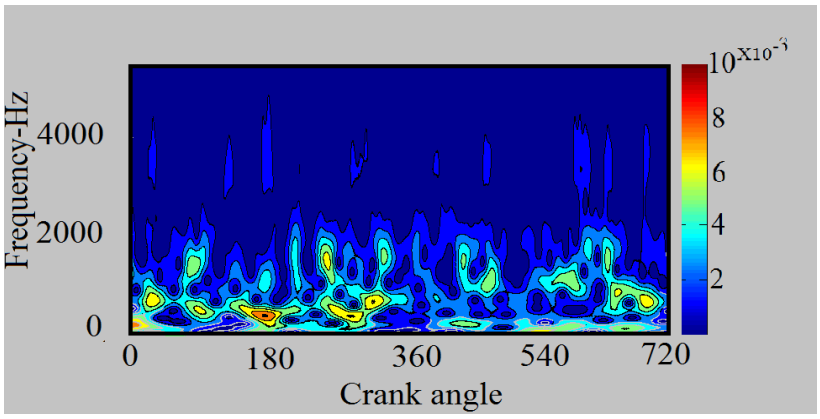

Figure no 4.44- Time-frequency plots -Accelerometer 2(Case 5)

These plots show that energy of block vibration signals is concentrated in 500Hz-4kHz range. Hence it can be concluded that energy of vibrations signals is located at higher frequency ranges as compared with in cylinder pressure signals. This is due to fact that these signals are propagated through engine block that acts as a kind of high pass filter.

4.4 Combustion based engine noise

This type of noise in engines originates from combustion taking place inside cylinders [18-21]. As fuel is injected inside the combustion chamber (where high pressure air is already present), part of ignitable gas starts to burn causing a rapid rise in pressure as well as temperatures inside the chamber. The pressure wave thus generated, strikes the walls of combustion chamber causing resonance of whole structure. Oscillations arising due to resonance have frequency (f_g) that can be estimated from engine bore diameter (D) & wave propagation speed (C_c) as:

$$f_g = \frac{C_c}{2D} \qquad (4.2)$$

These vibrations are next radiated in air through engine structure and are perceived as noise emissions. The intensity of combustion noise (I) is dependent on the values of maximum pressure value (P_{max}) and maximum value of pressure rise rate as [20]:

$$I\alpha[(\frac{dP}{dt})_{max} * P_{max}]^2 \qquad (4.3)$$

Further the analysis of spectrum plot of in cylinder pressure was done in figure no 4.45.

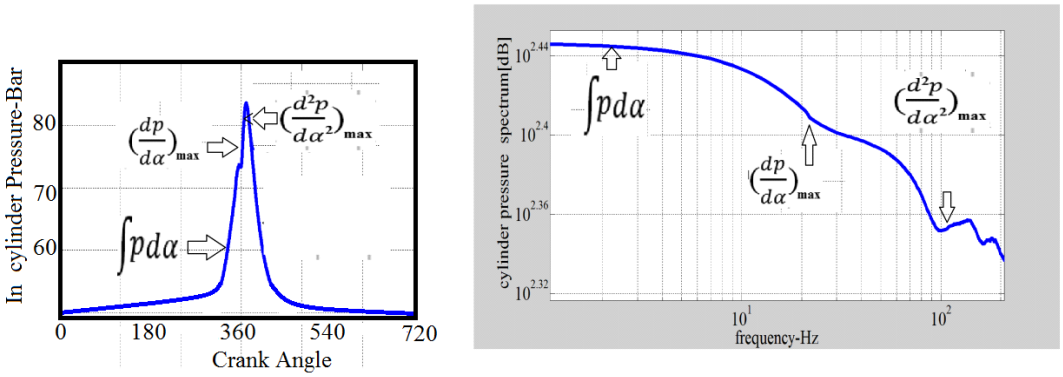

Figure no 4.45-Regions of combustion noise

The above plot is marked by following three distinct regions [20]:
a) Region 1 of low frequency ranges-in this region, the shape of curve depends upon peak cylinder pressure developed. Higher the maximum value of cylinder pressure, higher is the magnitude of peak in low frequency range.
b) Region 2 of medium frequency range-in this range the spectrum levels shows a logarithmic decrement with slopes depending on the rate of cylinder pressure rise. Larger values of pressure gradient causes steeper slopes.
c) Region 3 of higher frequency range –in this range rapid evolution of in cylinder pressure occurs due to onset of combustion process which results in high frequency vibrations of cylinder structure having amplitude dependent on second cylinder pressure derivative.

Figure no 4.46 shows the in cylinder pressure spectrum plot obtained by operating the test engine at 3600 RPM under full load condition with injection pressure maintained at 700 Bars. As observed from this figure region 3 of pressure spectrum begins around frequency of 2800Hz. In order to find the relevant frequency ranges corresponding to other regions, tests were further carried out by changing various injection parameters taking test case C as a base as reported in table no 4.6.

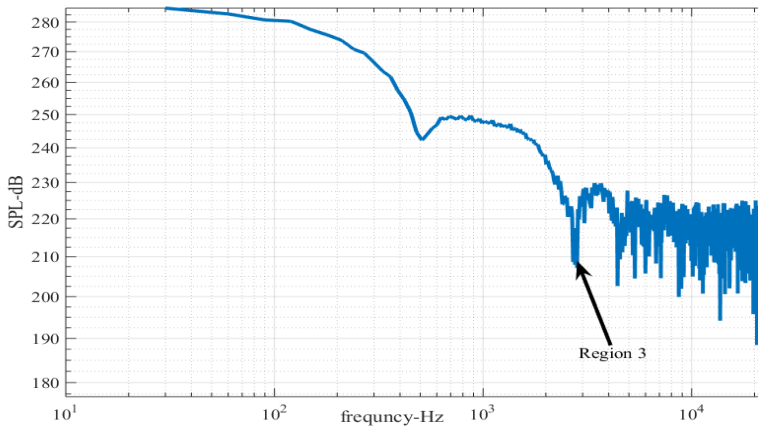

Figure no 4.46 -In cylinder pressure spectrum (3600RPM,100%Load)

Case	Parameter changed
A	Main injection timing retarded by 1º CAD
B	Injection pressure increased by 10 Bar
C, G	Base Case
D	Pre Injection Quantity of fuel increased by 1mm^3/stroke
E	Main injection timing retarded by 2º CAD
F	Injection pressure was reduced to 650 Bar
H	Speed reduced to 2000 RPM
I	Main injection timing retarded by 3º CAD
J	Main injection timing advanced by 3º CAD

Table no 4.6-Change in fuel injection parameters

Plots of in cylinder pressure and its spectrum were next analyzed from figure no 4.47-455. From these plots, it is clear that differences in the maximum value of in cylinder pressure levels were 5 Bars when the test cases denoted by A and B were compared and none for cases denoted by C and D.

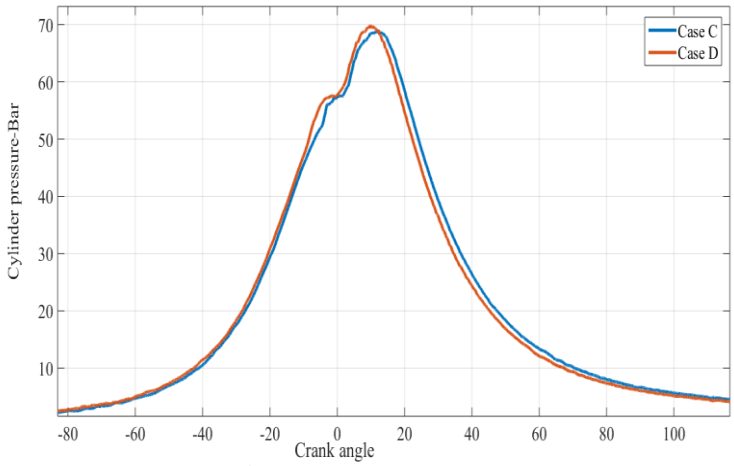

Figure no 4.47-Comparison of in cylinder pressure (Case C, Case D)

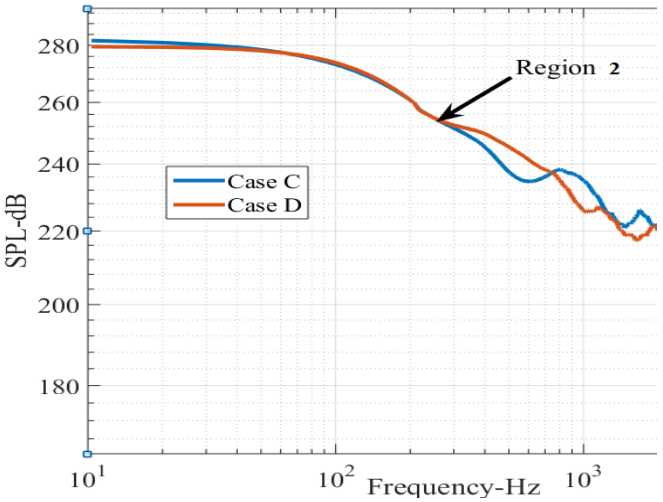

Figure no 4.48-Comparison of in cylinder pressure spectrum (Case C, Case D)

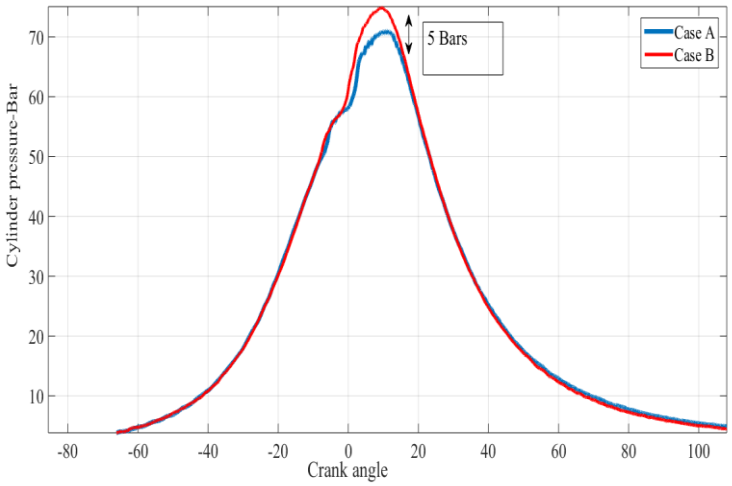

Figure no 4.49-Comparison of in cylinder pressure (Case A, Case B)

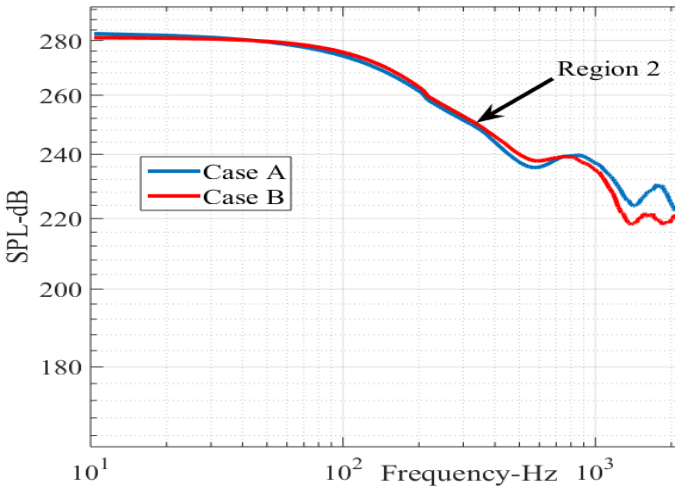

Figure no 4.50-Comparison of in cylinder pressure Spectrum (Case A, Case B)

Based on these plots it was observed that pressure spectrum for these testing conditions showed a similar trend in a common low frequency range of 10Hz-215Hz. Hence, this range denotes region 1 of pressure spectrum. By retarding the main injection timing by 2º CAD, the test case was denoted by condition E. Condition F denotes condition when injection pressure was reduced to 650 Bars. It is clear from figure no 4.51, 4.52 that engine noise for condition E is higher than condition F in spite of almost same peak pressure rise rates.

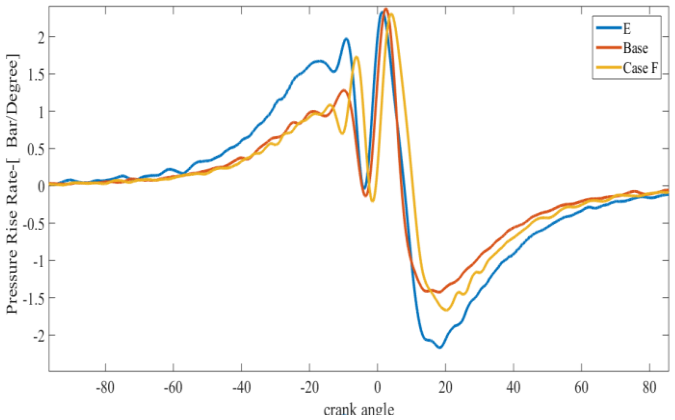

Figure no 4.51-Comparison of in cylinder pressure rise rate (Case E, Case F)

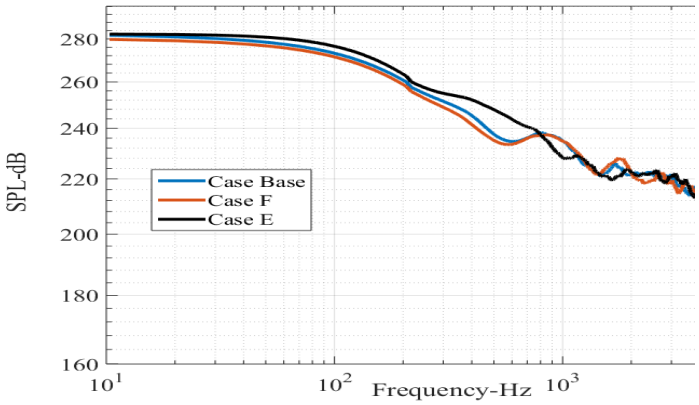

Figure no 4.52-Comparison of engine pressure spectrum (Case E, Case F)

Next engine noise levels and in cylinder pressure levels were analyzed for two other test cases marked by G and H. During these cases the injection pressure was kept same at 700 Bars, but speeds of engine were 3600 RPM and 2000 RPM respectively.

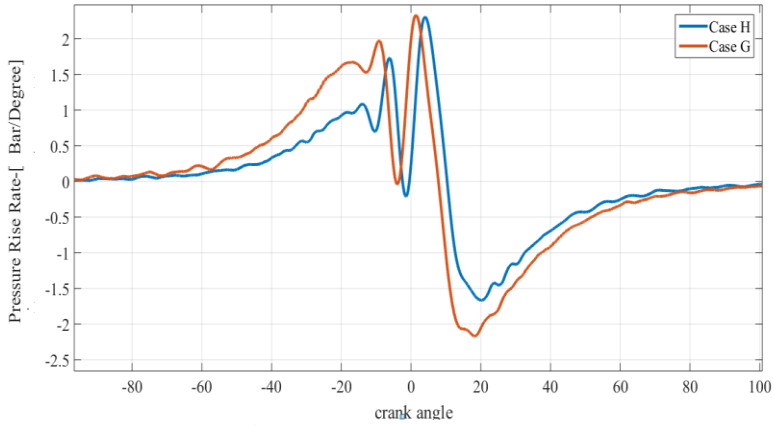

Figure no 4.53-Comparison of in cylinder pressure rise rate (Case G, Case H)

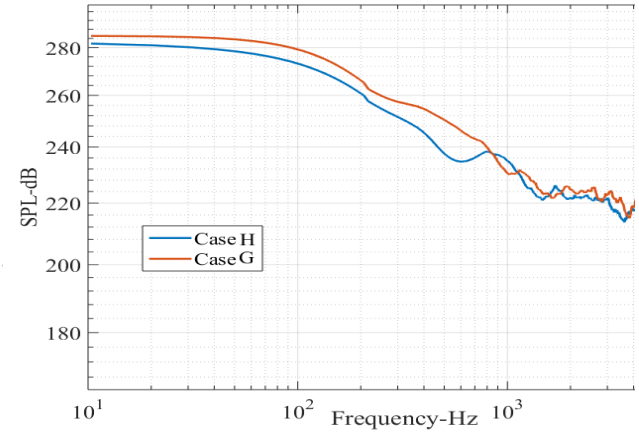

Figure no 4.54-Comparison of engine pressure spectrum(Case G, Case H)

It is clear from figure no 4.53,4.54 that even though peak pressure rise rates are almost equal, the noise emitted during case H was lower as compared to case G. Hence it can be concluded that pressure rise rates have poor correlation with engine noise levels. So other suitable index is needed as an alternative. Figure no 4.55 shows plots of cylinder pressure levels for two conditions denoted by Case I and Case J in which main injection timing was retarded by 3º CAD and advanced by 3 ºCAD respectively. It can be seen that a good correlation was observed in pressure spectrum for these two cases in frequency range of 215Hz-2800Hz of A-Weighted filter SPL.

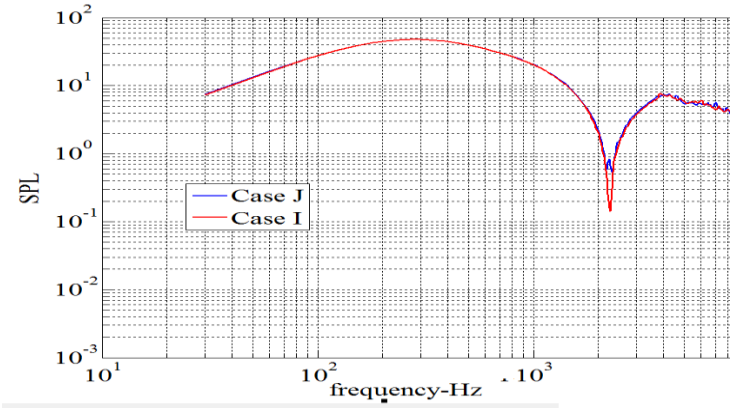

Figure no 4.55-Comparison of engine pressure spectrum (Case I, Case J)

Hence a new index defining combustion noise was developed which was based on the above mentioned frequency range. This index is defined as sum of in cylinder pressure spectrum in 215Hz-2800Hz frequency range i. e.

$CI=10*\log [10^{(215/10)}+...+10^{(2800/10)}]$ (4.4)

For this purpose, 5 different tests were done by operating engine at 3600 RPM under full load conditions as seen in table no 4.7.

Parameter	Mode 1	Mode 2	Mode 3	Mode 4	Mode 5
SOI_{pre}	16°	16°	20°	16°	19°
SOI_{main}	8°	8°	8°	6°	9°
Q_{pre}	1	2	1	1	1
Q_{Main}	13	13	13	13	13
$P_{injection}$	700	700	700	700	700

Table no 4.7-Comparison of various testing cases

Mode 1 was taken as a reference test case and various injection parameters were changed with respect to this case. During 2nd one, amount of fuel injected during pre-injection period was increased by $1mm^3$/stroke. During 3rd mode, the pre-injection timing was advanced by 4° CAD with respect to reference case. During 4th mode, the main injection timing was retarded by 2°CAD with respect to Case 1. During 5th one both pre as well as main injection timings were advanced with respect to mode 1 by 3° CAD and 1° CAD respectively. In order to devise a control system that utilizes noise emissions from engines as an effective method to monitor combustion process, the acquired signals were analyzed to formulate certain indices which could be correlated with quality of combustion and hence combustion noise. These indices have been defined as follows:

A) Combustion Index (CI)- As defined in previous section.

B) MBF50 and MBF100-Crank angle locations at which 50% and 100% of fuel is burnt as calculated from normalized values of heat release rates shown in figure no 4.56.

C) Peak pressure rise rate (MPRR)-It is defined as maximum value of in cylinder pressure observed during an engine cycle.

D) Least value of filtered accelerometer signals (LMA)-This denotes the crank angle locations corresponding to minimum value of filtered vertical accelerometer signals in previously defined frequency bands.

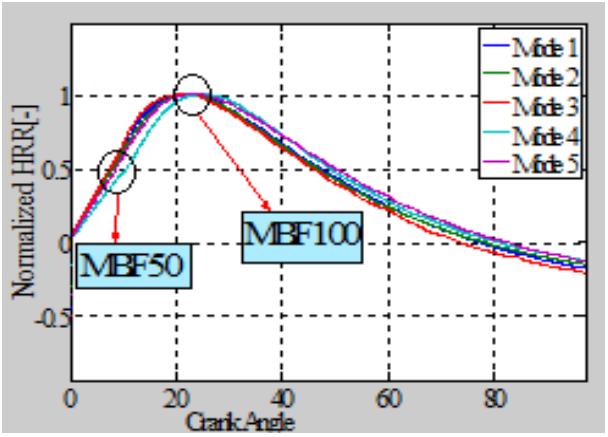

Figure no 4.56-MBF50 and MBF100

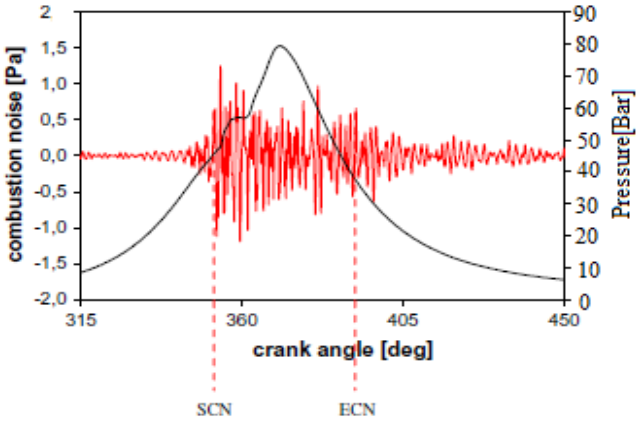

Figure no 4.57-Combustion Noise Indices

From the view point of radiated noise following indices are most relevant:

1. Start of combustion noise (SCN)-It is defined as value of crank angle at which filtered noise emissions (in frequency range dominated by combustion) from engine is higher than 0.5Pa for next 10º CAD.
2. End of combustion noise (ECN)-It is defined as value of crank angle at which filtered noise emissions (in frequency range dominated by combustion) from engine is lower than 0.5Pa for next 10 ºCAD.
3. Noise Index (NI)-It is defined as sum of noise spectrum in 0.5 kHz-3.8kHz frequency range (in which energy of combustion is concentrated).

Figure no 4.57 shows crank angles corresponding to various noise indices as defined above for the base testing case. Similar trends were observed for other cases. Further relationships between theses indices were investigated.

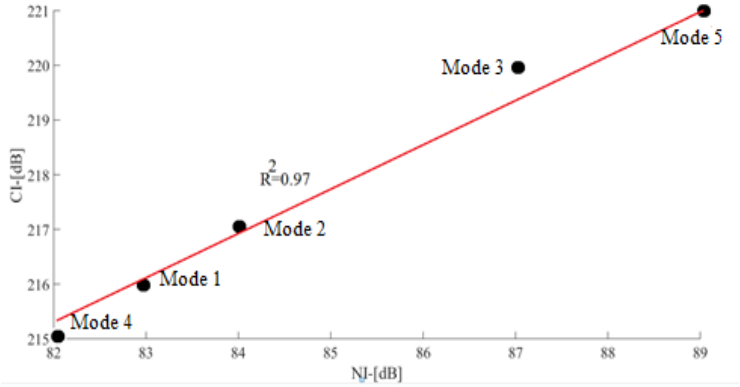

Figure no 4.58-Correlation between CI and NI

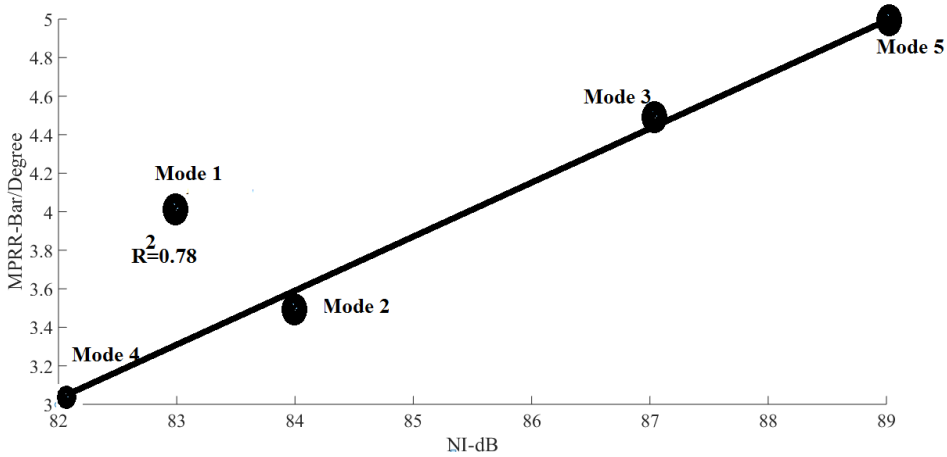

Figure no 4.59-Correlation between NI and MPRR

Figure no 4.58 shows relationship between NI and CI for the given testing conditions. Variations in the injection process was responsible for variations in CI which shows an almost linear correlation with NI. As seen from the above plots, the trends between two indices were coincident i.e. when NI increased, the CI also increased and vice versa. The relationship between two indices may be expressed in terms of proportionality coefficients as:

NI=CI *Ac (4.5)

Table no 4.8 shows values of coefficients Ac for various testing modes.

PARAMETER	Ac
Case 1	0.3813
Case 2	0.3862
Case 3	0.3855
Case 4	0.3925
Case 5	0.3998

Table no 4.8-Comparison of various proportionality coefficients

This trend was further analyzed using coefficient of correlation (R) which denotes an absolute correlation as its value reaches unity. From figure no 4.59-4.63, the lines of interpolation and values of R can be interpreted. The value of R between NI and CI were found to be 0.97. Further the value of R between maximum pressure rise rate (MPRR) and NI was found to be 0.7 as seen from figure no 4.60. This is lesser as compared to previous one. Thus CI can be perceived as a better parameter to diagnose combustion noise as compared to MPRR. This result can be justified by small range of crank angles in which MPRR develops when compared with wide range in which NI was computed.

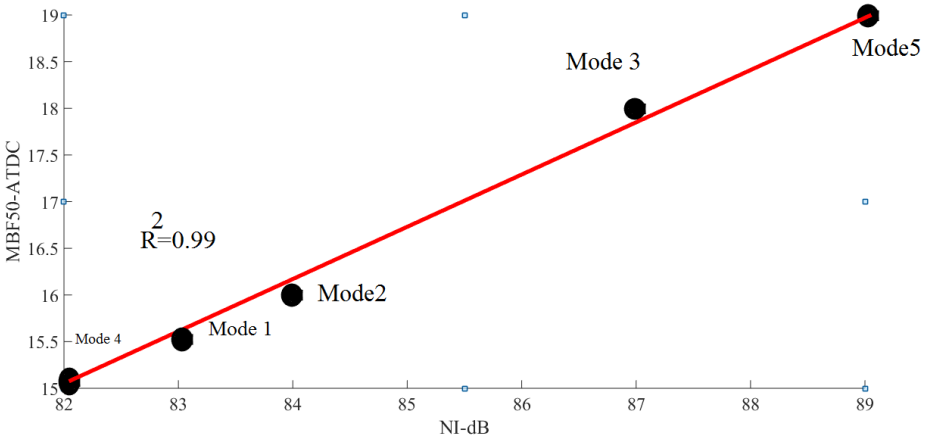

Figure no 4.60-Correlation between MBF50 and NI

In figure no 4.61 the relationship between SOI $_{pre}$ and SCN can be observed. Subsequently relationship between MBF100 and ECN is highlighted in figure no 4.62. The high correlation between data indicates that these indices are worth to analyze the combustion process. However, at higher speeds contributions due to mechanical sources dominates contributions due to combustion process.

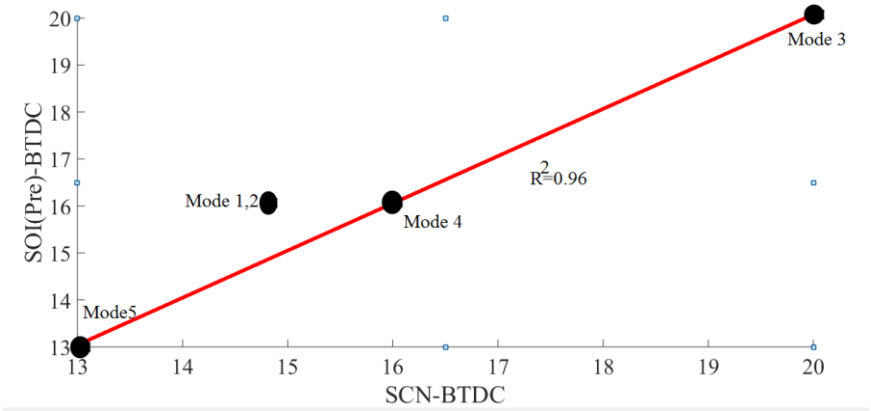

Figure no 4.61-Relationship between SOI $_{pre}$ and SCN

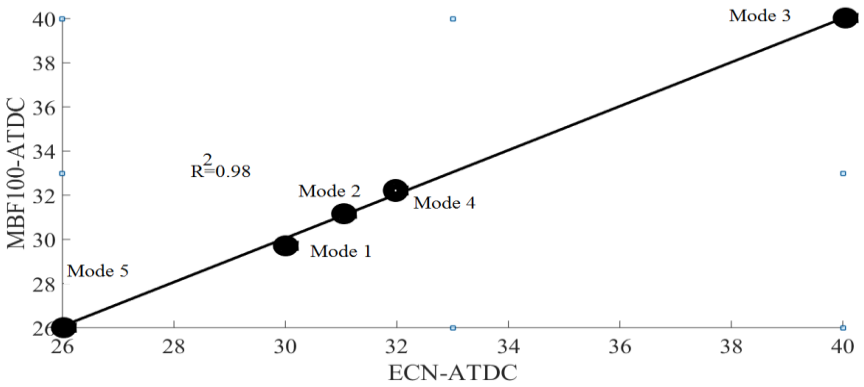

Figure no 4.62- Relationship between ECN and MBF100

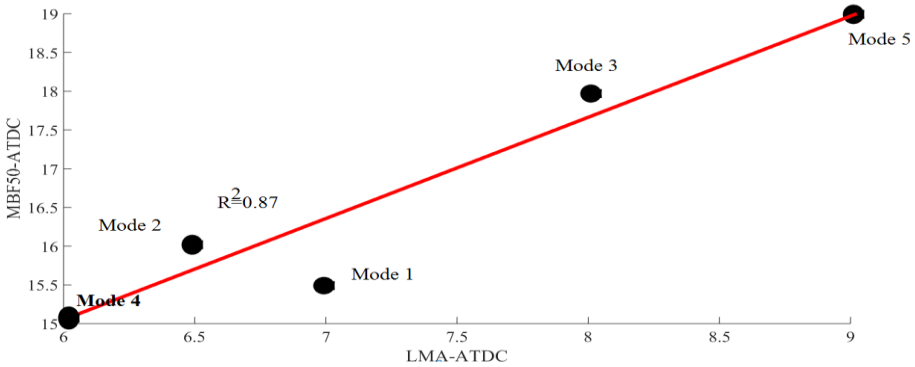

Figure no 4.63-Relationship between LMA and MBF50

Table no 4.9 summarizes relationship between various indices, where circles denotes the established link.

Parameter	NI	SCN	ECN	LMA
SOI_{pre}		●		
MBF 100			●	
MBF 50	●			●
MPRR	●			
CI	●			

Table no 4.9-Comparison of various indices

4.5 Factors effecting combustion noise [20]

The rate of pressure rise (which mainly depends on the ignition delay period) and quantities of combustion gas formed during this period are key parameters to analyze combustion based noise. A shorter delay period means lesser amount of combustible gas formed and hence lesser combustion noise. Hence delay period must be reduced as much as possible for effective reduction of combustion noise. Structure and layout of engine also plays a significant role. Anderton and Priede observed that an abrupt combustion led to high frequency contents of cylinder pressure spectrum [21, 22]. It was suggested that frequency contents up to 300 Hz were related to maximum cylinder pressure developed [23]. Between 300Hz-2000Hz they were related to first derivative of in cylinder pressure, whereas above 2000Hz they were related to second derivative of cylinder pressure.

Increase in the compression ratio and chamber temperature may shorten ignition delay period. However, an increase in compression ratio can cause a rise in noise due to slapping motion of skirt. Various parameters of fuel injection system like instance of fuel injection, injection pressure, number of nozzles and fuel supply rate also effects the combustion noise. Increasing the pressure of injection or engine speed leads to an increase in the amount of fuel accumulated during the delay period resulting in rise of combustion noise. There are many approaches to control combustion noise. One of these includes reducing cylinder pressure spectrum typically in middle and high frequency ranges. Others include increasing the stiffness of parts, use of turbo charging process and use of split injection methods.

4.6 Effects of heat release rate

Previous works have shown a relationship between peak of combustion noise and overall heat release rate [24]. Russell has developed a technique based on block attenuation curve which is still most reliable one for study of combustion noise [25]. It was observed that higher slopes of rate of heat release curves led to higher combustion noise irrespective of fuel injection timings [26]. There is a tradeoff between combustion efficiency and the noise generated due to combustion [27]. Efficient combustion leads to higher heat release rate near top dead center position which further gives rise to high frequency components in noise spectrum. Late release of heat release leads to lower pressures and subsequent lower frequencies in spectrum.

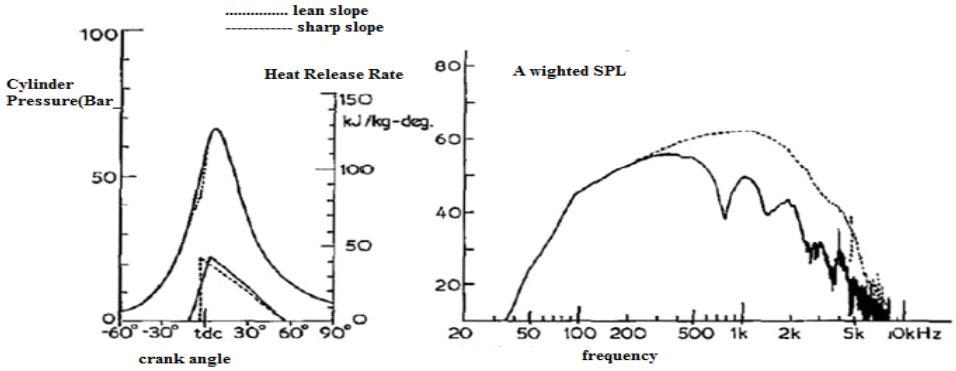

Figure no 4.64-Effects of heat release rate on combustion noise [27]

It has been observed that up to a 10dB reduction in sound pressure levels were possible by reducing the slopes of ROHR without change in fuel consumption as shown in figure no 4.64. However, there is a fall in efficiency of cycle and smoke emissions increase if ROHR is not terminated 50° after TDC position (ATDC) [28].

4.7 Effects of cyclic variations

Combustion process in diesel engines varies from cycle to cycle which may lead to variations in noise emissions as shown in figure no 4.65 [29]. These variations may be attributed due to different fuel injection rates, compression ratios as well as difference in fuel spray process, mixture formation and flame propagation.

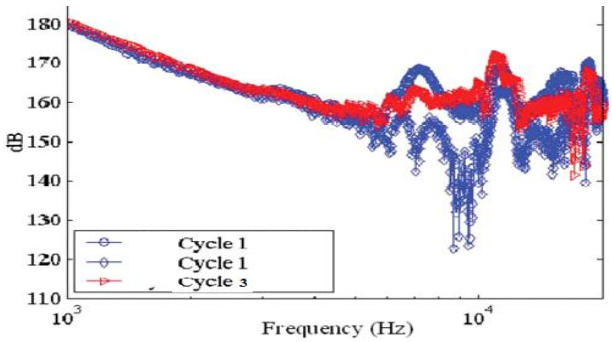

Figure no 4.65–Cyclic variations in combustion noise [29]

4.8 Resonance phenomenon

Resonance taking place inside combustion chamber also effects the noise emissions. Grover observed high peaks in the noise spectrum which may be attributed to this phenomenon [30, 31]. Hickling found peaks of higher amplitude by filtering data in range 20Hz-1500Hz which showed increased with engine load [32]. The amplitude of oscillations due to resonance depends on the geometry of bowl as well as temperature of gas formed [33]. Resonance phenomenon can be considered as an unsteady process as it changes continuously during course of combustion process [34]. The frequency of resonance (f_r) may be defined in terms of cylinder bore (B), axial length (L) and speed of sound (C) as:

$$f_r = \sqrt{\left(\frac{C}{2L}\right)^2 + \left(\frac{q_{m,n}}{B}\right)^2} \qquad (4.6)$$

Where m, m, k determines the circumfencial, axial and radial modes as shown in figure no 4.66.

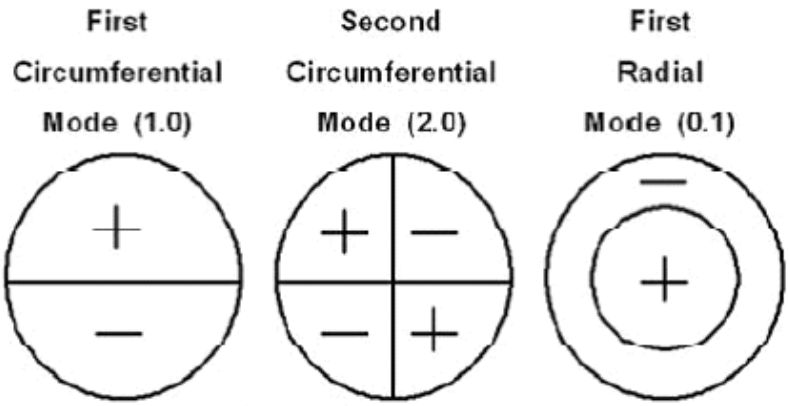

Figure no 4.66-Various modes of combustion chamber cavity [27]

4.9 In cylinder pressure decomposition method

A methodology to decompose the total in cylinder pressure signals was first proposed by Payri [35]. In this methodology the cylinder pressure was decomposed into three parts namely: combustion pressure, resonance pressure and motored pressure. The combustion part was dependent on injection process and hence resulting ROHR. Using suitable cutoff frequencies, resonance part of pressure can be isolated from excessive part (which is sum of combustion and resonance part). Figure no 4.67 shows results of this methodology as applied to in cylinder pressure at 3000 RPM under full load condition.

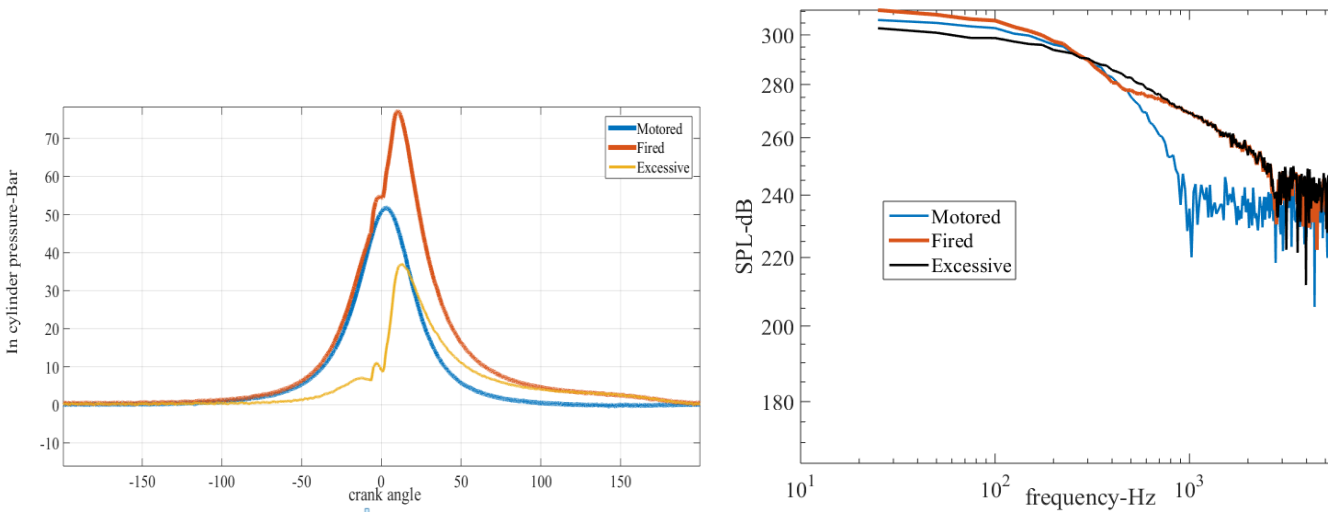

Figure no 4.67-Decomposition of cylinder pressure signal

As evident from these figures, motored part dominated at low frequency ranges. Excessive portion is clearly visible with fluctuating peaks at higher ranges. The contribution due to combustion process can be obtained by subtracting resonance portion from excessive portion. These contributions dominate in mid frequency ranges [35]. The decomposed signals thus obtained can be further used to calculate various indices defined in terms of ideal engine speed (N_{ideal}) as:

$$I_n = \log\left[\frac{N}{N_{ideal}}\right] \quad (4.7)$$

$$I_1 = \left[\frac{N}{N_{ideal}}\right]\left[\frac{(\frac{dp}{dt})_{pilot}+(\frac{dp}{dt})_{main}}{(\frac{dp}{dt})_{motored}}\right] \quad (4.8)$$

$$I_2 = 10*\log\left(10^6 \int \left(\frac{P_{residual}{}^2}{P_{motored}{}^2}\right)dt\right) \quad (4.9)$$

Where is maximum pressure gradient during pilot injection period, $(\frac{dP}{dt})_{main}$ is maximum pressure gradient during main injection, $P_{residual}$ is residual pressure and $(\frac{dP}{dt})_{motored}$ is maximum pressure gradient in motored pressure signal. These indices can be further used to express overall noise (ON) emitted from engine given by:

$$ON = C_0+C_1I_1+C_2I_2+C_nI_n \quad (4.10)$$

Where constants C_0,C_1,C_2 and C_n depend upon size of engine.

4.10 Mathematical Model of Generation of Combustion Noise [36]

In this part of work, a transient model for generation process of combustion noise has been discussed. For this purpose, a Morlet wavelet was used which was defined in terms of its central frequency f_c and bandwidth f_b as:

$$\psi(t) = \frac{1}{\sqrt{\pi f_b}} e^{i2\pi f_c t}\, e^{\frac{-t^2}{f_b}} \quad (4.11)$$

Figure no 4.68 shows real and imaginary parts of this wavelet having f_b = 1.5 and f_c = 1

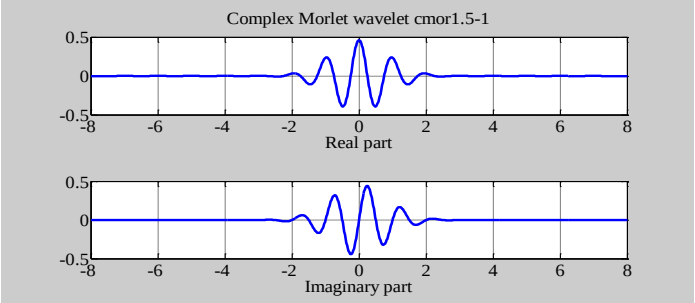

Figure no 4.68-Complex Morlet Wavelet

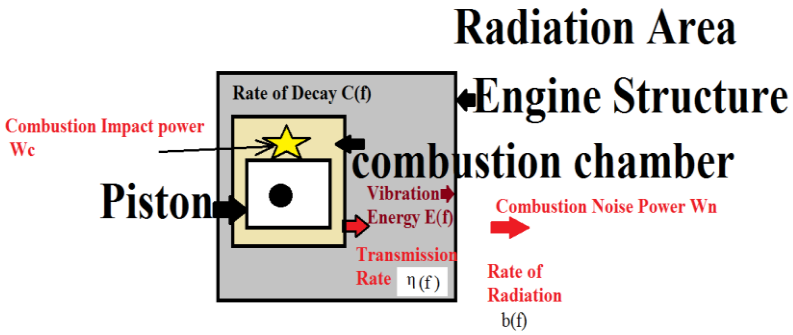

Figure no 4.69-Noise generation model

This model can be analyzed by following three processes: generation of vibrational energy inside chamber due to combustion process, transmission and decay of this energy and finally its radiation around the engine surface. The combustion process inside engines generates combustion impact power (W_c) shown in figure no 4.69. This is related to in cylinder pressure developed (p), impedance of medium (ρc) and cylinder surface area (A) as:

$$Wc = \frac{P^2}{\rho c} A \qquad (4.12)$$

The available energy at engine surface can be expressed in terms of transmission rate coefficient η(f) as:

$$E(f) = \eta(f) \int_0^t W_c dt \qquad (4.13)$$

Differentiating both sides of this equation we have:

$$\frac{d}{dt}\left(E(f)\right) = \eta(f) W_c \qquad (4.14)$$

Taking into account the decay rate C(f) this equation gets modified as:

$$\frac{d}{dt}\left(E(f)\right) = \eta(f) W_c - C(f)E(f) \qquad (4.15)$$

Where the decay constant C(f) may be defined as:

$$C(f) = -\frac{d[\log(Wn))]}{dt} \qquad (4.16)$$

$$\frac{d}{dt}\left(W_n\right) = b(f)\eta(f) W_c - C(f)\, W_n(f) \qquad (4.17)$$

Figure no 4.70-4.74 shows the plots of combustion impact power plotted for tests enlisted in table no 4.1 using reference power value of 10^{-12} Watts. It is clear from these results, that impact continued for longer crank angle durations at higher speeds.

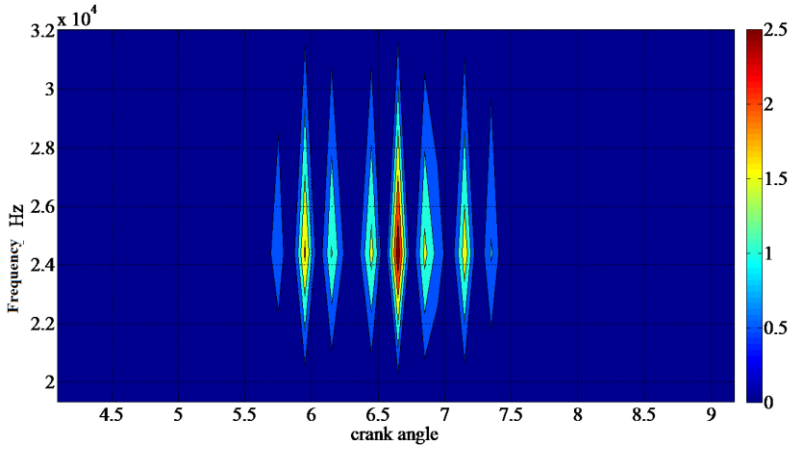

Figure no 4.70-Combustion impact power(Case1)

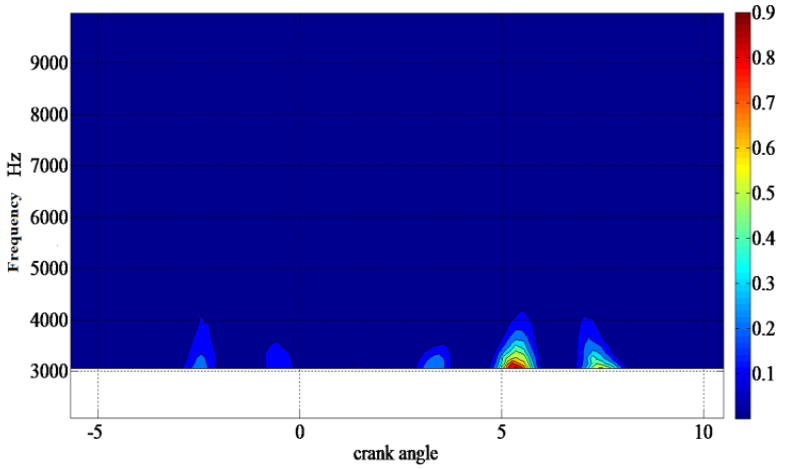

Figure no 4.71-Combustion impact power(Case2)

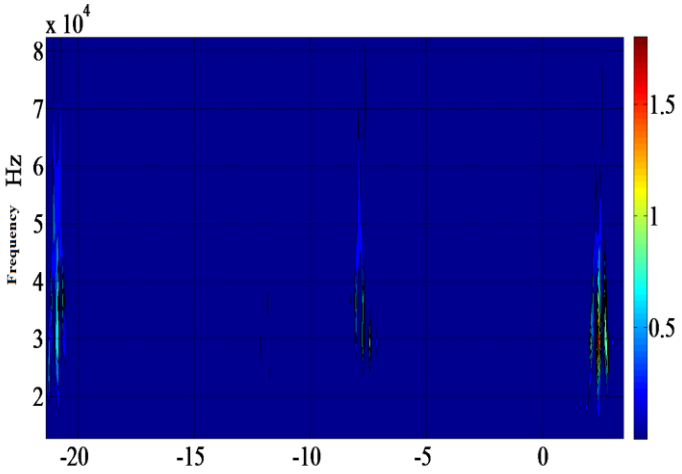

Figure no 4.72-Combustion impact power(Case3)

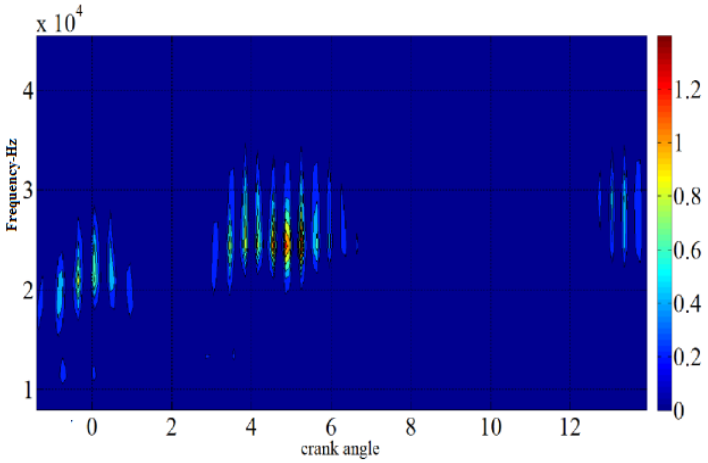

Figure no 4.73-Combustion impact power(Case4)

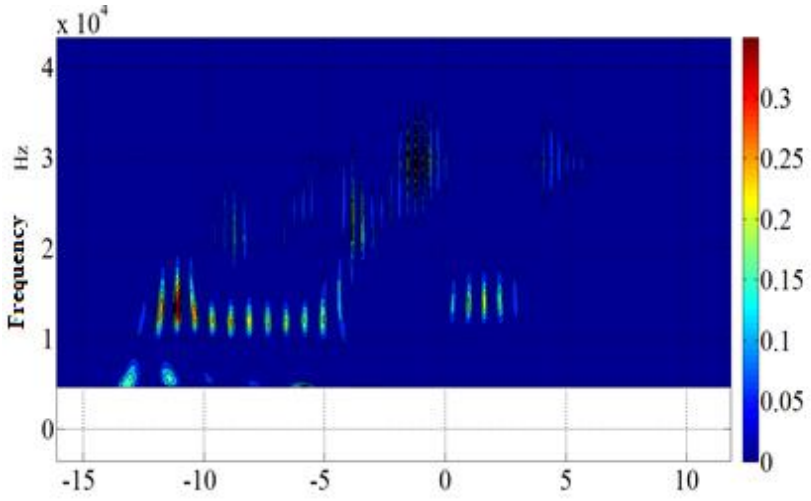

Figure no 4.74-Combustion impact power(Case5)

Further relationships between various noise emission rates were investigated in figure no 4.75-4.78 taking reference value of $1s^{-1}$. The values of transmission and decay rates was lesser at higher frequency ranges, so at these ranges the conversion efficiency of the impact energy into radiated noise was lower.

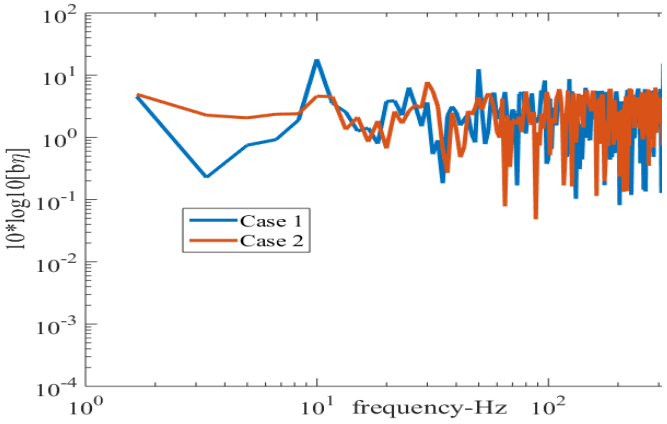

Figure no 4.75– Transmission rate[dB](2000RPM)

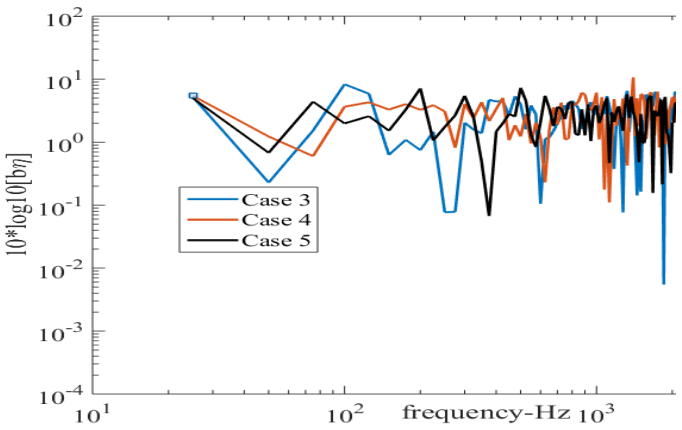

Figure no 4.76– Transmission rate[dB](3000RPM)

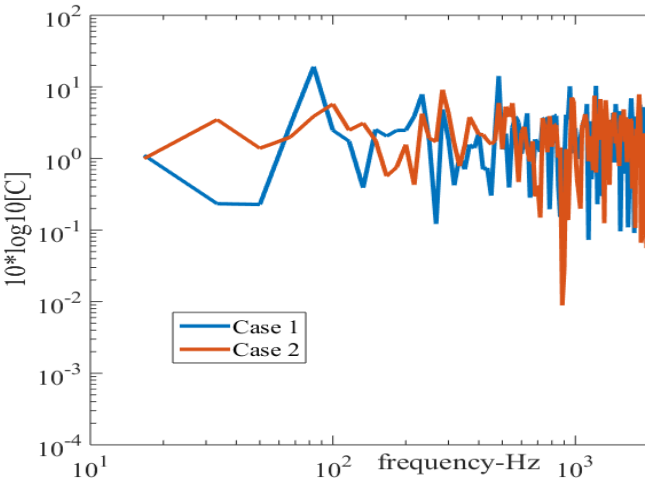

Figure no 4.77–Decay rate [dB](2000RPM)

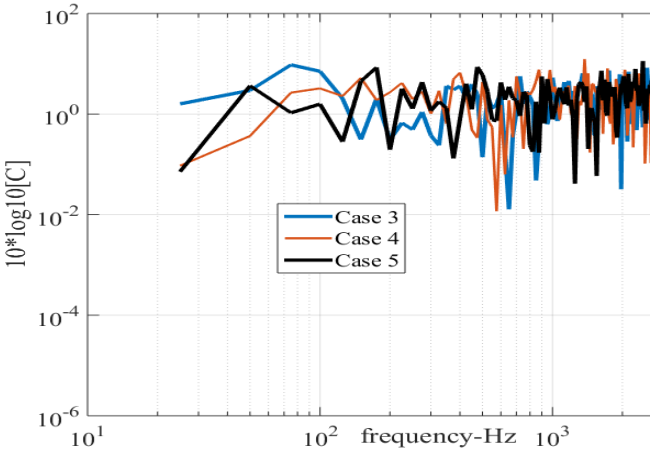

Figure no 4.78– Decay rate [dB](3000RPM)

4.11 Methods to evaluate combustion noise

Austin & Priede have shown that combustion based noise was most dominant in frequency range of 800Hz- 4kHz [37]. Acoustic measurements of noise outside the engine may be used for combustion noise analysis only when the engine is operated in such a way that contribution of combustion events towards the noise emissions becomes predominant. This can be achieved either by either advancing injection timing or by changing Cetane number of type of fuel. Russell used alkyl blended fuel to maximize in cylinder pressure so that combustion noise becomes dominant [25].

The magnitude of combustion noise generated also depends on the structural response and damping effects of engine under consideration. The difference between in cylinder pressure developed and radiated noise emissions is characterized by a decaying effect which represents the structural attenuation of engine which is seen in figure no 4.79.

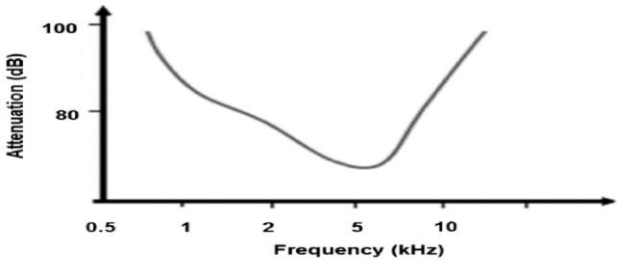

Figure no 4.79- Attenuation curve of engine

Various operational parameters of engine e.g. load, speed & fuel injection parameters have no significant effects on structural attenuation property of engine. This curve can be divided into three distinct regions:

a) Below 2000Hz-Low frequency range having high attenuation factor.
b) Mid frequency ranges of 2000Hz-5000Hz having decaying effect.
c) Above 5000Hz range having high attenuation factor.

Structural attenuation of engine structure also plays a vital role in determination of combustion based noise. Values of structure response functions was found to fall by about 10dBA in 500Hz -5kHz frequency range [33]. More recently AVL has developed a noise meter which is based on analysis of engine indicator diagram [38]. Figure no 4.80 shows structural response functions of a group of 9 engines as recorded by an AVL noise meter [33]. The response of direct injection high speed diesel engines falls by 12dB over 5kHz frequency range [33].

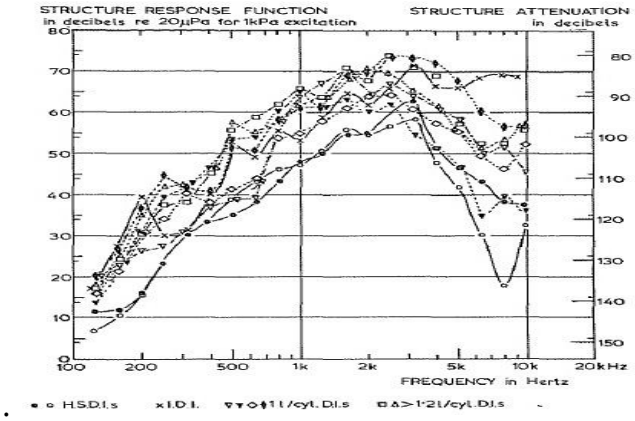

Figure no 4.80–AVL structural response function and structural attenuation [33]

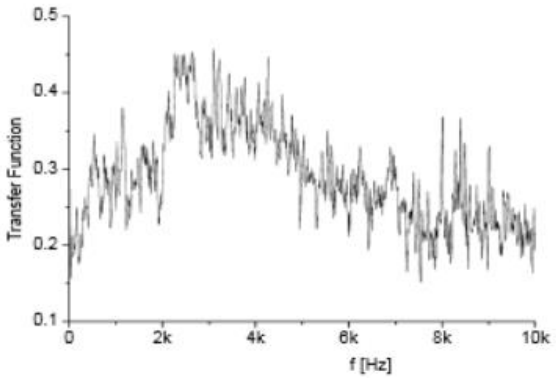

Figure no 4.81- Transfer function obtained by explosive charge [39]

Further Shu was able to predicted this transfer function by setting an explosive charge inside cylinder which was locked at fixed crank angle position as seen from figure no 4.81 [39]. Different functions for various designs of combustion chambers and different amounts of explosion charges have also been compared in his work.

All the methods discussed above use expensive and time consuming methodologies to analyze the transfer function of combustion noise, consequently an alternative method of analysis has been analyzed which involves use of Cepstrum analysis.

Cepstrum analysis is an important method of signal processing which has wide applications in source separation [40]. Psychoacoustic analysis of noise emissions from a S.I. engine has been carried out using Cepstrum analysis [41]. This methodology has also proved effective for cylinder pressure reconstruction [42], fault detection in gears [43] and condition monitoring of engines [44]. Mathematically Cepstrum can be defined as inverse spectrum of logarithmic power spectrum [40]. i.e.

$$C_a(q) = |IFFT[\log[G_x(f)]]| \quad (4.18)$$

Where q is frequency in milliseconds & G_x denotes the Fourier transformation of function.

Since auto power spectrum density function is even, both its inverse Fourier transformations & Fourier transformations are equal. i.e.

$$C_x(q) = |FFT\ [\log\ [G_x(f)]]| = IFFT[\log\ [G_x(f)]] \quad (4.19)$$

As a noise source x(t) reaches a measuring point as an output signal y(t) after passing through a system represented by h(t), the information may be expressed by following equation:

$$y(t) = x(t).h(t) = \int x(\tau)h(t-\tau)dt \quad (4.20)$$

Taking Fourier transformation, we have:

$$G_y(f) = G_x(f) * G_h(f) \quad (4.21)$$

Further, taking logarithm and Fourier transformations on both sides this equation gets modified as:

$$\log(G_y(f)) = \log(G_x(f)) + \log(G_h(f)) \quad (4.22)$$

$$FFT[\log(G_y(f))] = F[FT\log(G_x(f))] + FFT[\log(G_h(f))] \quad (4.23)$$

Or

$$IFFT[\log(G_y(f))] = IFFT[\log(G_x(f))] + IFFT[\log(G_h(f))] \quad (4.24)$$

$$C_y(q) = C_x(q) + C_h(q) \quad (4.25)$$

Figure no 4.82-4.84 shows the plots of structural response function as obtained by Cepstrum analysis for various test cases listed in table no 2.1 using windows positioned around TDC. For motored condition noise emissions was taken as output signal and in cylinder pressure as input. In case of firing conditions, the rate of heat release was taken as input parameter.

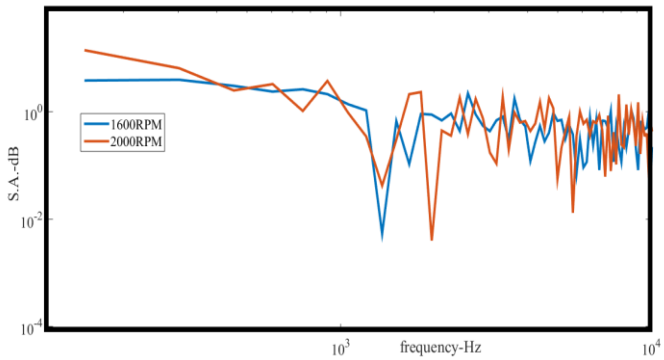

Figure no 4.82- Structural Attenuation Function (Motored)

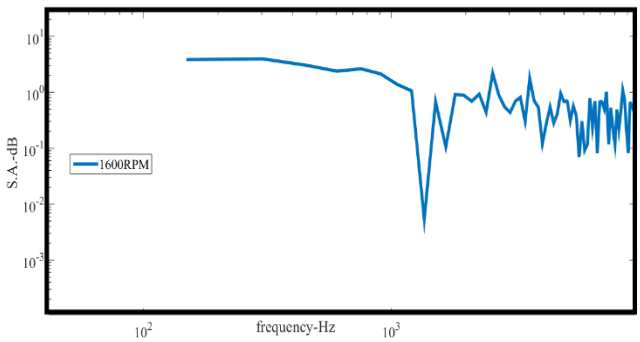

Figure no 4.83- Structural Attenuation Function (1600RPM-100%load)

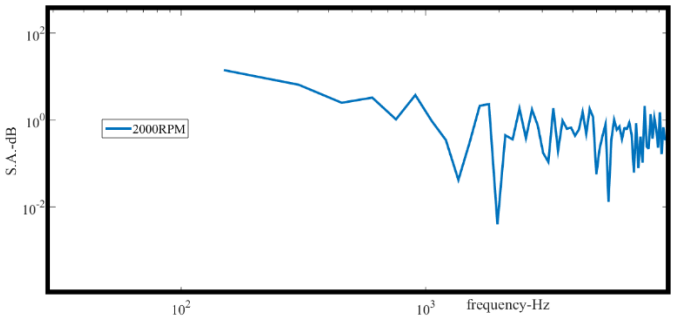

Figure no 4.84- Structural Attenuation Function (2000RPM-100%load)

It is clear from plots that transfer function for various cases showed same trends in spite of load and speed variations. The values of attenuation were higher in lower frequency ranges gradually decreasing reaching minimum value at 2kHz and then rose again. At low frequency ranges, various parts of engine have high rigidity and hence radiation efficiency was very low. Significant differences were seen in higher frequency ranges. These variations may be attributed to differences in the designs of cylinder heads, engine block and cover which also play a vital role. Engines may use same materials for different parts, hence engines of different make may show same variations in structural response function. Based on these results all curves show a minimum contributions in frequency range of 1kHz-2kHz range and hence combustion process may be seen to dominate noise emissions in this range.

Further the combustion noise is transmitted to the exterior through the engine block and the head cover. Assuming this transmission is linear and invariant, the overall noise emissions (ON) from engine can be written as sum of direct combustion noise (CN) and motion based noise (MN). i.e.

$$ON = CN(H_1) + MN \qquad (4.26)$$

Where H_1 is structural attenuation factor of combustion noise.

Assuming that mechanical noise levels (motored conditions) do not change significantly, various noise levels for the given testing conditions were evaluated using transfer functions previously described as seen in figure no 4.85,4.86. Increase of engine speed caused a slight increase in mechanical noise levels.

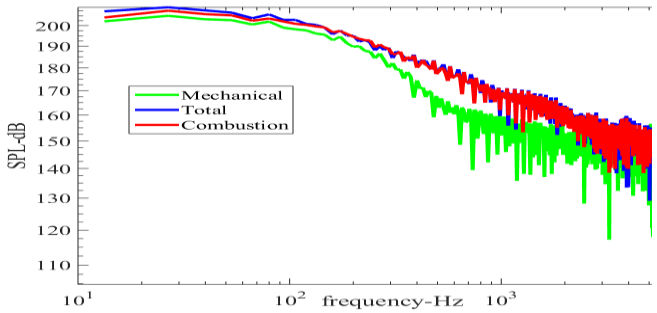

Figure no 4.85- Source separation -1600RPM ,100%Load

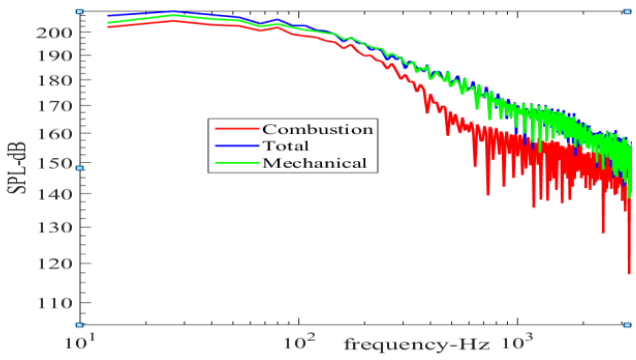

Figure no 4.86- Source separation -2000RPM, 100%Load

4.12 Summary

This part of work investigated use of various experimental data for diagnosis of combustion based noise. Block vibrations were used to identify various phases of combustion process in diesel engine cycle. Coherence analysis was able to identify suitable frequency ranges in which combustion based noise was dominant. Various regions of cylinder pressure spectrum and noise indices were developed by changing fuel injection parameters.

High levels of correlations were observed between these indices and actual pressure developed, showing the applicability of vibration signature of engine as a possible input feedback parameter in case of a closed loop control system shown in figure no 4.87 [45]. Thus an effective control mechanism over combustion noise can be achieved by devising optimum MBF50/MBF100 timings [46].

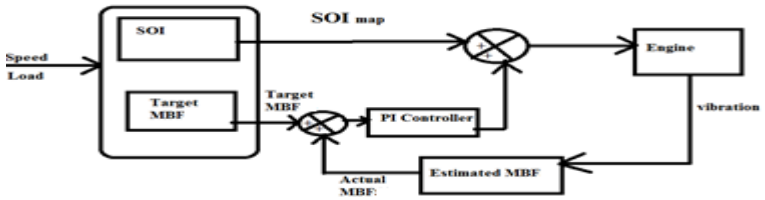

Figure no 4.87 –Use of vibration signals as a feedback [45]

Further a transient model of combustion noise generation was also analyzed. Cepstrum analysis was used to obtain the transfer function of combustion noise. As evident from various results, this function remained same in spite of variations in testing conditions. This function is also dependent on the resonance frequencies of combustion chamber, hence temperature variations inside chamber also need to be taken into account for future analysis.

4.13 References

[1] Rakopoulos**,** Constantine D., Giakoumis, Evangelos G.,2009, "Diesel engine transient operation- Principles of Operation and Simulation Analysis",Springer,London, ISBN -978-1-84882-374-7.

[2] Rakopoulos**,** Constantine D., Giakoumis, Evangelos G.,2011, "Experimental study of combustion noise radiation during transient turbocharged diesel engine operation", Vol 36,no.8,pp.4983-4995.

[3] Anderton, D., Baker, J., 1973,"Influence of operating cycle on noise of diesel engine", SAE Technical Paper 730241.

[4] Carlucci, P., Ficarrela, A., Laforgia, D.,2001, " Study of the influence of the injection parameters on combustion noise in a common-rail diesel engine using ANOVA and neural networks", SAE Technical Paper 2001-01-2011.

[5] Head , Wake ,J.D.,1980, "Noise of diesel engines under transient conditions", SAE Technical Paper 800404.

[6] Torregrosa, A.G., Broatch , A.,Novella,R., Monico, L., 2011,"Suitability analysis of advanced diesel combustion concepts for emissions and noise control", Energy,Vol 36,no 2,pp.825–838.

[7] Russell., Haworth, R.,1985, "Combustion noise from high speed direct injection diesel engines", SAE Technical Paper 850973.

[8]Baumgarten,C.,2006,"Mixture formation in internal combustion engines", Springer Verlag, Heidelberg, ISBN 13798-3-540-30835-5.

[9]Flynn,P.,Durrett,R.,Hunter,G.,Loye,A.,Akinyem,O.,Dec,J.,andWestbrook,C.,1999,"Diesel Combustion :An integrated view combining laser diagnosis chemical kinetics and empirical validation", SAE Technical Paper 1999-01-0509.

[10]Hammer,J.,Durnholz,M.,Dohle,U.,2004,"Entwicklungstrends bei Einspritzsystemen fur PKW-Diesel motoren",Dieselmotorentechnik,pp.36-52.

[11]Ricaud,J.,Lavoisier,F.,2002, "Optimizing the multiple injection settings on an HSDI diesel engine ,THIESEL conference on Thermo and fluid dynamic processes in diesel engines ".

[12]Drake,M.,Ratcliffe,J.,Blint,R.,Carter,C.,Laurendeau,N.,1990, "Measurements and modelling of flame front NO_x formation and super Equilibrium radical concentrations in laminar high pressure premixed flames",23 rd symposium on combustion, The combustion institute,pp.387-395.

[13]Duret,P.,Gatellier,B.,Miche,M.,Montreiro,L.,Zima,P.,Marotaux,D.,Blundell,D.,Gase,M.,Zhao,H.,Perozzi,M.,Araneo,L.,2003, "Innovative diesel HCCI combustion process for passenger cars: European Space light project, EAEC congress ,paper no C108.

[14] Arnone,L.,Manelli, S.,Chiatti,G.,and Chiavola,O.,2009," In cylinder pressure analysis through accelerometer signal processing for diesel engine combustion optimization", SAE Technical Paper 2009-01-2079.

[15]Arnone,L.,Manelli, S.,Chiatti,G.,and Chiavola,O.,2009," Engine block vibration measures for time detection of diesel combustion phases, SAE Technical Paper 2009-24-0035.

[16]Chiavola,O.,Chiatti,G., Arnone,L.,Manelli, S.,2010, "Combustion characterization in diesel engines via block vibration analysis", SAE Technical Paper 2010-01-0168.
[17]Arnone,L.,Boni,M.,Manelli,S.,Chiavola,O.,Conforto,S.,Recco,E.,2010, "Diesel engine combustion monitoring through engine block vibration signal analysis", SAE Technical Paper 2009-01-0765.

[18]Chiavola,O.,Chiatti, G., Recco,E.,2012, "Accelerometer measurements to optimize injection strategy", SAE Technical Paper 2012-01-1341.
[19] Chiatti, G., Recco,E., Chiavola,O.,2011, "Vibration processing to optimize pressure development in CR diesel engine ", SAE Technical Paper 2011-01-1560.
[20]Gang, Sheng.,2012,"Vehicle noise, vibration, and sound quality", SAE International , ISBN 978-0-7680-7513-7.
[21]Anderton, D., 2003,"Noise source identification techniques", ISVR course notes.
[22]Schaberg,P.,Priede,T.,Dutkiewicz,R.,1990, "Effects of a rapid pressure rise on engine vibration and noise", SAE Technical Paper 900013.
[23]Priede,T.,Grover,E., Anderton,D.,1968, "Combustion induced noise in diesel engines", Proceedings of diesel engines users association congress, London.
[24]Russell,M.,1972, "Reduction of noise emissions form diesel engine surface", SAE Technical Paper 720135.
[25]Russell,M.,Haworth,R.,1985, "Combustion noise from high speed direct injection diesel engines ", SAE Technical Paper 850973.
[26]Russell,M.,Cavanagh,E.,1979, "Establishing a target for control of diesel combustion noise", SAE Technical Paper 790271.
[27]Monelletta,L.,2010, " Contribution to the study of combustion noise of automotive diesel engines",Phd Thesis, University polytechnic Velencia
[28]Lyn,W.,1960, "Calculation of the effect of rate of heat release on the shape of cylinder pressure and cycle efficiency", Proceedings of IMECH conference on automobiles ,Vol 14,no.1,pp.34-46.
[29]Torregrosa,A.,Broatch, A., Maratin,J.,Monelletta,L.,2007, "Combustion level assessment in direct injection diesel engines by means of in cylinder pressure components", Measurements science and technology ,Vol. 18,no.7,pp.2131-2142.
[30]Priede,T.,Grover,E.,1966, "Noise from industrial diesel engines", Proceedings of symposium on noise from power plant equipment, Southampton.
[31] Priede, T., Grover, E., and Lalor, N.,1969, "Relation between noise and basic structural vibration of diesel engines," SAE Technical Paper 690450.
[32] Hickling,R., Feldmaier, D.,and Sung,S.,1979, "Knock induced cavity resonances in open chamber diesel engines", JASA, Vol 65,no.6,pp.1474-1479.
[33]Anderton, D.,1979,"Relation between combustion system and noise ", SAE Technical Paper790270.
[34]Anderton, D.,1990,"Basic origins of automotive noise ", ISVR course notes.
[35] Payri,F.,Broatch,A.,Tormos,B.,and Marant,V.,2005, "New methodology for in cylinder pressure analysis on DI diesel engines-application to combustion noise", Measurement Science and technology, Vol 16,no.2,pp.540-547.
[36]Nguyen,T.,Kai,Y.,Miami,M.,2012, "Study on combustion noise from a running diesel engine based on transient combustion noise generation model ",International Journal of automotive engineering, Vol 3,no.4,pp.131-140.
[37] Austen, A. and Priede, T.,1965, "Noise of automotive diesel engines: Its causes and reduction," SAE Technical Paper 650165.
[38]AVL450 combustion noise meter, AVL manual, August 2000.
[39] Ge-qun, S., Hai-qiao, W., and Rui, H.,2005, "The transfer function of combustion noise in D.I. diesel engine ", SAE Technical Paper 2005-01-2486.
[40] Liang, X., Yang, K., Shu, G., Dong, L.,2012, " The identification of noise source in diesel engine based on the Cepstrum analysis of sound and vibration signals", SAE Technical Paper 2012-01-0802.

[41]Andrés, Camacho., Gema,Pinero., Maria de diego, Miguel, Ferrer., 2004,"On the use of complex Cepstrum in psychoacoustic evaluations of engine noise",11th ICSV, Saint Petersburg, Russia
[42]Ghamry, Steel, Reuben, Fog,2005, "In direct measurement of in cylinder pressure using acoustic emissions", Mechanical Systems and signal processing ,Vol 19,no.4,pp.751-765.
[43]Robert B Randall ,2013, "A history of Cepstrum analysis and its applications to mechanical problems", 7th Surveillance International Conference ,October 29-30, Institute of Technology of Chartres, France.
[44]Chamay,M., Oh,S., and Kim,Young., 2013,"Development of a diagnostic system using LPC/Cepstrum analysis in machine vibration", Journal of Mechanical Science and Technology Vol 27,no.9,pp.2629-2636.
[45]Scafati, Lavorgna,Mancaruso, E.,2011, "Use of vibration signal for diagnosis and control of a four cylinder diesel engine", SAE Technical Paper 2011-24-0169.
[46]Kanda, Y. and Mori, T., 2015."Diesel combustion noise reduction by controlling piston vibration," SAE Technical Paper 2015-01-1667.

Chapter 5
Piston slapping noise

5.1 Introduction

In combustion engines, a small gap between piston skirt and walls of liner allows a movement of skirt along lateral direction as well as its rotation about piston pin axis in addition to its usual reciprocating motion [1]. This motion is known as piston slapping motion and the magnitude of piston-liner gap puts a limit on its amplitude [2-7]. Flores has presented a computational methodology based on slider crank mechanism dynamics to analyze this motion [8]. The existence of clearance in this mechanism makes system highly dynamic and nonlinear in nature. The motion of skirt tends to be chaotic with increase in gap.

Coefficient of restitution also plays a vital role in the piston dynamics. As this coefficient decreases and reaches unity values, the motion of skirt transforms from bouncing chaotic to periodic one [9]. This has been confirmed from the study of Farahanchi and Shaw [10]. Geng and Chen have studied a dual degree of freedom system showing a close correlation between slapping motion and resulting vibrations of engine block [11]. The slapping motion of piston also gets suppressed due to hydrodynamic action of oil which acts as a damper between skirt and liner.

Several simulations have been done previously in order to simulate various two dimensional models of this lateral motion [12]. Various parameters considered included offset of center of gravity [13], skirt profile [14], effects of variable inertial forces [15], effects of frictional forces [16] and effects of lubricating oil [17]. The skirt comes in contact with liner if its lateral displacement is greater as compared to skirt-liner gap. There can be several methods by which skirt may come into contact liner as seen from figure no 5.1.

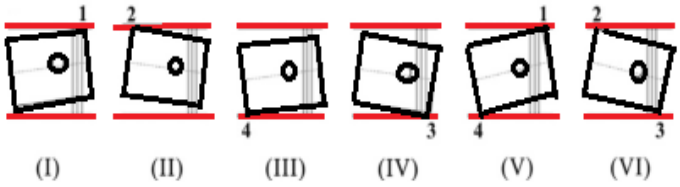

Figure no 5.1-Modes of contact during piston slap [18]

Corners 1 or 4 or both of these can come into contact with liner as skirt rotates in counter clockwise direction. Similarly corners 3 or 2 or both can touch liner as rotation occurs in clockwise direction.

Various conditions for impacts to occur are enlisted as [19]:

Corner 1 in Contact, $\frac{X_c}{2} < X_p < X_c, \theta > 0$

Corner 2 in Contact, $\frac{X_c}{2} < X_p < X_c, \theta < 0$

Corner 3 in Contact, $0 < X_p < \frac{X_c}{2}, \theta < 0$

Corner 4 in Contact, $0 < X_p < \frac{X_c}{2}, \theta > 0$

Corner 1,4 in contact, $\frac{X_c}{2} < X_p < X_c, \theta = \theta_{max}$

Corner 2,3 in contact, $0 < X_p < \frac{X_c}{2}, \theta = -\theta_{max}$

5.1

Subsequently various modes of piston secondary motion may be classified as in figure no 5.2.

Figure no 5.2-Modes of slapping motion [19]

These modes are defined as follows:

a) Rattling motion-During this motion, skirt rotates in counter clock wise direction before reaching the ignition TDC position and turns its direction rotating in clock wise direction after TDC position. This results in top part of skirt striking anti thrust side of liner as shown in the above figure. Amplitude of this motion was seen to increases with increase in engine speed and load [20]. During this motion the inertial force component (F_{Si}) of side thrust force acts towards thrust side of liner, whereas in cylinder gas component of side thrust force (F_{Sp}) acts towards anti thrust side of liner as seen in figure no 5.23.

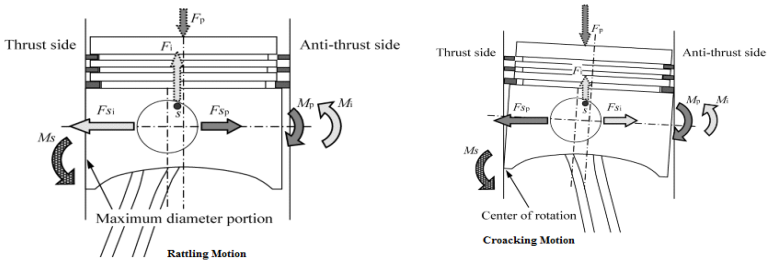

Figure no 5.3-Force analysis during various modes of lateral motion

b) Croaking motion-During this motion the top part of skirt strikes thrust side of skirt. The inertial force component (F_{Si}) of side thrust force acts on the anti- thrust side, whereas in cylinder gas component of side thrust force (F_{Sp})acts towards the thrust side of liner. This mode of motion has been found to be least effected by engine speed or load conditions [19].

c) Clatter motion -Bottom part of skirt strikes thrust side of liner which is typically observed at low speeds [19].

Major factors that affect piston slap include [20]:
a) Cylinder bore temperature
b) Lubrication oil film thickness
c) Oil viscosity
d) Engine speed
e) Skirt profile
f) Skirt roughness
g) Skirt waviness
i) Skirt size
j) Wrist pin offset
k) Piston-liner gap

Motion of crankshaft picks up the lubrication oil from sump. This oil is then transported along cylinder bore due to motion of piston skirt, piston rings and gravity. Oil is consumed either inside the combustion chamber or it returns back to sump, or is blown away by residual gases.

According to Stribeck curve (shown in figure no 5.4), various lubrication zones can be classified into following three major types: boundary zone, hydrodynamic zone and mixed zone [21]. In the boundary lubrication zone, asperities in mating parts come into contact with each other, whereas in hydrodynamic zone there is no direct contact and hence the film of lubricant separates mating surfaces. The function of piston rings of skirt assembly is to seal pressure inside the combustion chamber and prevent leakages of oil from crankcase into combustion chamber. Type of lubrication zone changes with variations in operating conditions of engine. As piston reaches towards dead center positions, its speed approaches zero and hence boundary lubrication zone dominates. At mid strokes, where piston speed is at its maximum values, the hydrodynamic zone dominates.

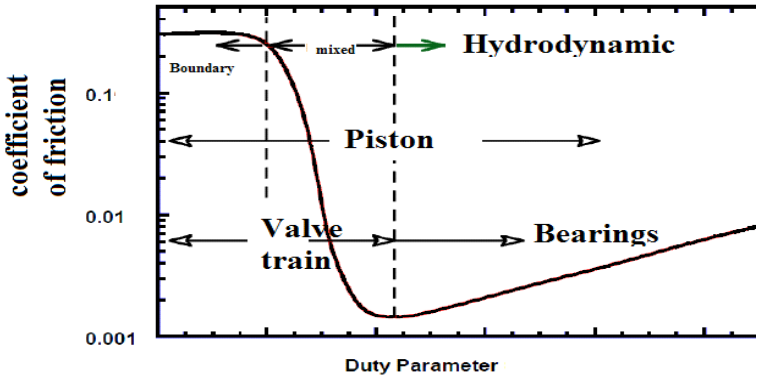

Figure no 5.4–Stribeck lubrication curve [20]

5.2 Background

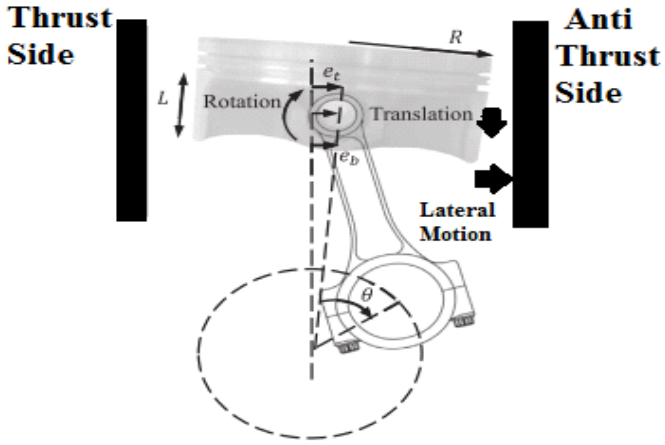

Figure no 5.5-Piston secondary motion [21]

Increasing demand for noise, vibration and harness (NVH) comfort levels have led to detailed study of dynamic motion of skirt as skirt-liner contact plays an important role in various frictional losses occurring in engines [21]. Piston may impact either on thrust side (TS) or anti-thrust side(ATS) of liner as seen in figure no 5.5. These contacting motions cause vibrations in liner which are further transmitted from various surfaces of engine. In general, three major approaches have been identified to locate the crank angle instances of skirt-liner contact during this motion [22]. First one includes study of piston secondary motion without taking into consideration lubrication effects of oil and rotatory motion of skirt. This approach is known as static method. In second method, piston side force is analyzed by taking into account lubrication pressure distribution as represented by Reynolds equations [22]. Variations in oil film thickness is the third parameter to analyze the lateral motion of skirt. Skirt -liner contact may occur if this thickness is minimum which may occur either towards thrust or anti thrust side [23]. As the slope of film thickness changes, the squeezing action is initiated indicating a possible instance of piston slap. Other methods to study slapping motion includes energy transfer method and angular duration method [23].

Instances at which the maximum energy is transferred to liner wall can indicate a possible location of skirt-liner contact [22]. The angular duration method includes study of crank angle duration starting from initiation of squeezing action of oil film and terminating at occurrence of minimum oil thickness [22]. Up to 6-10 instances of actual skirt-liner contacts have been practically observed [24]. In order to validate various possible instances of slap, block vibration data from accelerometers mounted at various locations on engine block has been analyzed [22,25]. However, this data may include contributions due to other sources of noise such as combustion based noise [25]. Pruvost has used spectro filters to separate the above mentioned sources [26]. Liu and Randall used blind source separation (BSS) algorithm to achieve effective source separation [27]. Chen analyzed the concept of pseudo angular acceleration to study phase and frequency variations of slapping noise of skirt [28].

5.3 Reynolds equation for lubrication oil pressure distribution

The tribology of lubricating oil plays an important role in mechanical losses occurring in assembly of piston. About 3-5% of the total energy losses take place in the piston skirt assembly [29]. Figure no 5.3 shows a typical breakdown of various losses for case of a diesel engine, wherein it is clear from the figure that share of piston assembly accounts for about 30% -40% [30-34].

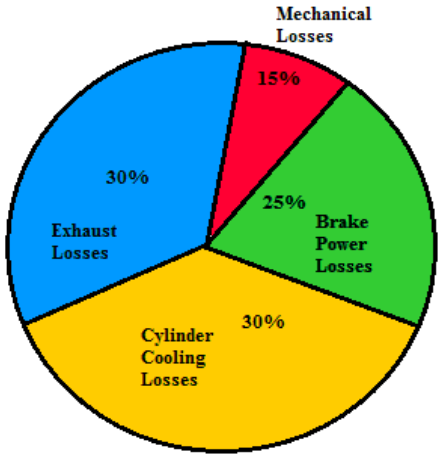

Figure no 5.6 –Break up of total dissipation of fuel energy [29]

In 1886, Osborne Reynolds studied hydrodynamic pressure generated between two sliding surfaces. For an incompressible fluid with constant density he proposed an equation given by [32]:

$$\frac{\delta}{\delta x}\left(\frac{h^3}{12\eta}\frac{\delta P}{\delta x}\right)+\frac{\delta}{\delta z}\left(\frac{h^3}{12\eta}\frac{\delta P}{\delta z}\right)=\frac{1}{2}\frac{\delta(U_2-U_1)h}{\delta x}+(V_2-V_1)+\frac{1}{2}\frac{\delta(W_2-W_1)h}{\delta z} \qquad (5.2)$$

In this relationship, the left hand side terms are called pressure terms, whereas the right hand side terms are known as source terms. The terms of $\frac{\delta U}{\delta x}$ & $\frac{\delta U}{\delta z}$ depict stretching action, whereas $\frac{\delta h}{\delta x}, \frac{\delta h}{\delta z}$ represent the wedging action. The velocity difference term (V_1-V_2) is known as squeezing action as shown in figure no 5.7 [32].

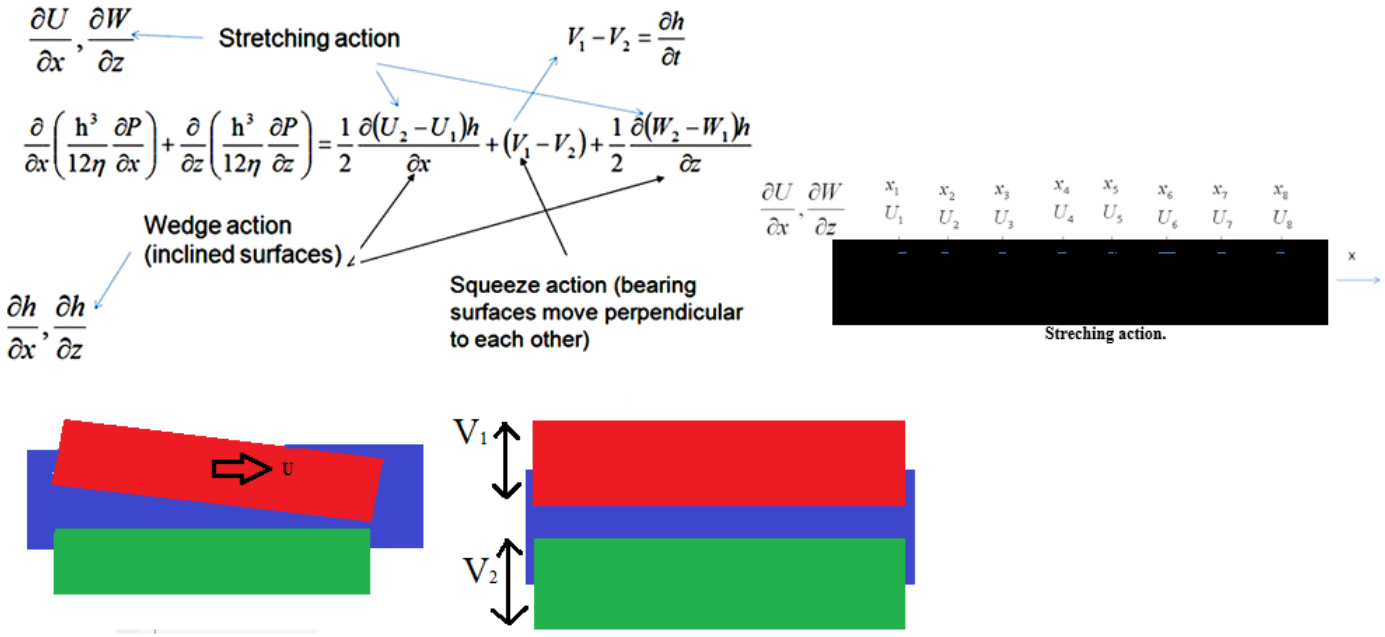

Figure no 5.7-Interpretation of terms in Reynolds equation [33]

Assuming that the lubrication oil used is a Newtonian fluid, flow is incompressible, value of viscosity is constant and neglecting various effects e.g. inertial forces, slip, angle of inclination, pressure gradient and stretching action, the Reynolds equation may be simplified as:

$$\frac{\delta}{\delta x}\left(h^3\frac{\delta p}{\delta x}\right)+\frac{\delta}{\delta z}\left(h^3\frac{\delta p}{\delta z}\right)=6\eta\,\frac{\delta(U_2-U_1)h}{\delta x}+12\eta\frac{\delta h}{\delta z} \qquad (5.3)$$

In order to estimate the oil pressure distribution, this equation needs to be solved. One way to do this, is by considering pressure variations in one direction as shown in figure no 5.8. The piston may be assumed to be as a kind of short bearing and circumfencial pressure gradient can be neglected as compared to axial one. Using these assumptions, the equation discussed above gets modified as:

$$\left[\frac{\delta}{\delta z}\left(h^3\frac{\delta p}{\delta z}\right)\right]=6\eta\,\frac{\delta h}{\delta x} \qquad (5.4)$$

Using boundary conditions of P (θ, z= $\pm\frac{L}{2}$) = 0, the closed form of pressure distribution P can be expressed as :

$$P=\frac{-3\eta\omega}{c^2}\,(x^2-\frac{L^2}{4})\,\frac{\xi\sin\theta}{(1+\xi\cos\theta)^3} \qquad (5.5)$$

Where c is skirt-liner gap and ξ is skirt-liner eccentricity.

The density of lubricant is dependent on the generated oil pressure (P) and density at mean liner temperature (ρ_0) as expressed from following equation [35]:

$$\rho=\rho_0\left[1+\frac{0.6\times10^{-9}\times P}{1+1.7\times10^{-9}\times P}\right] \qquad (5.6)$$

Grade of lubricant oil used also effects its viscosity. Table no F presents values of viscosity coefficients for different grades of SAE oils. The oil used in present study was of SAE30W grade for which viscosity may be expressed as [33]:

$$\eta=0.1531*\quad 9.8*10^4*a*e^{\left(\frac{b}{c}\right)} \qquad (5.7)$$

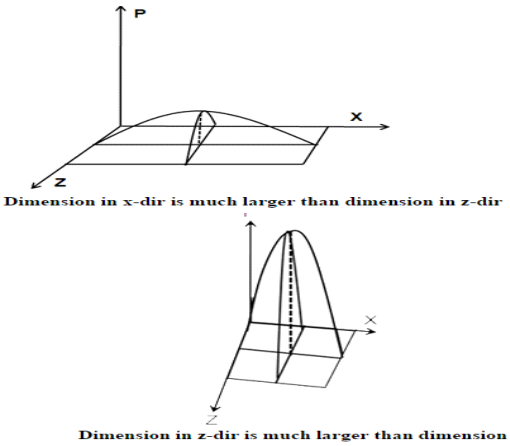

Figure no 5.8- Variation of pressure along one direction [32]

Since pressure terms have magnitude of order MPa and the oil film thickness are in microns, there may be some inconsistencies while solving the Reynolds equation. These may be sorted out by considering the Non-dimensionalization in which space coordinates may be written as:

$$\left.\begin{aligned} \bar{x} &= \frac{x}{X} \\ \bar{y} &= \frac{y}{Y} \\ \bar{z} &= \frac{z}{Z} \\ \bar{h} &= \frac{h}{C} \\ \bar{p} &= \frac{pC^3}{6\eta U X^2} \\ \bar{t} &= \frac{tU}{C} \end{aligned}\right\} \quad (5.8)$$

Substituting these non-dimensional values, the new equation gets modified as:

$$\frac{\delta}{\delta \bar{x}}\left(\bar{h}^3 \frac{\delta \bar{p}}{\delta \bar{x}}\right) + \frac{X^2}{Z^2}\frac{\delta}{\delta \bar{z}}\left(\bar{h}^3 \frac{\delta \bar{p}}{\delta \bar{z}}\right) = \frac{C}{X}\frac{\delta \bar{h}}{\delta \bar{x}} \qquad (5.9)$$

In order to solve this equation, finite element analysis (FEA) method has been used for which the mating surfaces were analyzed into number of nodes as shown in figure no 5.9 [32]. A mesh was made so that nodes on the lubrication zone of skirt correlates with those used in finite element analysis (FEA) to analyze the pressure distribution of lubricating oil.

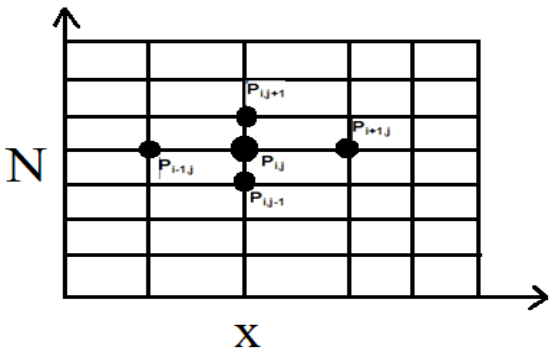

Figure no 5.9–Nodal representation of surface [32]

Various gradient terms of Reynolds relationship can be solved using Taylors approximation which yields following results [33]:

$$\bar{h}^3 \frac{\delta \bar{p}}{\delta \bar{x}} = \frac{\bar{h}_{i,j+0.5}{}^3 \bar{p}_{i,j+1} + \bar{h}_{i,j-0.5}{}^3 \bar{p}_{i-1,j} - (\bar{h}_{i,j+0.5}{}^3 + \bar{h}_{i,j-0.5}{}^3)\bar{p}_{i,j}}{\Delta \bar{x}^{-2}} \qquad (5.10)$$

$$\bar{h}^3 \frac{\delta \bar{p}}{\delta \bar{z}} = \frac{\bar{h}_{i,j+0.5}{}^3 \bar{p}_{i,j+1} + \bar{h}_{i,j-0.5}{}^3 \bar{p}_{i-1,j} - (\bar{h}_{i,j+0.5}{}^3 + \bar{h}_{i,j-0.5}{}^3)\bar{p}_{i,j}}{\Delta \bar{z}^{-2}} \qquad (5.11)$$

$$\frac{\delta \bar{h}}{\delta \bar{x}} = \frac{\bar{h}_{i+1,j} - \bar{h}_{i-1,j}}{2\,\Delta \bar{x}} \qquad (5.12)$$

Substituting these relationships and rearranging them we have:

$$P_{i,j} = A_{i,j} P_{i,j+1} + B_{i,j} P_{i,j-1} + C_{i,j} P_{i+1,j} + D_{i,j} p_{i-1,j} + E_{i,j} \qquad (5.13)$$

Most of values of nodal pressure ($P_{i,j}$) are unknown so an iterative loop must be used with suitable convergence limits (£) to get values of pressure. i.e.

$$\frac{(\sum_{i=1}^{n}\sum_{j=1}^{m} \bar{p}_{i,j})_{iteration\,k} - (\sum_{i=1}^{n}\sum_{j=1}^{m} \bar{p}_{i,j})_{iteration\,k-1}}{(\sum_{i=1}^{n}\sum_{j=1}^{m} \bar{p}_{i,j})_{iteration\,k}} \leq £ \qquad (5.14)$$

A MATLAB code was used to analyze the lubrication behavior of oil between piston skirt and liner considering its motion of skirt analogous to that of journal inside a bearing [32].

Plots of oil pressure distribution on the piston skirt plane were next analyzed for each 90° crank angle rotation of skirt in case of a single cylinder of engine for a compete cycle as shown in figure no 5.10-5.13. Rotation operating speed of engine was taken as 2000 RPM with skirt-liner gap of 0.05mm and SAEW30 type oil.

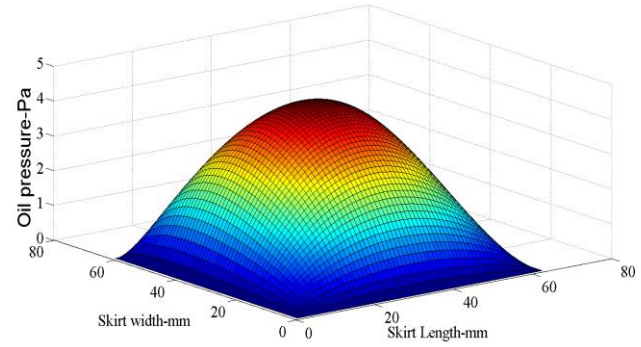

Figure no 5.10-Oil pressure distribution (180° crank angle)

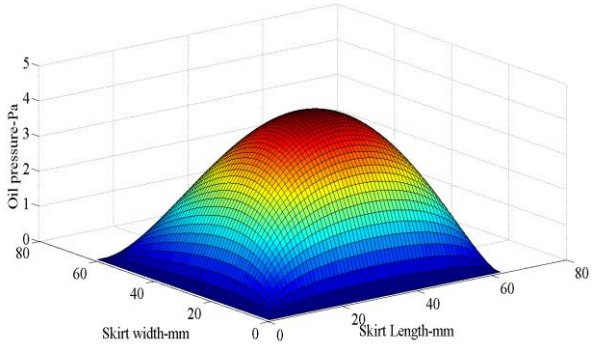

Figure no 5.11-Oil pressure distribution(360° crank angle)

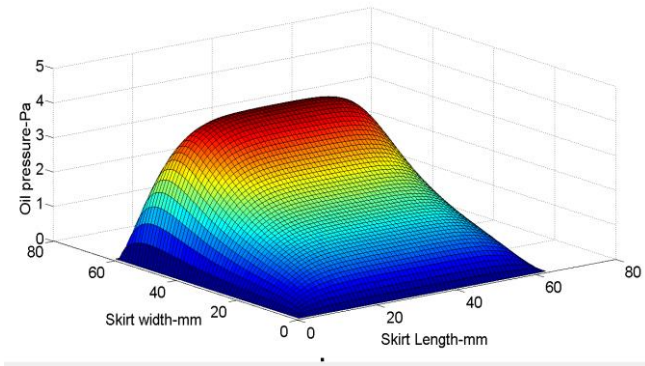

Figure no 5.12-Oil pressure distribution (540°crank angle)

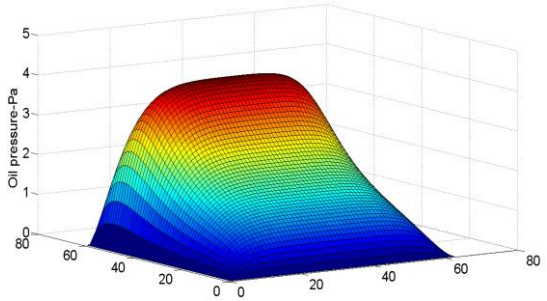

Figure no 5.13-Oil pressure distribution(720°crank angle)

At 180° crank angle position at the end of intake stroke, peak pressures were observed towards the midpoint of skirt. At 360° crank angle position, as the end of compression stroke approaches, the slopes of pressure curves starts shifting slightly towards right hand side. At 540° crank angle, the peak values of oil pressures were seen to shift towards the bottom part of skirt. During the exhaust stroke peak of slopes again shifted slightly towards right side. The energy transferred to liner due to impacts ($W_{I,J}$) can be calculated using average of local force ($\tilde{F}_{I,J}$) between two time steps as [32]:

$W_{I,J} = \tilde{F}_{I,J} (h_{2I,J} - h_{1I,J})$ (5.15)

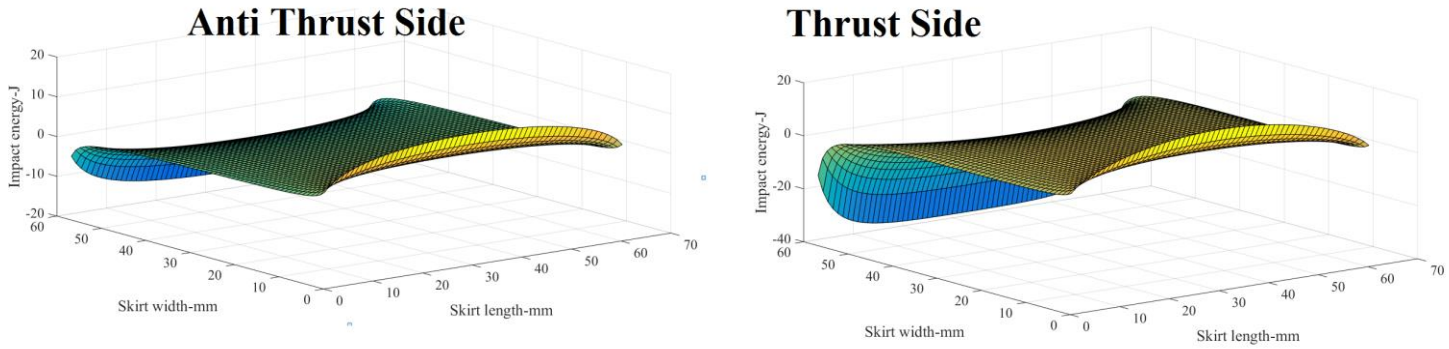

Figure no 5.14–Impact Energy (720°crank angle)

Figure no 5.14 shows variations of impact energy transferred to liner walls at 2000 RPM speed at 720˚ crank angle position. It is clear that energy is transferred both on thrust as well as anti -thrust sides at the same time. When value of $W_{I,J}$ is positive, lubricant is squeezed and oil film absorbs the impact energy. Otherwise this energy is utilized in skirt deformation.

The acoustic power available at surface of engine (P_a) is written in terms of radiation efficiency (σ), density of air (ρ_a), wave speed (c_a), area of noise radiating surface (A_r) and surface velocity (v_r) as [32]:

$P_a = \sigma * \rho_a * c_a * v_r^{\,2} A_r$ (5.16)

Impact power (P_v) can be expressed in terms of impedance (Z) and impact velocity V_v by the following relationship:

$P_v = Z V_v^2$ (5.17)

Hence overall transmission efficiency (η_t) can be written in terms of these responses and expressed as:

$\eta_t = \frac{Pa}{Pv} = \frac{\sigma V^2 r \rho_a C_a A_r}{Z V_v^2}$ (5.18)

Using law of conservation of energy, it may be assumed that impacting energy is transmitted without any loss to outer surface of skirt and may be expressed in terms of thickness of structure (h), area (A), velocity (V) and density (ρ). i.e.[32]

$\frac{1}{2}\rho_v h_v A_v V_v^{\,2} = \frac{1}{2}\rho_R h_R A_R V_R^{\,2}$ (5.19)

Where subscript v denotes liner structure and R denotes engine block.

Hence the transmission efficiency at each node (i, j) at both thrust and anti -thrust side may be expressed by [32]:

$\eta_t(i,j) = \frac{\sigma \rho_v \rho_a h_V C_a A_v(i,j)}{Z_{i,j}\, \rho_R h_R}$ (5.20)

Where $Z(i,j) = \frac{F_v(i,j)}{V_v(i,j)}$

The SPL at each node can be estimated taking reference pressure level P_{ref} ($2*10^{-6}$ Pa) and expressed in terms of distance of microphone from engine block (R) as [32]:

$SPL_{i,j} = L_{i,j} + 10\log\left(\frac{S^-}{4\pi R^2}\right)$ (5.21)

Where $L_{i,j} = 10\log\left(\frac{P_{a\ i,j}}{P_{ref}}\right)$

For far field conditions, the value of S^- is taken as 2 as acoustic field is assumed as semi spherical one. The total sound pressure level (SPL) may be expressed as sum of levels both at thrust as well as anti-thrust side. For comparisons, SPL levels under both steady state (no lubrication effects) and transient conditions (with effects of lubrication oil) were compared with actual measurements for test case no B3 listed in table no 2.1 as seen in figure no 5.15.

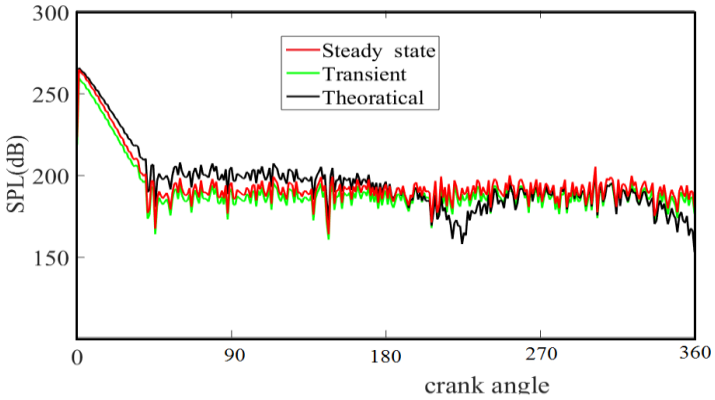

Figure no 5.15–Variations in SPL

The experimental data has contributions due to all other sources, whereas the theoretical one focuses just on skirt-liner interactions. Hence during suction and compression strokes the theoretical data is seen to achieve higher values as compared to experimental data as the gas pressure is reduced and the contributions due to other sources are more dominant.

5.4 Occurrence of Piston Slap Events

Figure no 5.16 shows various forces and moments acting on skirt assembly. Various forces acting on skirt includes frictional force between liner and skirt (F_f), gas force (F_g) and oil reaction force (F_h). Piston skirt having moment of inertia depicted J tilts by an angle β and has some pin offset distance (d_p) and center of gravity offset (d_{COG}). Connecting rod exerts a lateral force depicted by F_t on liner which is given by following equation [22]:

$F_t = m_p X_p'' - F_{hyd} = F_L \sin\phi = [F_G - m_p Y_P'' + F_f] \tan\phi$ (5.22)

Hydrodynamic reaction forces are given by solution of Reynolds equation [34-37].

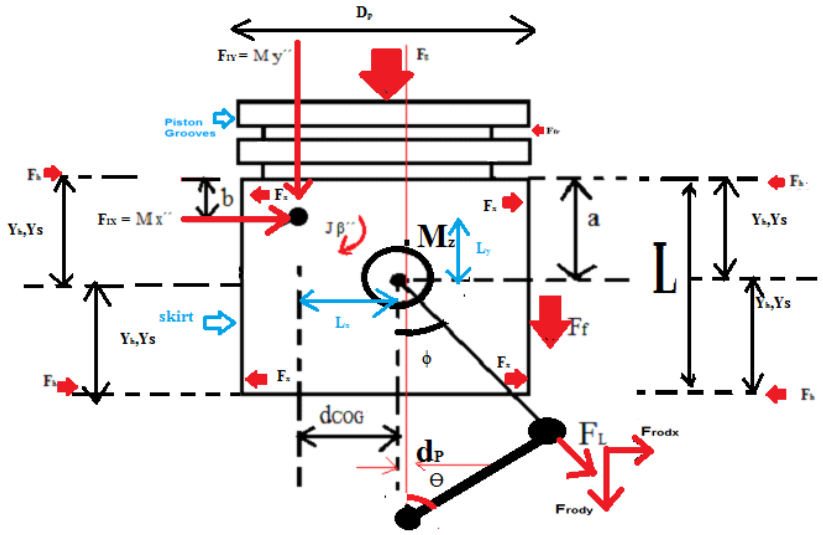

Figure no 5.16 -Piston skirt assembly forces and moments

Applying moment balance equation, we have [38]:

$$(J+M\,[d_{COG}{}^2-(a-b)^2])\,\beta''+M\,X_p''(a-b)-My''d_{COG}=-T_f+T_G+F_h Y_h \qquad (5.23)$$

Changes in the direction of lateral forces is an important way to diagnose the instances of piston slap motion. This occurs when Tan $\phi = 0$ at TDC ($\phi=0$) and BDC ($\Theta = k\pi$, k=0,1,2...) positions. Exact values of ϕ can be determined using following relation which has been expressed in terms of connecting rod length (l), crank radius (r), crank case offset (C) as [37]:

$$\Phi = \sin^{-1}\left(\frac{r\cos\Theta+C}{l}\right) \qquad (5.24)$$

When gas force is greater than inertial force, slap occurs at thrust side of liner and vice versa.

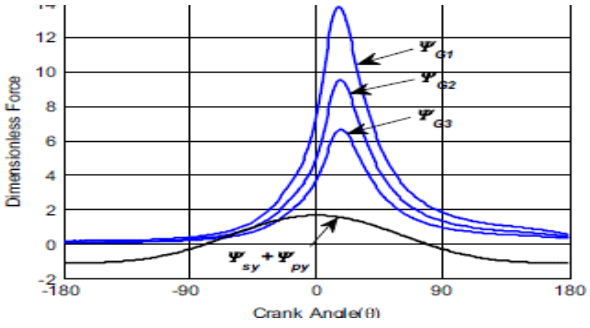

Figure no 5.17 -Piston force distribution [37]

Figure no 5.17 shows the graphical representation of balance between various forces acting on piston skirt. The coincidence points between dimensionless form of gas forces (ψ_G) and total inertial forces ($\psi_{SY} + \psi_{PY}$) indicates possible locations of slapping motion [37]. Higher numeric subscripts in Ψ_G denotes higher operational speeds of engine. For lower values of engine speeds (Ψ_{G1}), the graphs of gas forces and inertial forces do not meet at any point. For case of Ψ_{G3}, up to five intersections points were observed.

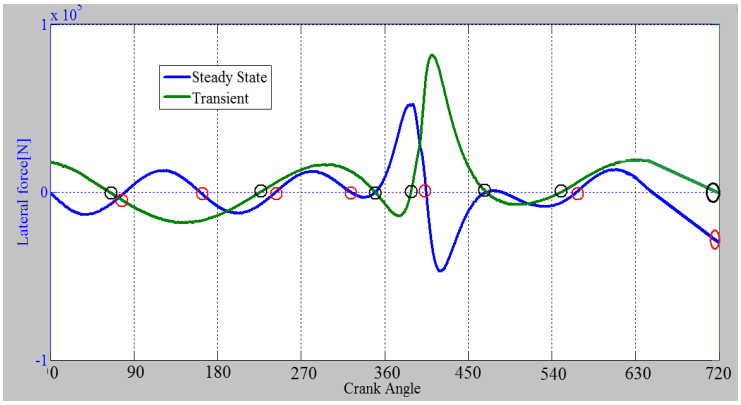

Figure no 5.18-Piston side thrust force (2000 RPM)

The concept of lateral force (also known as side thrust force) as represented by equation no 5.22, has been analyzed next for prediction of slapping events. Whenever values of this force changes its direction crossing the zero markings, an instant of slapping event is expected to occur as depicted by circles in figure no 5.18. Negative values of this force depicts contact along the thrust side (T.S.), whereas positive values indicate contact with anti -thrust side (A.T.S). Gas forces acting on skirt are dominant during the compression stroke up to 360º crank angle position. Hence during this interval, side thrust forces calculated using both steady state and transient approaches shows some match, whereas during later parts of engine cycle there is a greater mismatch as inertial forces dominate. There were at least 9 potential events of slapping motion identified in Table no 5.1 using the above mentioned approaches.

Slap no	Steady state method	Transient state method
1	70°	60°
2	170°	240°
3	240°	340°
4	320°	390°
5	340°	470°
6	400°	550°
7	470°	720°
8	560°	-
9	720°	-

Table no 5.1-Summary of locations of slap events (Lateral Force method)

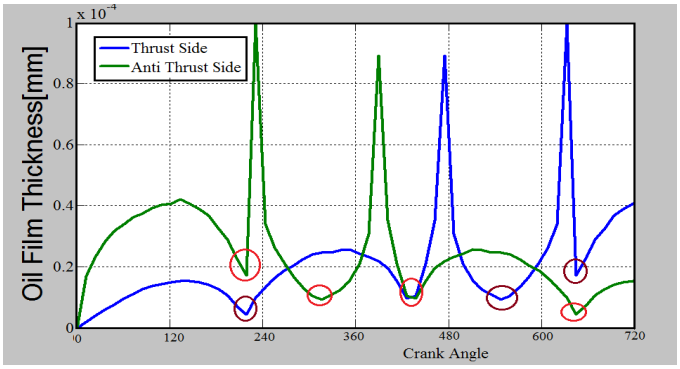

Figure no 5.19-Oil film thickness behavior at 2000 RPM

The concept of oil film thickness (as represented by equation no 5.4) was examined next in figure no 5.16 by assuming that skirt-liner gap is fully flooded with lubricant flow. Perera has previously studied oil film thickness using multi-physics model considering piston as a rigid body [36].

The thickness of oil film was evaluated over the entire length of skirt with its minimum value labelled as a possible instance of skirt-liner contact. During the intake stroke the film thickness falls and then again rises during compression stroke reaching its maximum value. This indicates lesser magnitude of lateral motion of skirt. During the expansion stroke film thickness again drops to minimum value indicating development of full hydrodynamic lubrication. During the exhaust stroke the film thickness falls again reaching minimum value at 650 °crank angle position. Based on the minimum values of oil film thickness, four possible events of skirt-liner contact were identified occurring both at thrust as well as anti-thrust side. These locations were found to be [220°,300°,420°,630°] for anti-thrust side and [230°,420°,540°,620°] for the thrust side. The positions of minimum oil film thickness may not always coincide with those of maximum pressure developed.

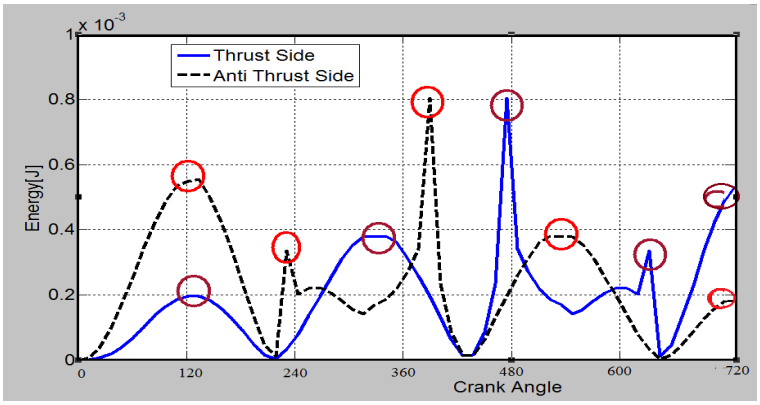

Figure no 5.20-Transferred energy behavior at 2000 RPM

Locations of instances of slapping motion on basis of maximum energy transfer method were seen as [120°,240°,370°,500°,720°] for anti -thrust side and [130°,200°,480°,630°,710°] in case of thrust side as marked in figure no 5.21.

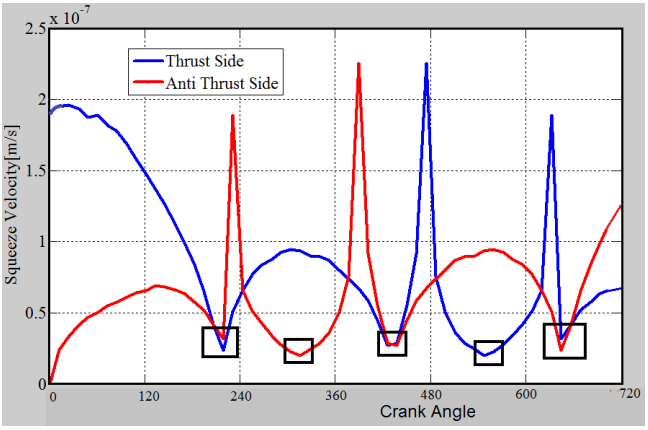

Figure no 5.21 -Squeeze velocity of lubricant at 2000 RPM

In the Reynolds equation, the term $\frac{\delta h}{\delta t}$ denotes the rate of change of oil film thickness which may be negative (squeezing action) or positive(separation). Hence a change in sign of this term indicates a possible event of piston slap. Locations of instances of slapping motion on the basis of analysis of squeezing velocity were found to be [220°,270°,420°,630°] for anti -thrust side and [230°,420°,540°,620°] for thrust side as seen in figure no 5.21.

The above mentioned location of events were validated next by recording actual engine block vibrations both towards thrust as well as anti- thrust side by operating the test engine at 2000RPM under full load condition. Vibration signals were filtered in frequency range [450Hz-3000Hz] which was found to be dominated by piston-slapping events based on the previous works [20, 21, 22]. Wavelet analysis of signals can be seen in figure no 5.22, 5.23. Events having higher energy are seen having wider frequency ranges.

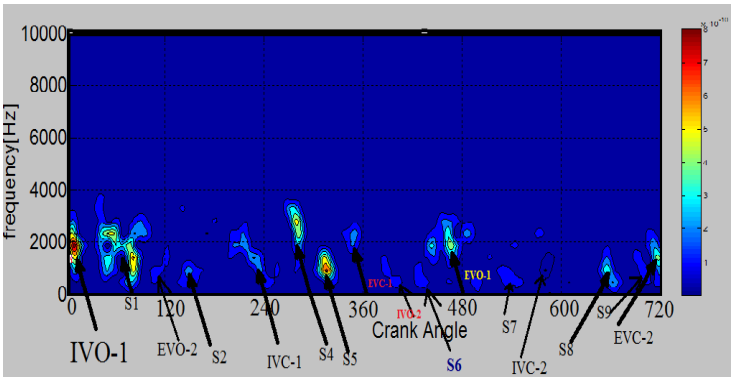

Figure no 5.22-Time frequency analysis of Filtered acceleration (Thrust Side)

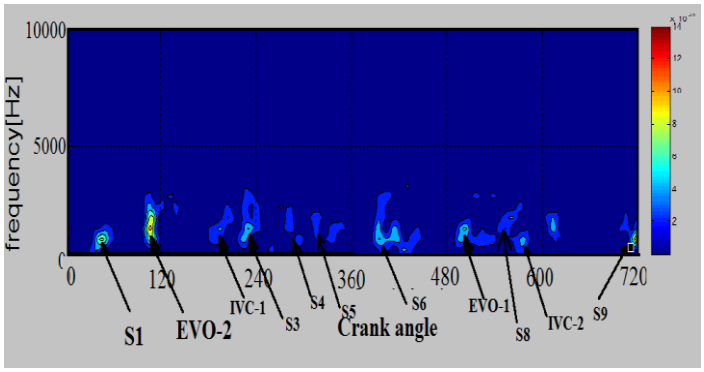

Figure no 5.23-Time frequency analysis of Filtered acceleration signals (Anti Thrust Side)

There were some traces of energy levels visible which may be contributed to other cyclic events occurring during course of operation cycle of engine. Inlet valve opens (IVO) at 10° crank angle before TDC position, whereas its closure (IVC) occurs 42°after BDC during compression stroke. Opening of exhaust valve (EVO) takes place at 58° before BDC position and closure occurs 10° after TDC (EVC). Contributions of these cyclic events towards vibration signature was observed for case of both cylinders.

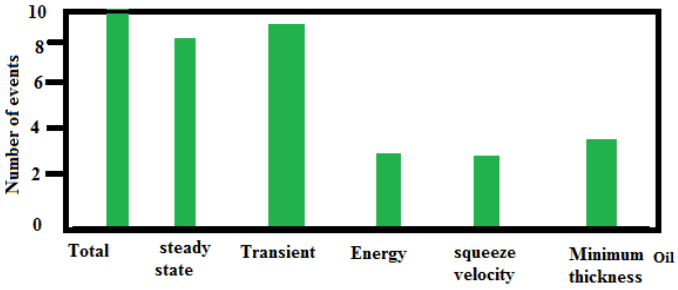

Table no 5.2- Comparison of accuracy of various methods

The actual locations of events were compared with theoretical methods discussed above. Transient approach was found to be more precise than steady state method to predict instances of various events as shown in table no 5.2. Slight deviations in prediction of exact location of events may be attributed to negligence of various parameters like inertia of connecting rod, bearings and crank shafts.

5.5 Piston Motion analysis using software

A multi body dynamics model of piston skirt using COMSOL Multi physics-7 was used for analysis of its lateral motion. Tetrahedral elements were used to mesh the quarter part of skirt. Material used for simulation was Al alloy having density 2700kg/m^3, Young's modulus 72GPa and poison ratio of 0.31. Figure no 5.24-5.28 shows various profiles of skirt analyzed for various testing cases enlisted in table no 4.2.

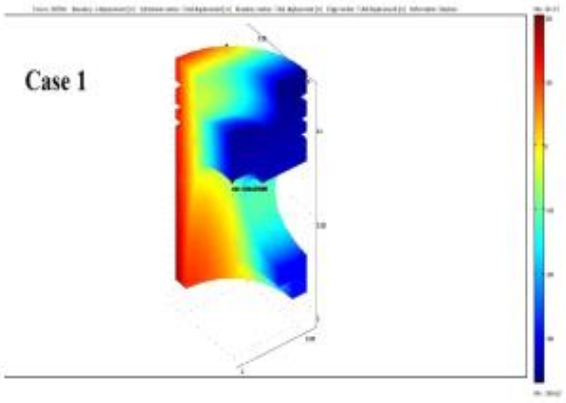

Figure no 5.24 -FEA model of piston skirt(Case1)

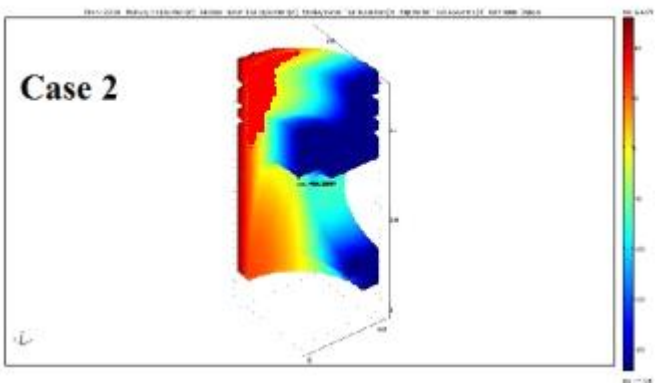

Figure no 5.25-FEA model of piston skirt(Case2)

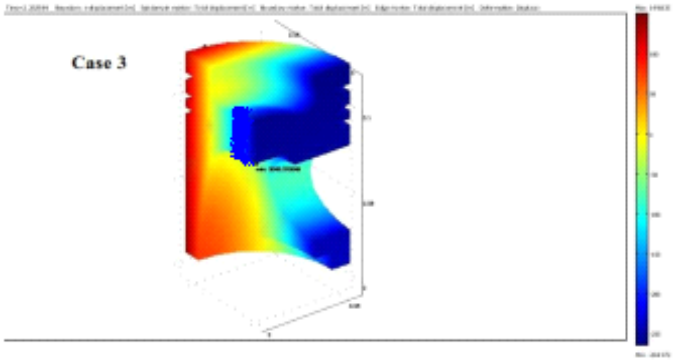

Figure no 5.26-FEA model of piston skirt(Case3)

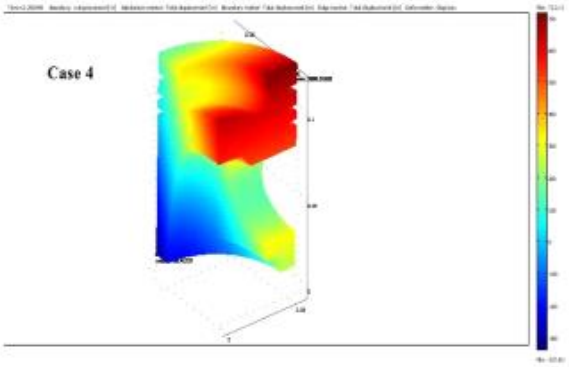

Figure no 5.27-FEA model of piston skirt(Case4)

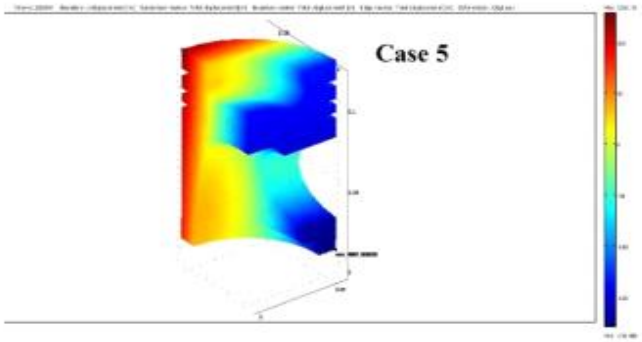

Figure no 5.28 -FEA model of piston skirt(Case5)

Results were obtained for the lateral surface velocity of skirt as seen in figure no 5.29, 5.30. This velocity was seen to decrease with increase of engine speed as hydrodynamic action of oil becoming more dominant.

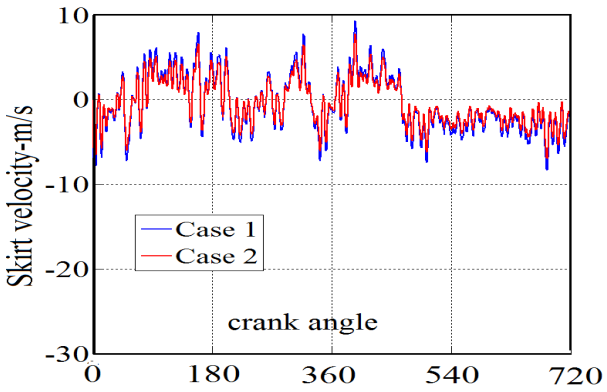

Figure no 5.29-Lateral velocity of piston skirt (2000 RPM-100% load)

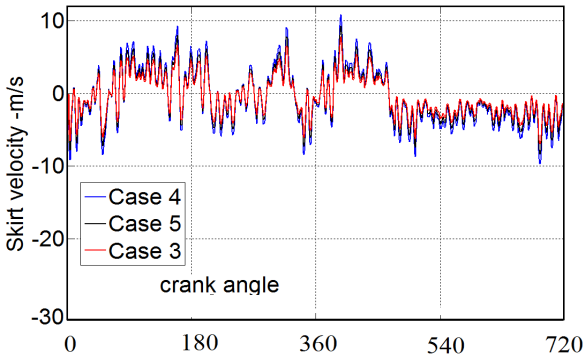

Figure no 5.30-Lateral velocity of piston skirt(3000RPM-100%load)

5.6 Force Analysis

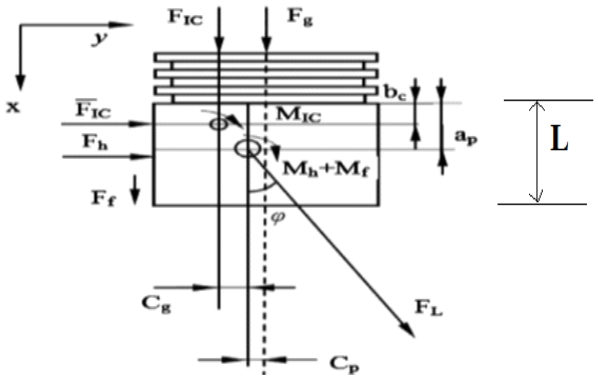

Figure no 5.31 -Piston skirt force and moments [39]

Parameter	Value
S	68 mm
r_p	34 mm
l	121mm
L	62.65 mm
μ	0.03Pa-s
ω	2000RPM,3000RPM
m_{piston}	179g
m_{pin}	84g
m_{sl}	100g
m_t	363g
b_c	31.3250mm
a_p	36.9mm
I_{piston}	$6.6*10^{-8}$kg-m^2
Cp	0 mm
Cg	0 mm
C	0.05mm

Table no 5.3-Engine parameters

Various forces and moments acting on skirt are shown in figure no 5.31. As the gas force (F_g) acts on top part of skirt, the hydro dynamic oil film force (F_h) creates a moment M_h about piston pin axis. Tiling angle of connecting rod is denoted by φ.

The axial displacement of piston along liner (Z) can be expressed as [39]:

$Z = -r_p \cos\theta - (l^2 - B_s^2) + \sqrt{(l + r_P)^2 - C_p^{\,2}}$ (5.25)

Where $B_s = r_p \sin\theta + C_p$

This equation was differentiated to get values of axial velocity of skirt as plotted in figure no 5.32.

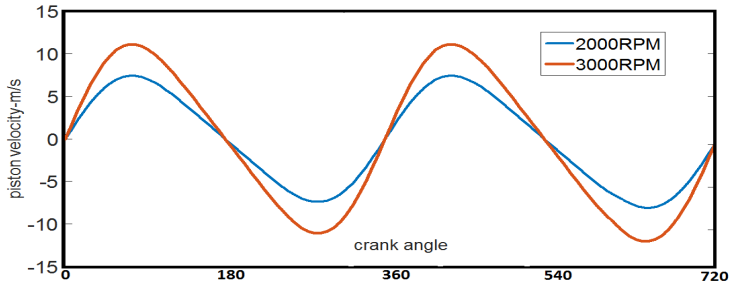

Figure no 5.32 -Axial velocity of skirt

The inertial force acting along X axis (F_{IC})may be expressed as [39]:

$$F_{IC} = -(m_{piston} + m_{pin} + m_{sl})\left[r_p w \cos\Theta + \frac{(r_p w B_s \cos\theta)^2}{\sqrt{l^2 - B_s^{\,2}}} + \frac{r_p w^2 (r_p \cos\theta^2 - cos\theta\, B_s)}{\sqrt{l^2 - B_s^{\,2}}}\right] \quad (5.26)$$

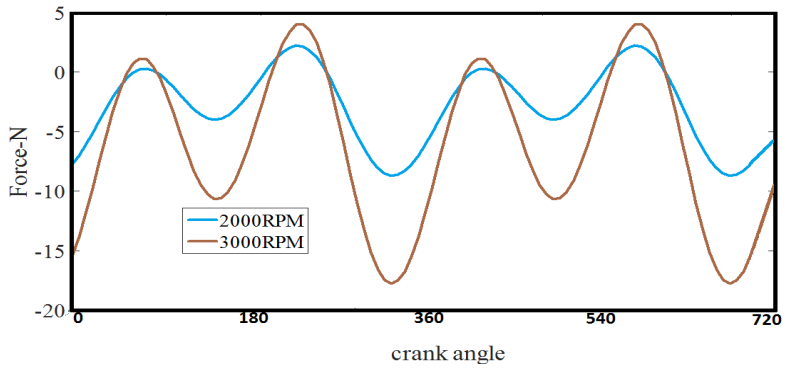

Figure no 5.33-Variations in Inertial force along X axis

Gas force acting on piston top (F_g) may be expressed in terms of in cylinder pressure (P_g) and piston diameter(D) as:

$F_g = P_g * \pi \frac{D^2}{4}$ (5.27)

Inertial forces along Y axis (F^{-}_{IC}) may be expressed as [39]:

$$F^{-}_{IC} = (m_{piston} + m_{pin} + m_{sl})\left[\frac{de^2{}_t}{dt^2} - \frac{b_c}{L}\left(\frac{de^2{}_t}{dt^2} - \frac{de^2{}_b}{dt^2}\right)\right] \quad (5.28)$$

As piston slides along the liner, frictional force between liner and skirt cause a shear force (τ) in oil film which can be expressed as [40]:

$\tau = \mu \frac{U}{h}$ (5.29)

Where U is axial skirt velocity, h is oil film thickness and μ is dynamic viscosity of oil.

The friction force between skirt and liner (F_f) and resulting moment about the wrist-pin (M_f) can be calculated based on the shear stress as [39] :

$F_f = R \iint \tau(x, \theta) dx\, d\theta$ (5.30)

$M_f = R \iint \tau(x, \theta)(R\cos\theta - C_p) dx\, d\theta$ (5.31)

The oil film force (F_h) and its moment about wrist pin (M_h) due to the nonlinear pressure distribution $p(x, \theta)$, can be written as [39]:

$F_h = R \iint [p(x,\theta)] \cos\theta \, dx \, d\theta$ (5.32)

$M_h = R \iint [p(x,\theta)](a_p - x) \cos\theta \, dx \, d\theta$ (5.33)

The rotatory moment about wrist pin (M_{IC}) can be calculated as:

$M_{IC} = -\frac{I_{piston}}{L}\left(\frac{de^2_t}{dt^2} - \frac{de^2_b}{dt^2}\right)$ (5.34)

Further various force and moment balance equations for the system may be expressed as:

$F_g + F_{IC} + F_f + F_L \cos\varphi = 0$ (5.35)

$F_h + \bar{F}_{IC} + F_L \sin\varphi = 0$ (5.36)

$M_h + M_{IC} + \bar{F}_{IC}(a_p - b_c) + F_g C_p - F_{IC} C_g + M_f = 0$ (5.37)

Magnitude of piston secondary motion is defined by skirt displacements normal to axis of liner. These are represented as top eccentricity (e_t) and bottom eccentricity (e_b) as represented in figure no 5.5. In matrix form the numerical model may be expressed in the form:

$$\begin{bmatrix} m_{pis}\left(1-\frac{b_c}{L}\right)+m_{pin}\left(1-\frac{a_p}{L}\right) & m_{pis}\left(\frac{b_c}{L}\right)+m_{pin}\left(\frac{a_p}{L}\right) \\ m_{pis}\left(1-\frac{a_p}{L}\right)(b_c-a_p)+\left(\frac{I_{piston}}{L}\right) & m_{pis}\left(\frac{a_p}{L}\right)(b_c-a_p)-\left(\frac{I_{piston}}{L}\right) \end{bmatrix} \begin{bmatrix} e''_t \\ e''_b \end{bmatrix} = \begin{bmatrix} F_h-(F_{IC}+F_g+F_f)Tan\,\phi \\ M_h+M_f+F_g C_P-F_{IC}C_g+\bar{F}_{IC}(a_p-b_c) \end{bmatrix} \quad (5.38)$$

These equations of piston lateral motion were solved by using various skirt design parameters enlisted in table no 5.3. Input parameter used was in cylinder pressure data acquired for a single cylinder of engine at 2000 RPM speed under full load condition.

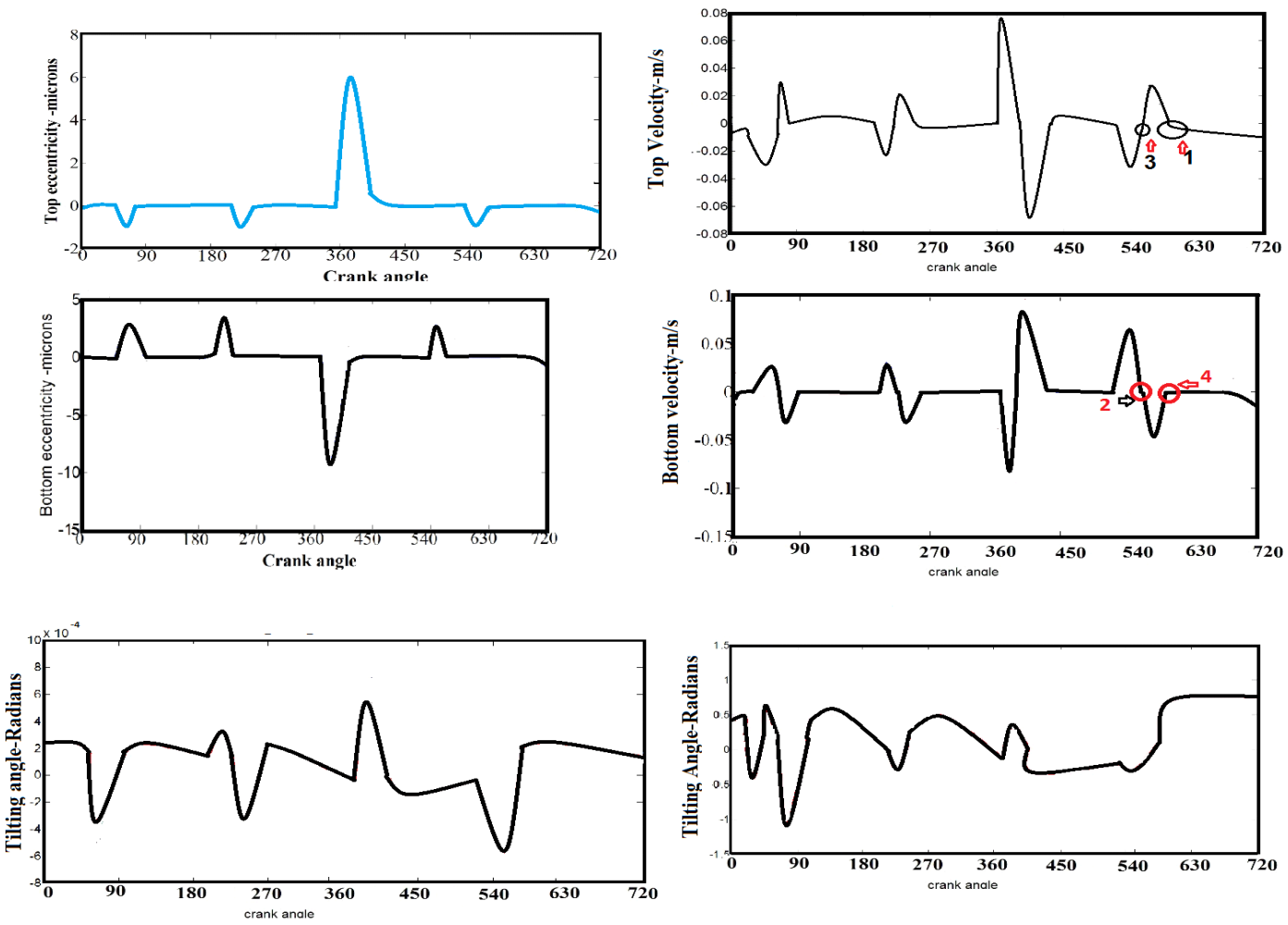

Figure no 5.34-Variations of piston dynamic parameters

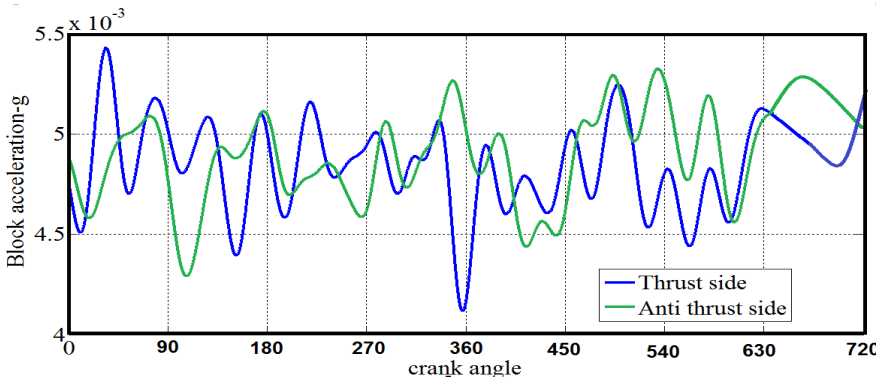

Figure no 5.35 -Block vibrations

Figure no 5.34 shows variations of different parameters that quantify lateral motion of skirt. Largest variations in skirt eccentricities are seen around TDC position (360˚ crank angle) which indicates possible instance of impact. However, there may be certain uncertainties, hence surface vibration signals acquired both at sides of liner were analyzed as seen from figure no 5.35. The amplitudes of these vibrations were found to be inconsistent mostly during power stroke as combustion pressures reached their peak values. Two events during exhaust stroke (540°-720°) in top skirt velocity curve (marked as 3 and 1) as well as in bottom velocity curve (2 and 4) were identified at which lateral velocities of skirt are almost zero, but corresponding block vibrations shows high amplitudes. Hence it can be concluded that prediction of slapping events using skirt velocity profile has a higher degree of uncertainty.

5.7 Effects of various skirt design parameters on lateral motion of skirt

a) Effects of piston pin offset distance

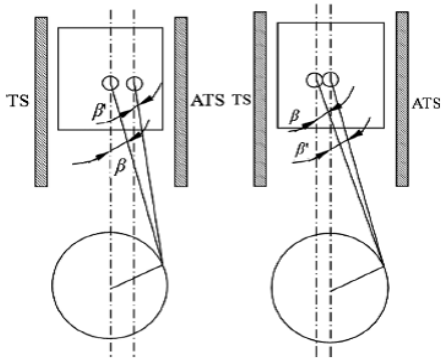

Figure no 5.36-Variations of piston pin offset distance [39]

The location of piston pin may be designed in order to offset either towards the thrust side or anti thrust side of liner with a typical amplitude of 0-2mm as shown in figure no 5.36. Suitable values of piston pin offset not only effects the dynamic motion of skirt but also load equilibrium. There is a tradeoff between these two offset positions as in order to reduce lateral motion, the piston pin should offset towards thrust side, whereas to reduce the wear it must be offset towards the anti- thrust side [38]. In present analysis, the piston pin offset distances (Cp) inclines towards anti thrust side when values of Cp are positive and towards thrust side as for negative values. Figure no 5.37-5.39 shows comparisons of various dynamic features of piston lateral motion using three different offset values of -1mm,0mm, +1mm respectively. As the skirt moves towards BDC after mid stroke (90˚-180˚crank angle duration), various dynamic parameters remain almost unchanged and hence lubrication of skirt can be assumed to be stable. After the onset of expansion stroke, at around 387°crank angle position these parameters have shown noticeable changes which may induce noise and vibrations due to lateral motion of skirt.

The results show that maximum values of lateral tilting velocities of top part of skirt were 0.055m/s,0.06m/s,0.07m/s when offset distances were -1mm,0mm and 1mm respectively, and these were observed at 350º, 340º and 330º crank angle positions. The values of top eccentricities were found to increase as offset moves towards the anti-thrust side. The values of moment about piston pin due to gas force (M) decreases as the offset is made towards thrust side, hence lateral displacements are lesser with Cp = -1. This along with increased value of side thrust force $F=(F_g+F_{IC})\ Tan\beta$ prevents further tilting of skirt.

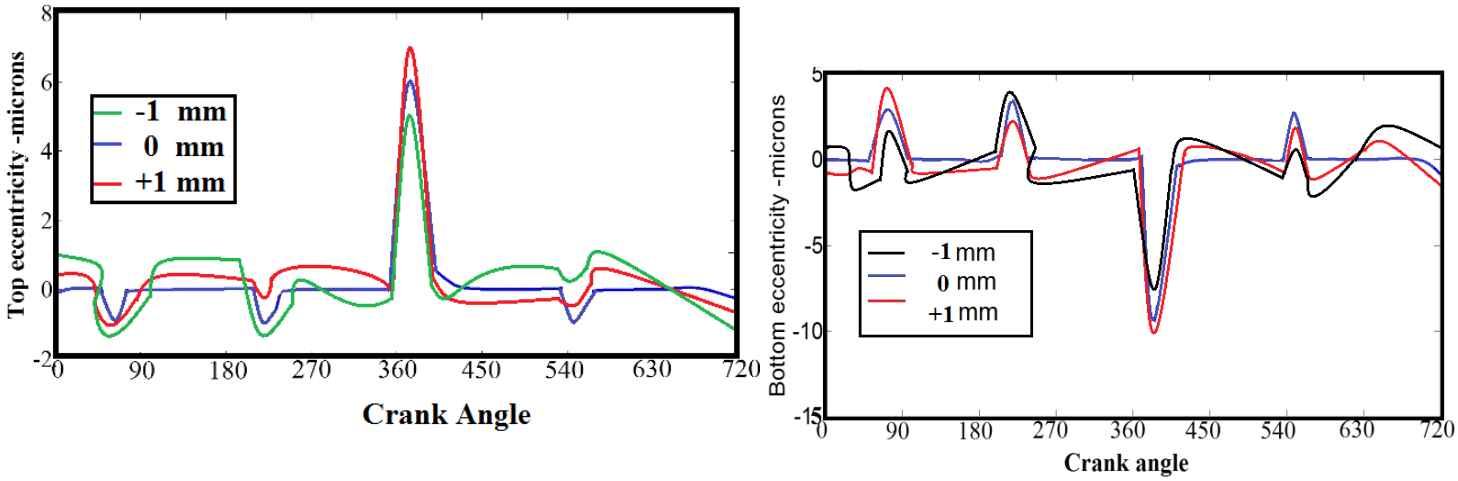

Figure no 5.37-Variations of eccentricities with piston pin offset distance

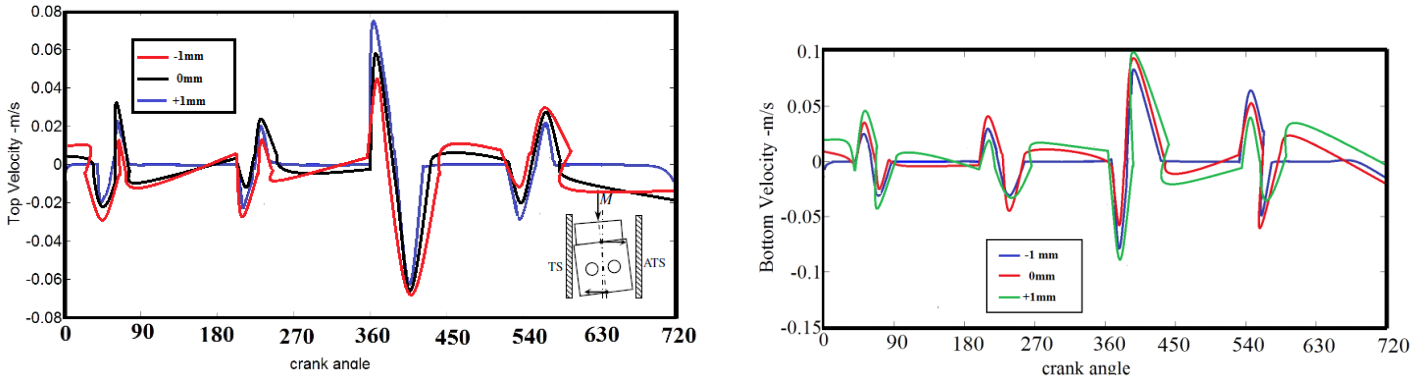

Figure no 5.38-Variations of tilting velocities with piston pin offset distance

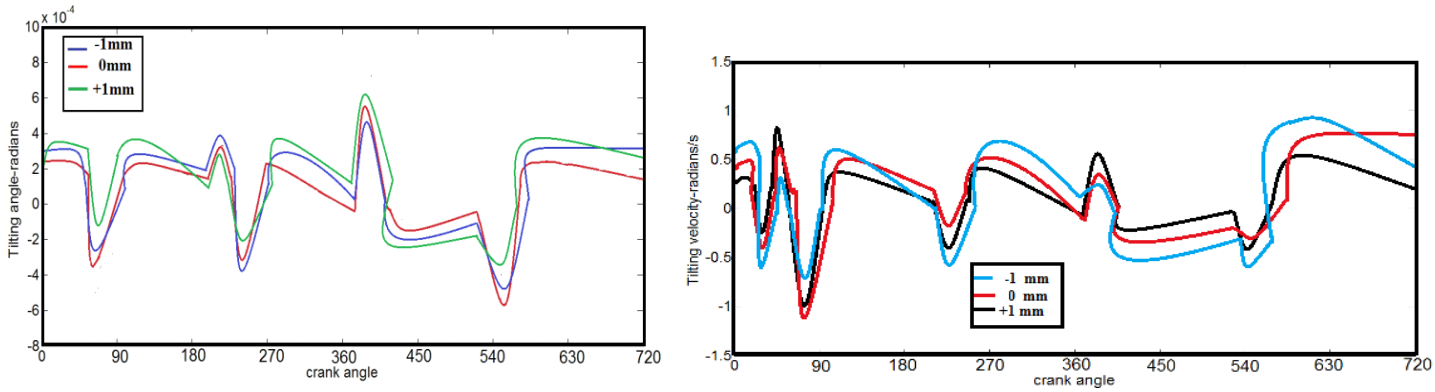

Figure no 5.39-Variations of tilting parameters with piston pin offset distance

b) Effect of skirt-liner gap

The gap between piston skirt and liner walls is a crucial factor to control thickness of lubrication oil film formed. Suitable values of this gap not only increases the load bearing capacity of skirt but also helps to control secondary motion of skirt. It has been suggested that optimum value of this gap must be kept in range of 0.01mm-0.09mm [39]. However, it is difficult to predict exact values of this gap due to thermal deformations of skirt as well as manufacturing tolerances. The energy of impacts due to piston secondary motion (E_I) consists of contributions due to both rotational as well lateral components. i.e.

$$E= \frac{1}{2}MV^2 + \frac{1}{2}J\theta'^2 \qquad (5.39)$$

As a major portion of slap occurs near TDC, so major focus is on these crank angle positions. In order to simulate the dynamic features of secondary motion three values of clearances were chosen as seen in figure no 5.40-5.42. The results show that skirt changes its direction near 360° crank angle positions. The maximum values of displacements of top part of skirt are 8µm,7µm and 6µm for clearance values of 0.08mm,0.07mm and 0.05mm respectively and these occurred at 372°crank angle position. Greater values of clearances provide larger space for lateral movement of skirt. However, lateral velocity of piston also contributes towards slapping noise. Increase in the skirt-liner gap also increases this velocity. The maximum values of e_t' for the three clearances were observed to be 0.08m/s,0.075ms/s and 0.07m/s for skirt-liner gaps of 0.08mm,0.07mm and 0.05mm respectively, whereas e_b' values were -0.1m/s, -0.09m/s and-0.08 m/s.

When clearances are small, higher shear forces will be generated leading to greater surface asperity contacts which in turn causes higher frictional losses. At smaller gaps the sliding motion of skirt along liner is for longer duration with few rebounds. With an increase in values of the lateral motion of skirt shifts from periodic to chaotic one. So larger oil film reaction forces are needed to prevent contact of skirt with liner. From the plots of velocity of skirt, it is clear top edge is moving away from the thrust side of liner and tilting towards anti-thrust side before TDC. Bottom edge is tilting towards thrust side. After TDC position reverse trends were observed.

Apart from rotational velocity of skirt must also be taken into account. The rotational moment about piston pin falls with a decrease in clearance values which prevents further rotation of skirt about piston pin. Hence the rotational velocity falls with a decrease in skirt-liner gap.

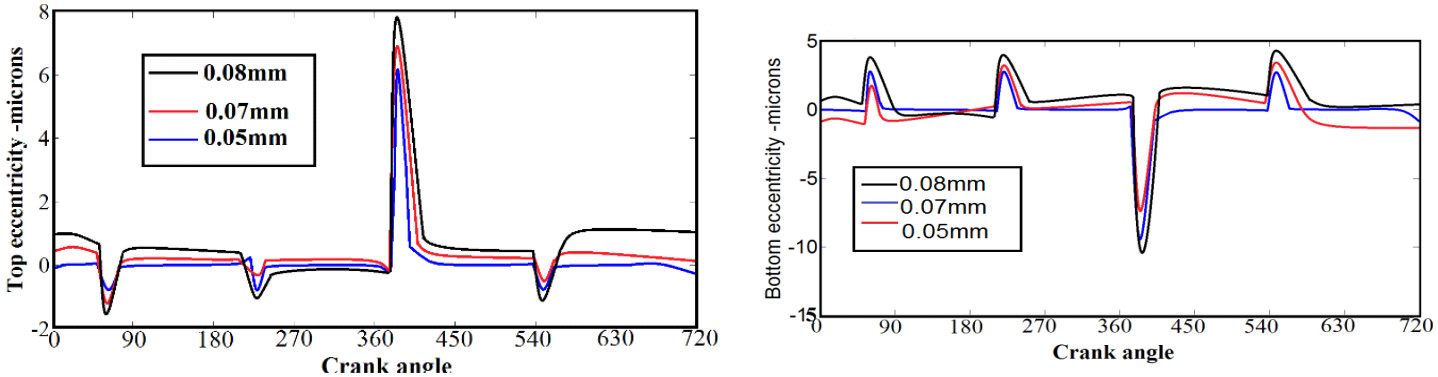

Figure no 5.40-Variations of eccentricities with skirt-liner gap

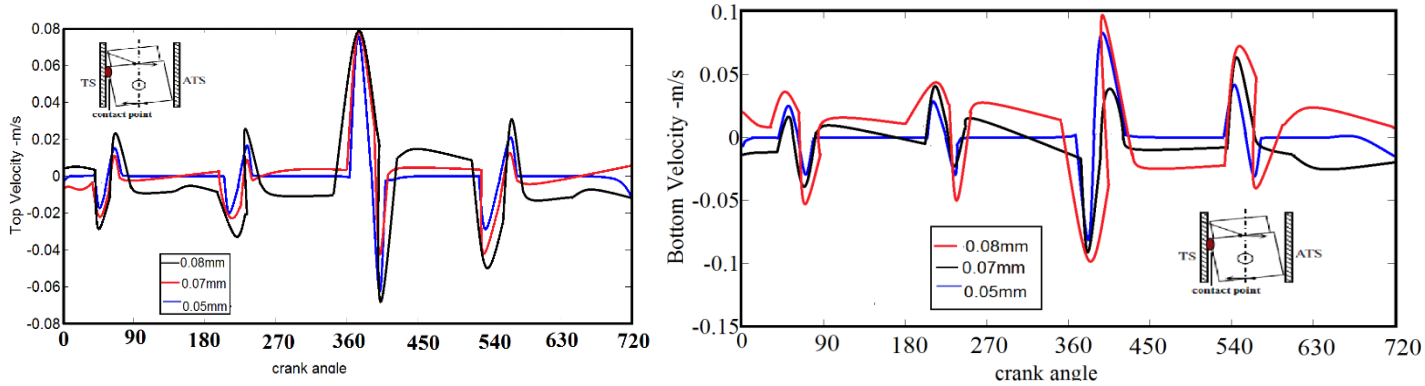

Figure no 5.41-Variations of tilting velocities with skirt-liner gap

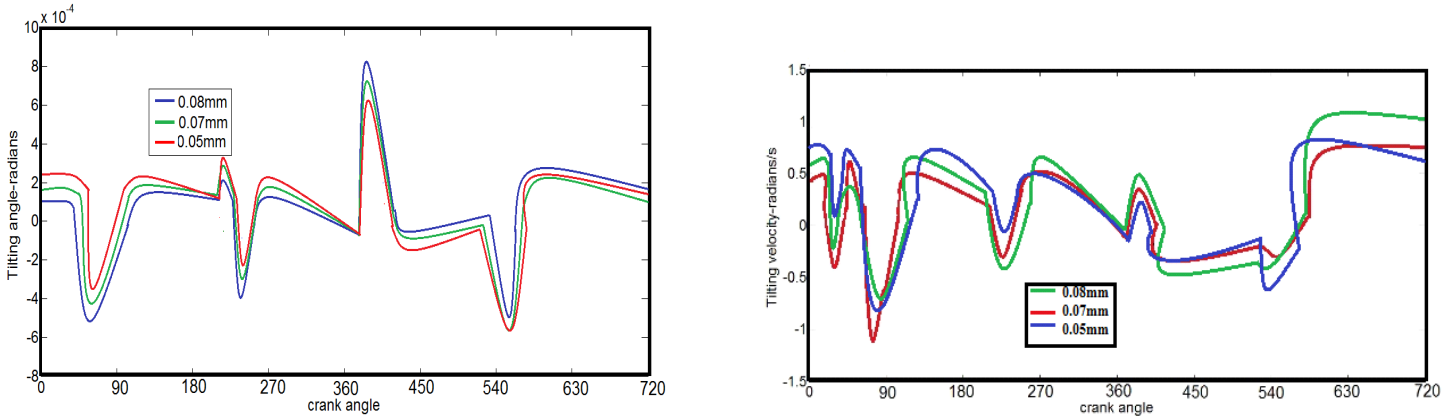

Figure no 5.42-Variations of tilting parameters with skirt-liner gap

c)Effects of variations in length of skirt

Length of piston skirt is designed according to according to compact pressure ratio and guidance length of skirt. An increase in skirt length causes a rise in its mass, hence an optimum value must be chosen. Effects of length of skirt were investigated on the its lateral motion by taking three values of 62mm, 62.65mm and 63mm respectively as seen in figure no 5.43-5.45. Load compacting area rises with an increase in the length of skirt, which in turn leads to fall in oil pressure P=$\frac{F_h}{\pi D}$. This causes a fall in oil film force (F_h) and moment associated with it (M_h). Hence various dynamic parameters of skirt show a decreasing trends with an increase of skirt length.

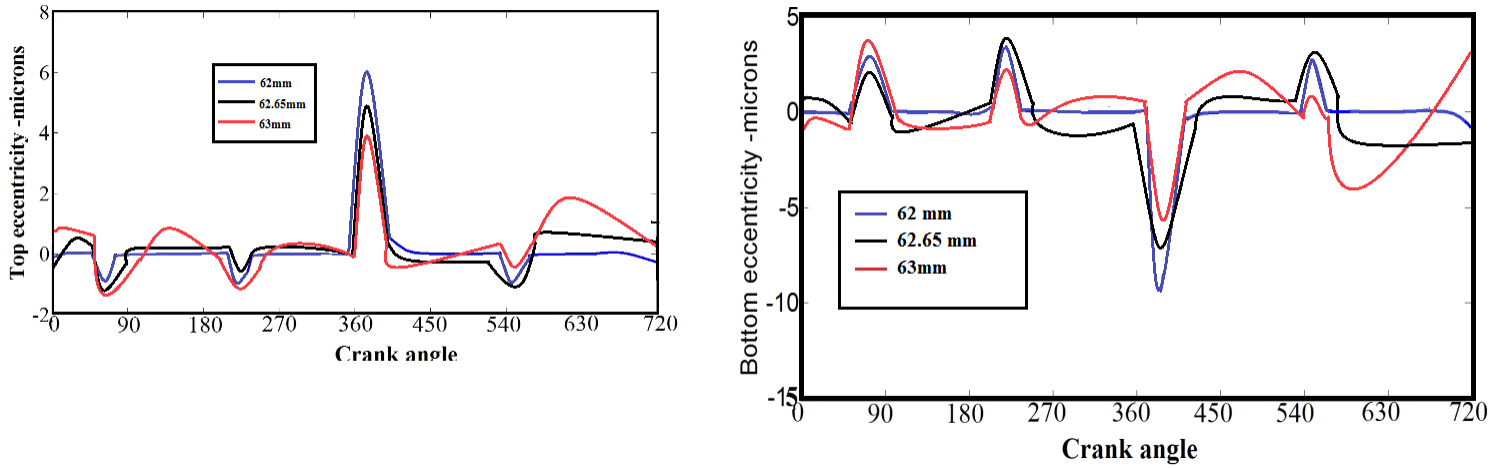

Figure no 5.43-Variations of eccentricities with skirt length

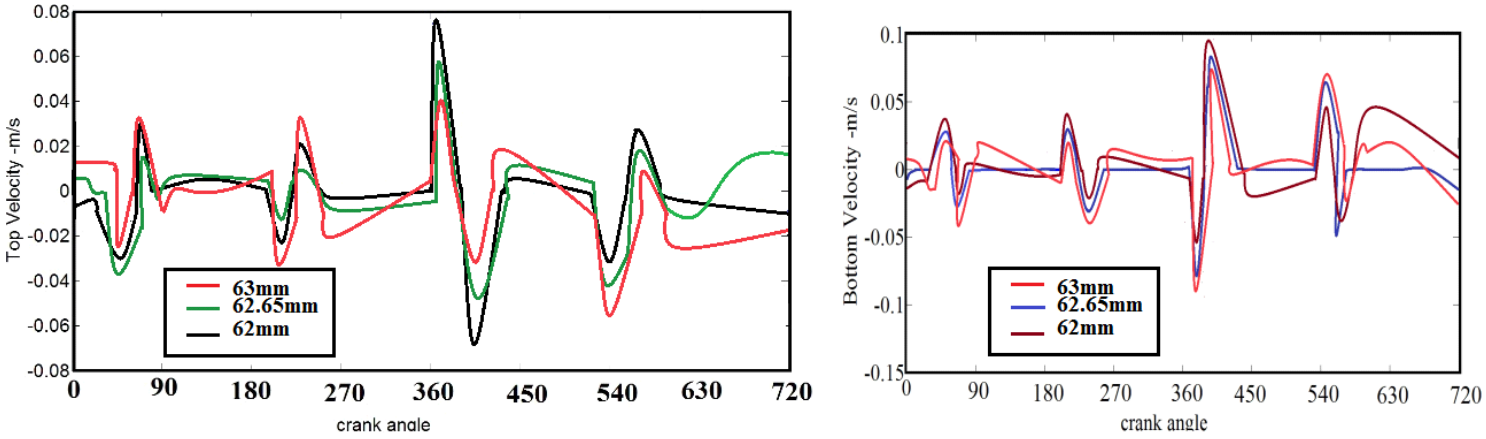

Figure no 5.44-Variations of tilting velocities with skirt length

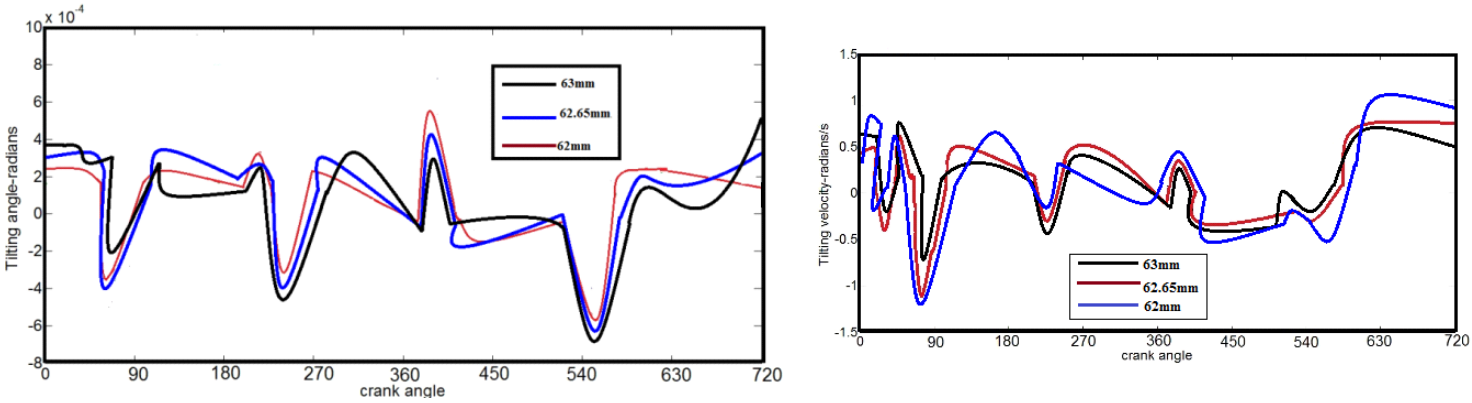

Figure no 5.45-Variations of tilting parameters with skirt length

d) Effects of operational speed of engine

An increased speed of engine causes changes in in cylinder pressure development due to increased mass of fuel injected inside combustion chamber. This leads to increased thermal deformations as higher temperatures are reached. Figures no 5.46 shows the variations of eccentricities with engine speed. As speed increases, lubrication changes to hydrodynamic type and hence higher oil pressures developed reduce the lateral motion of skirt. As combustion pressure is maximum during compression stroke, the values of frictional forces and associated power losses are their peak during this stroke as seen from figure no 5.47, 5.48.

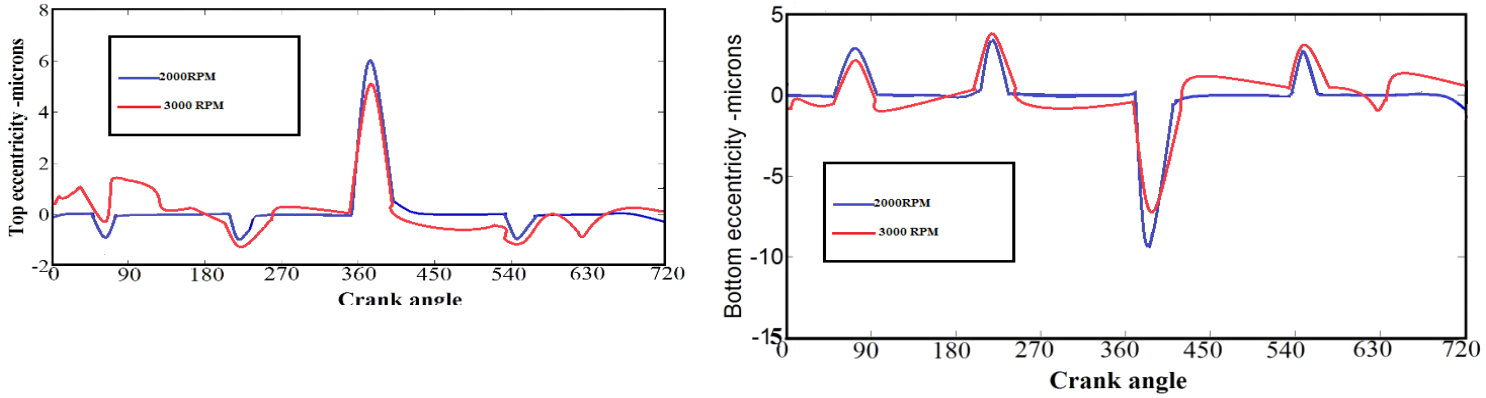

Figure no 5.46-Effect of engine speed on eccentricities

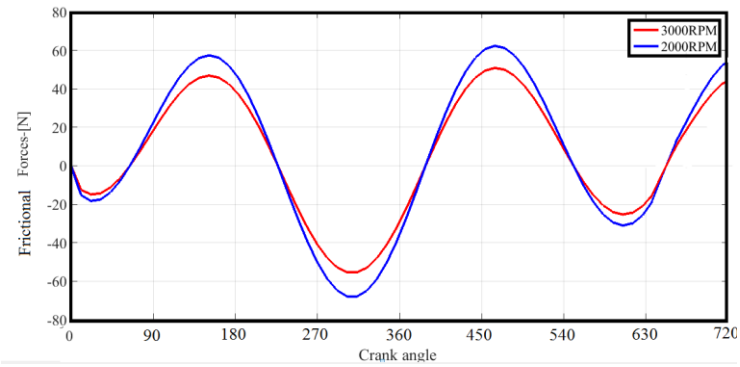

Figure no 5.47 -Effect of engine speed on skirt friction

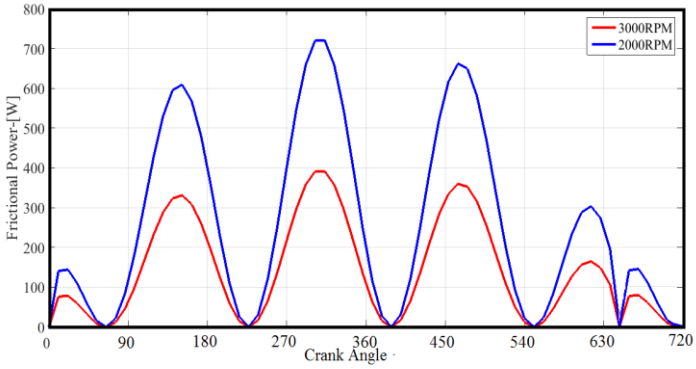

Figure no 5.48 -Effect of engine speed on friction power

Figure no 5.49 and 5.50 shows the effects of lighter piston skirt mass (2/3 rd of original mass) and heavier wrist pin mass (double original mass) on piston secondary motion. A slight increase was observed in the eccentricities with a decrease in skirt and pin masses.

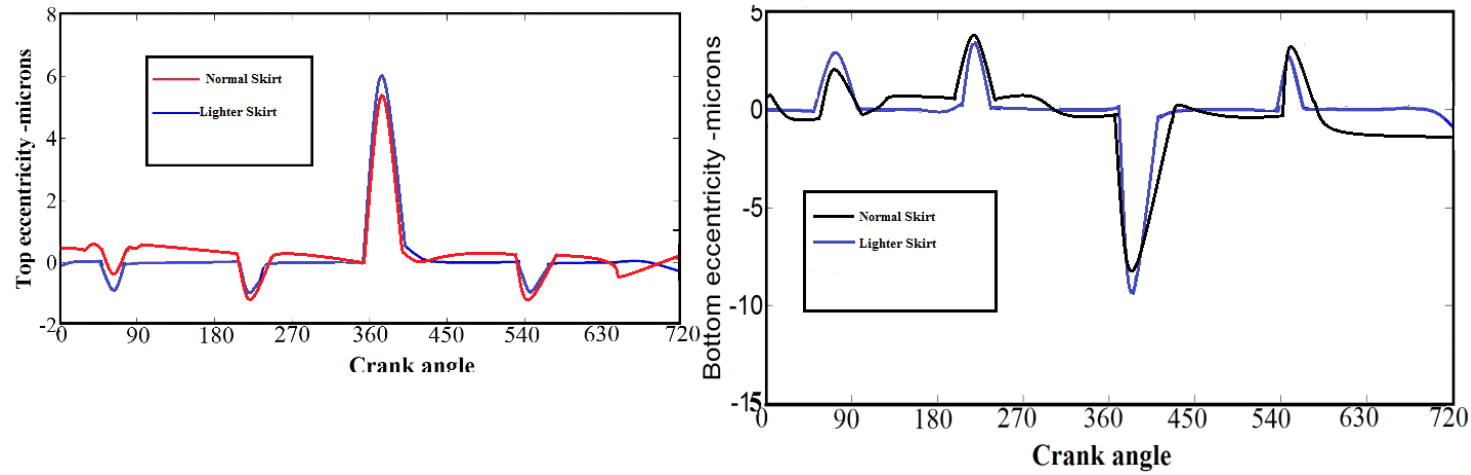

Figure no 5.49-Effect of skirt weight on eccentricities

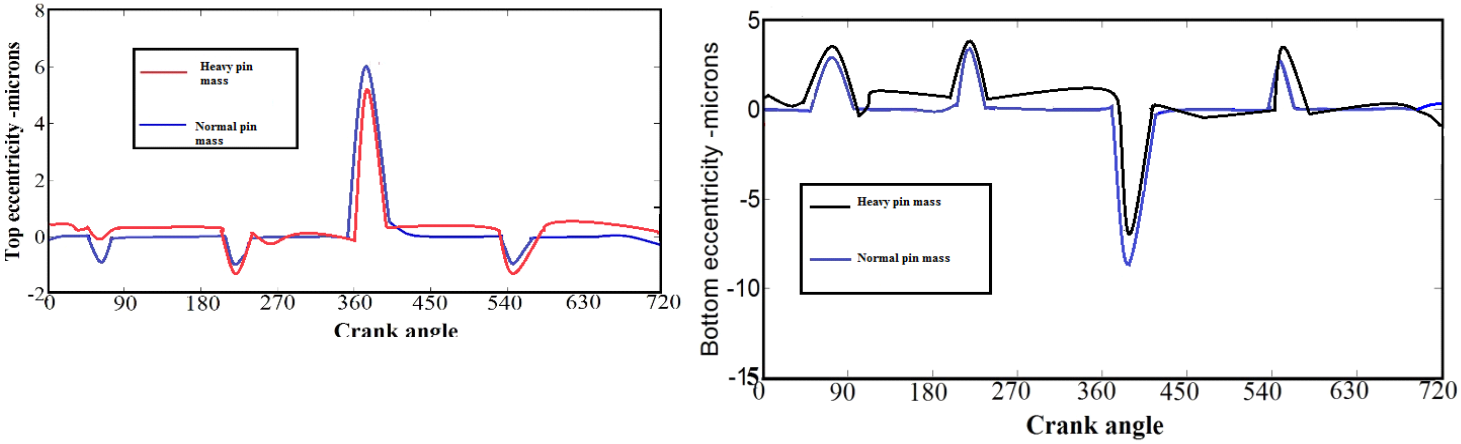

Figure no 5.50-Effect of pin mass on eccentricities

e) Effects of engine load

As the load increases, the amount of charge to be brought into cylinder must increase in order to maintain a constant speed range. Hence peak in cylinder reached inside cylinder increases. As it is evident from figure no 5.29,5.30, the lateral velocity of skirt showed no significant increase with changing load values. Hence it may be interpreted that this factor has least influence on lateral motion of skirt.

In addition to above discussed factors, the inertia of connecting rod has also pronounced effects on piston lubrication and it needs to be taken into account for further analysis especially at higher engine speeds [40].

5.8 Numerical model of slapping motion

A numerical model of lateral motion of piston skirt has been analyzed in this part of work considered lumped system approach having three degree of freedom as depicted in figure no 5.51[41]. The skirt has a dual degree of freedom (X_p, θ) having dynamic mass (m_p) and moment of inertia (I_P) 7.8540 $X10^{-9}$ kg-m^2. The engine block was considered having a single degree of freedom (X_b) with dynamic mass (m_b).

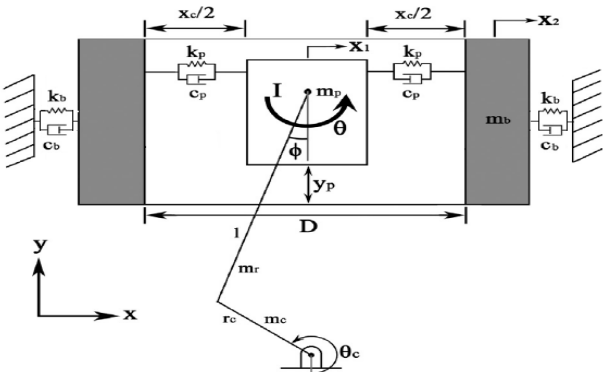

Figure no 5.51-Numerical model of piston secondary motion [41]

Motion of system can be represented mathematically in matrix form of equation no 5.40.

$$\begin{bmatrix} m_p & 0 & 0 \\ 0 & m_b & 0 \\ 0 & 0 & I_p \end{bmatrix}\begin{bmatrix} X_p'' \\ X_b'' \\ \theta'' \end{bmatrix} + \begin{bmatrix} C_p & -C_p & 0 \\ -C_p & C_b + C_p & 0 \\ 0 & 0 & C_\theta \end{bmatrix}\begin{bmatrix} X_p' \\ X_b' \\ \theta' \end{bmatrix} + \begin{bmatrix} K_p & -K_p & 0 \\ -K_p & K_b + K_p & 0 \\ 0 & 0 & K_\theta \end{bmatrix}\begin{bmatrix} X_p \\ X_b \\ \theta \end{bmatrix} = \begin{bmatrix} F_x \\ 0 \\ M_Z \end{bmatrix} \quad (5.40)$$

Where $M_z = m_p L_x X''_p + \sum F_x Y_s + F_g(X_p - X_{ob}) - \sum F_f(X_b - X_p) + T_p$, $T_p = \mu R F_L$ (5.41)

5.9 Driving forces

The lateral side thrust force imparted by connecting rod on walls on liner plays a major role in lateral motion of skirt. This force exerted can be vertically decomposed along X and Y directions. As the tilting angle of connecting rod changes, there will be a lateral component of force which pushes the skirt on liner walls. This lateral side thrust force takes into consideration both inertial as well as gas forces and is expressed in terms of crank radius-connecting rod length ratio (K) by following equation [35]:

$$F_x = [F_g - m_p r\omega^2(\cos(\theta) + K\cos(2\theta)])\lambda \quad (5.42)$$

Where $\lambda = \frac{Sin2\theta}{\sqrt{l^2 - (r\sin\theta)^2}}$

Various frictional forces between skirt and liner (F_f) as well as those between skirt rings and liner (F_{fr}) act vertically along Y axis. The center of mass of piston assembly is at horizontal offset distance of L_X and at vertical offset distance of L_y from connecting rod position as seen in figure no 5.16**.**

5.10 Determination of mobility

Mechanical mobility (M) can be defined as the ratio of resulting velocity of structure to input force causing excitation. This parameter was used to analyze the dynamic mass, stiffness and damping coefficients for the skirt-liner system. In frequency domain, the mechanical mobility M(Jω) can be expressed as [41]:

$$M(J\omega) = \frac{V(J\omega)}{F(J\omega)} \qquad (5.43)$$

$$M(J\omega) = \frac{-J\omega[\left((K-M\omega^2)+JC\omega\right)]}{M\omega^2(K+JC\omega)} \qquad (5.44)$$

Where F(Jω) is exciting force spectrum and V(Jω) is velocity response spectrum function. The analysis of mechanical mobility was carried out to compute various lumped mass parameters of skirt-liner system. For this purpose, the response of cylinder block was captured using accelerometer mounted normal to the axis of piston motion, whereas the response of piston skirt was analyzed using COMSOL-7 software.

Frequency domain plots of mobility have shown that frequency range below first resonant frequency ($\omega_a = \frac{K}{m}$) is dominated by dynamic mass of system. Hence the point mobility equation can be written as:

$$M(J\omega) = \frac{-J}{m\omega_a} \qquad (5.45)$$

Above this resonant frequency, response of system is spring dominated and hence the point mobility may be expressed as [38] :

$$M(J\omega) = \frac{-J\omega_a}{K} \qquad (5.46)$$

Figures no 5.52 shows the plots of lateral side thrust forces for testing cases enlisted in table no 4.1. As seen from these plots, lateral side thrust force changes its direction six times in a complete engine cycle (as marked by circles) indicating possible instances of piston-liner contact.

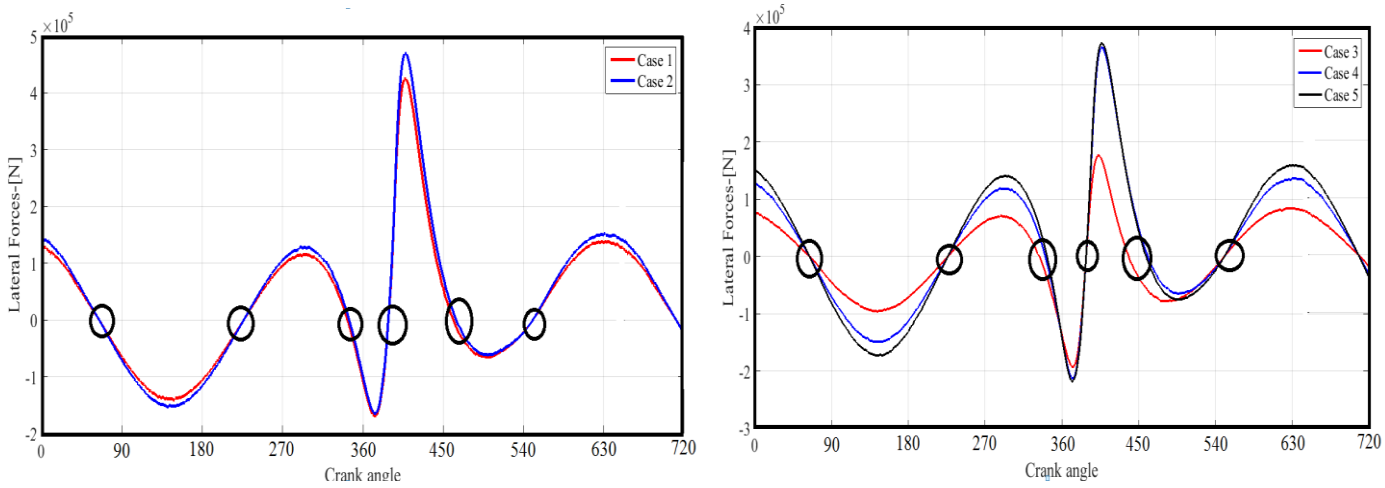

Figure no 5.52–Piston side thrust force

Further from values of lateral velocities of skirt (as obtained from COMSOL -7) in equation no 5.43, mechanical mobility of skirt was computed as depicted in figure no 5.53.

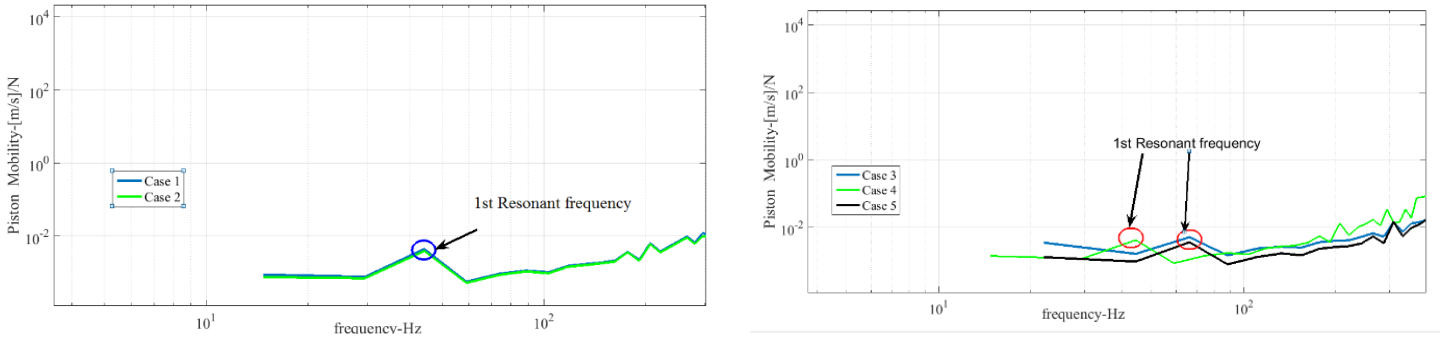

Figure no 5.53-Piston Mobility

Variations in values of mobility shows same trends hence confirming that mobility is least effected by change in the engine operational conditions. First resonant frequency for skirt was found to be in 40Hz-70Hz range. Block velocities of engine were simulated next using numerical integration of accelerometer data as shown in figure no 5.54.

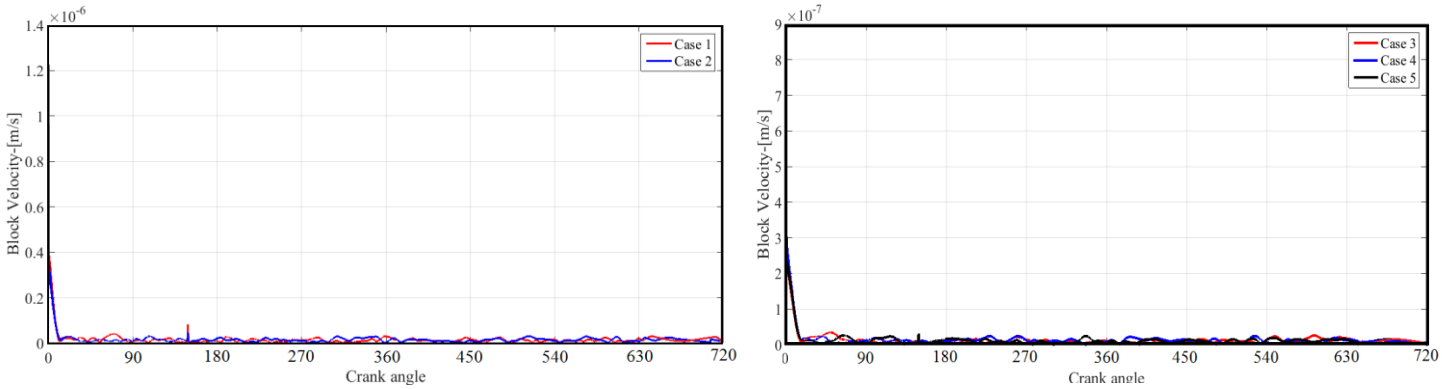

Figure no 5.54–Block Velocity

These were used to plot graphs of engine block mobility as seen in figure no 5.55. Gas forces acting on skirt play a major role in mechanical mobility of system, hence despite of almost same values of first resonant frequency, the values of block mobility were found to be lower as compared with piston mobility.

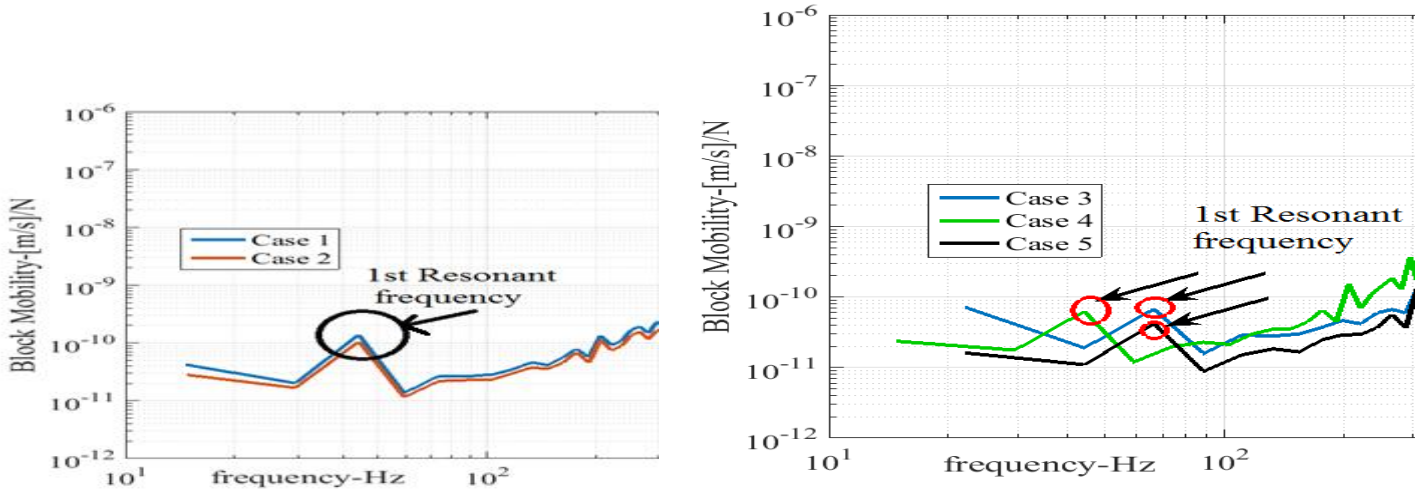

Figure no 5.55- Block Mobility

Using the concept of first resonant frequency as discussed in the previous section, various dynamic parameters of lumped mass system were computed for given test conditions. The results can be seen in table no 5.4.

Case	Block Parameter	Piston Parameter
1	f_a=44Hz	f_a=44Hz
	$[M_b (J\omega)]$ = 1.4*10^{-10} [m/s]/N	$[M_P(J\omega)]$ = 0.005 [m/s]/N
	C_b=5.9*10^9(kg/s)	M_P=0.72(kg^{-1})
	K_b=1.9*10^{12} (kg/s^2)	K_P=5.5*10^4 (kg/s^2)
	M_b=2.5*10^7 (kg)	C_P=141(kg)
2	f_a=44Hz	f_a=44Hz
	$[M_b(J\omega)]$ = 1*10^{-10} [m/s]/N	$[M_P(J\omega)]$ = 0.004[m/s]/N
	C_b=7.7*10^9(kg/s)	M_P=0.9(kg^{-1})
	K_b=2.7*10^{12} (kg/s^2)	K_P=6.3*10^4(kg/s^2)
	M_b=3.5*10^7 (kg)	C_P=176(kg)
3	f_a=65Hz	f_a=66Hz
	$[M_b(J\omega)]$ = 10^{-10} [m/s]/N	$[M_P(J\omega)]$ = 0.0050[m/s]/N
	C_b =7.7*10^9(kg/ s)	M_P=0.4(kg^{-1})
	K_b=4*10^{12} (kg/s^2)	$K_{P'}$=8.2*10^4(kg/s^2)
	M_b=2.5*10^7 (kg)	C_p=141(kg)
4	f_a=44Hz	f_a=44Hz
	$[M_b(J\omega)]$ = 10^{-10} [m/s]/N	$[M_P(J\omega)]$ =0.0032 [m/s]/N
	C_b =7.7*10^9(kg/ s)	M_P=1.1(kg^{-1})
	K_b=2.7*10^{12} (kg/s^2)	K_P=8.5*10^4 (kg/s^2)
	M_b=3.6*10^7(kg)	C_P=220(kg)
5	f_a=65Hz	f_a=67Hz
	$[M_b(J\omega)]$ = 10^{-10} [m/s]/N	$[M_P(J\omega)]$ =0.0035 [m/s]/N
	C_b =7*10^9(kg/ s)	M_P=0.7(kg^{-1})
	K_b=4*10^{12}(kg/s^2)	K_P=1.3*10^5(kg/s^2)
	M_b=2.4*10^7(kg)	C_P=220(kg)

Table no 5.4-Dynamic Parameters of system

5.11 Results and discussions

Figure no 5.56-5.60 shows comparisons of the simulated and measured vibratory response of engine block (as captured at accelerometer-2 location). Both trends showed a good agreement. In these figures, the impact of the piston on the liner walls resulted in a sudden increase of the amplitude of vibrations which increases with engine speed. These vibrations gradually decay and were induced again upon next instance of impact after some crank angle duration. At lower engine speeds, the vibration response of the cylinder block induced by the slapping contact of the skirt has a longer duration till decay. As the measured data has contributions due to various other sources, the amplitudes of resulting vibrations of engine block measured experimentally were higher than those of simulated ones.

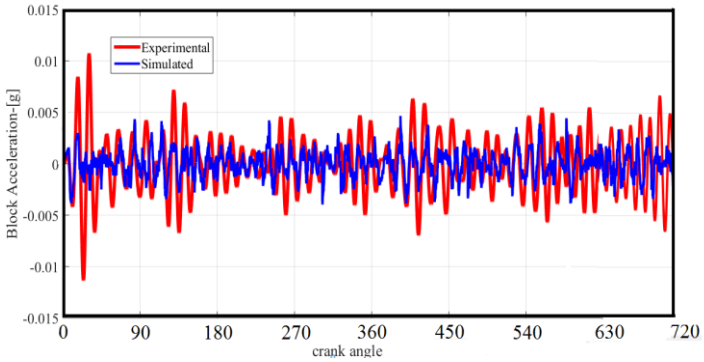

Figure no 5.56- Block Vibrations(2000RPM-80%Load)

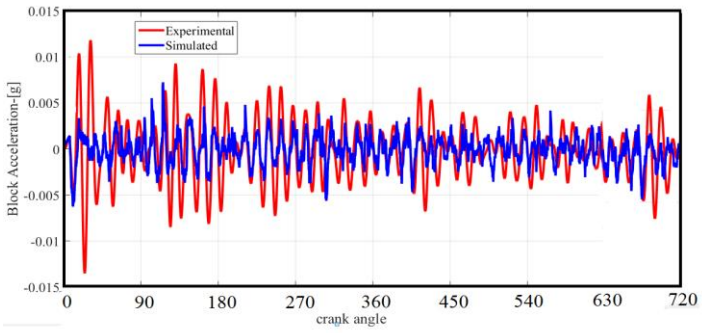

Figure no 5.57- Block Vibrations(2000RPM-100%Load)

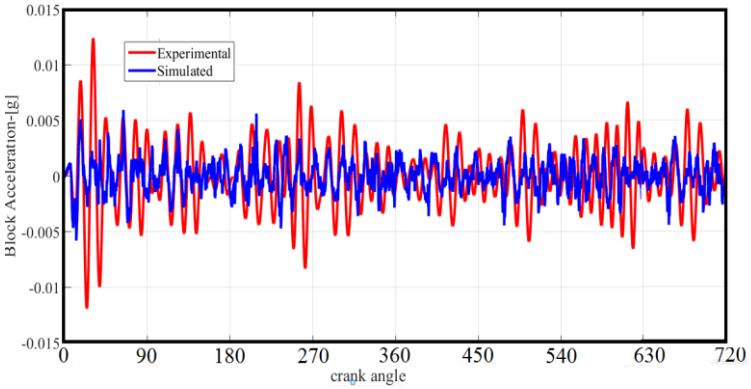

Figure no 5.58-Block Vibrations(3000RPM-motored)

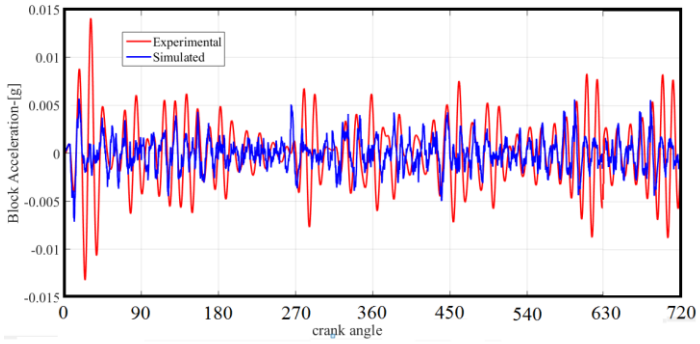

Figure no 5.59- Block Vibrations(3000RPM-80%Load)

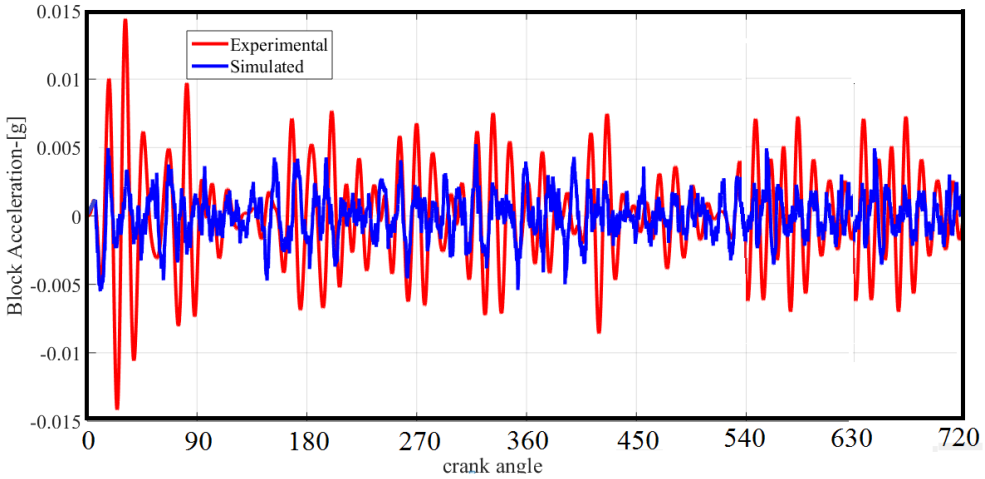

Figure no 5.60- Block Vibrations(3000RPM-100%Load)

The effects of variations in engine load and on piston lateral motion of skirt were next investigated from figure no 5.61,5.62. Due to gap between skirt and liner, a non-linear saw toothed pattern was observed in the lateral motion with amplitudes in range[0-8μm]. With an increase of engine speed, the side thrust force also increases. This results in fall of duration of sliding motion of skirt as it bounces off more frequently for longer durations.

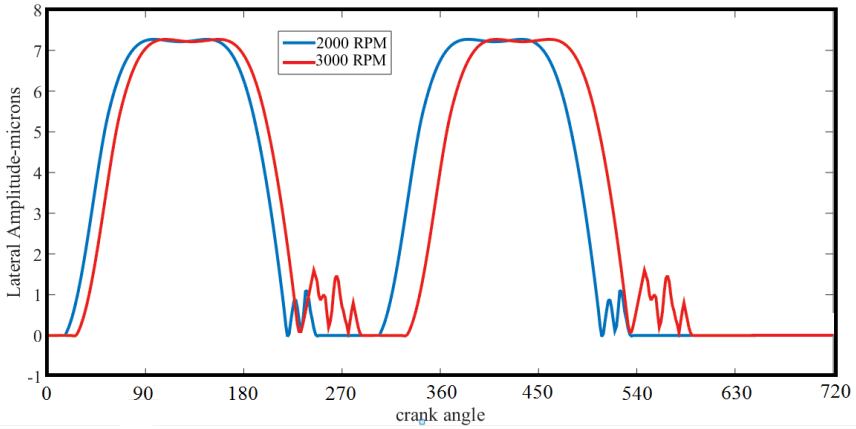

Figure no 5.61– Piston lateral motion (80% load)

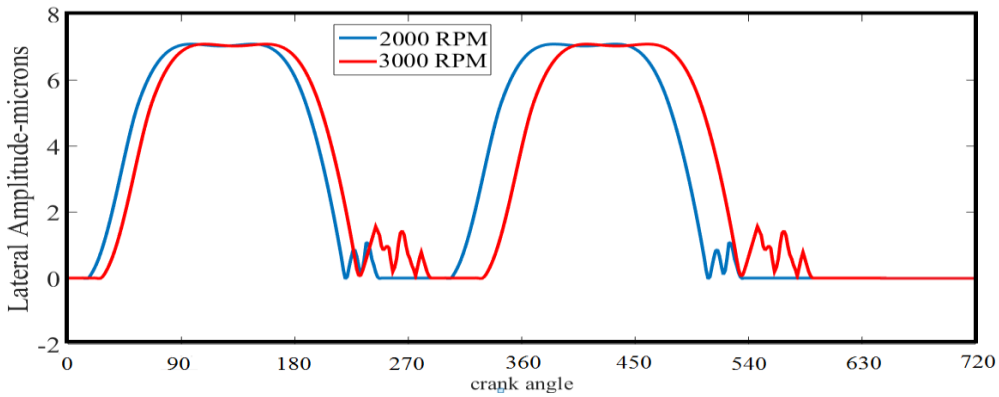

Figure no 5.62– Piston lateral motion (100%load)

5.12 Summary

Piston slapping motion is a major cause of noise and vibrations in engines. In first part of this chapter, various methods to locate the crank angles at which skirt may laterally strike walls of liner were discussed and further validated using filtered engine block vibrations. The dynamic equations of piston secondary motion were solved and effects of various skirt design were analyzed.

Further in order to understand this motion, a lumped system approach was also discussed. The values of first resonant frequencies of both skirt and liner were found to be near 40Hz-70Hz range. Lateral impacts of skirt with liner caused peaks in block vibrations. Effects of load and speed were also investigated on lateral motion of piston skirt. The sliding motion of skirt along liner was less dominant during suction and power strokes as the bouncing tendency dominated the dynamic motion of skirt. Skirt was found to slide a few crank angle duration before reaching TDC position. The duration of this sliding motion was observed to decrease with increase in engine speed which is in agreement with previous available literature.

5.13 References

[1]Chen,J.,Randall,R.,Peeters,B.,2016, "Advanced diagnostic system for piston slap faults in IC engines based on the non-stationary characteristics of the vibration signals", Mechanical Systems and Signal Processing,Vol.75,pp.434–454.
[2] Zhang, Z., Xie, Y., Zhang, X., Meng.,2009, " Analysis of piston secondary motion considering the variation in the system inertia ", Proceedings of the Institution of Mechanical Engineers, Part D-Journal of Automobile Engineering, Vol.223, no.4, pp.549-563.
[3]Kim, T.,2003, " Numerical analysis of the piston secondary dynamics in reciprocating compressors ", Journal of Mechanical Science and Technology, Vol.17,no.3,pp.350-356.
[4]Offner, G.,Herbst, H.,Priebsch, H.,2001, " A Methodology to Simulate Piston Secondary Movement Under Lubricated Contact Conditions ", SAE Technical Paper ,2001-01-0565.
[5]Comfort, A.,2003, " An introduction to heavy-duty diesel engine frictional losses and lubricant properties affecting fuel economy ", SAE Technical Paper,2003-01-3225.
[6]Ruggiero, A., and Senatore, A.,2003, " Computer model for the prediction of the impact force induced by piston slap in internal combustion engines", The Annals of the University Dunarea de Jos of Galati, Fascicle VIII,Tribology, pp 129–134.
[7]Wilson, R., and Fawcett, J. ,1974, " Dynamics of the slider-crank mechanism with clearance in the sliding bearing ", Mechanism and Machine Theory, Vol.9,no.1,pp.61–80.
[8] Flores, P., Ambrosio, J., Claro, H., and Lankarani,2008, " A Translational joint with clearance in rigid multibody systems ", Journal of Computational and Nonlinear Dynamics, Vol.3, no.1, pp.107-103.

[9]Rong, F., and Hung, H.,1996, " Dynamic analysis of flexible connecting rod of a slider crank mechanism using finite element analysis ", Journal of the Chinese Institute of Engineers, Vol.19,no.3,pp.381-391.
[10]Farahanchi, F.,and Shaw.,1994, "Chaotic and periodic dynamics of a slider-crank mechanism with slider clearance, Journal of Sound and Vibration,Vol.177,no.3,pp. 307-324.
[11]Geng, Z., and Chen, J.,2005, "Investigation into piston-slap-induced vibration for engine condition simulation and monitoring", Journal of Sound and Vibration,Vol.282,no.3-5,pp.735–751.
[12]Nakashima,K.,Yajima,Y.,Suzuki,K.,1999, "Approach to minimization of piston slap force for noise reduction–investigation of piston slap force by numerical simulation", JSAE Review, Vol.20,no.2,pp.211-216.
[13] Haddad, S., and Tjan, T.,1995, "An analytical study of offset piston and crankshaft designs and the effect of oil film on piston slap excitation in a diesel engine", Mechanism and Machine Theory,Vol.30,no.2,pp.271–284.
[14] Jang, S.,and Cho, J.,2004, "Effects of skirt profiles on the piston secondary movements by the lubrication behaviors",International Journal of Automotive Technology,Vol.5,no.1,pp 23–31.
[15] Guzzomi, A.,Hesterman, D.,Stone, B.,2008, "Variable inertia effects of an engine including piston friction and a crank or gudgeon pin offset", Proceedings of the Institution of Mechanical Engineers, Part D-Journal of Automobile Engineering,Vol.222,no.3,pp.397–414.
[16]Liu, L.,Xie, Y.,Gui, C.A,1998, "Comprehensive study of the friction and dynamic motion of the piston assembly", Proceedings of the Institution of Mechanical Engineers, Part J-Journal of Engineering Tribology,Vol.212,no.3. pp. 221–226.
[17] McFadden, P., and Turnbull, S.,2011, "Dynamic analysis of piston secondary motion in an internal combustion engine under non-lubricated and fully flooded lubricated conditions", Proceedings of the Institution of Mechanical Engineers, Part C- Journal of Mechanical Engineering Science, Vol.225,no.11,pp.2575–2585.
[18]Tan, Y.C., and Ripin, Z.,2012, "Technique of measuring piston secondary motion using laser displacement sensors", Experimental Mechanics,Vol.52,no.9,pp.1447–1459.
[19] Takahashi, M., Isarai, R., and Hara, H.,2013, "Measurement of Piston Secondary Motion Using the New Digital Telemeter," SAE Int. J. Engines,Vol.6,no.1,pp.577-586.
[20]Han, D.,and Lee, S., 1998," Analysis of the piston ring lubrication with a new boundary condition", Tribology International, Vol.31,no.12,pp.753–760.
[21] Nakashima.,K,Yajima,Y.,Suzuki.,K,1999, "Approach to minimization of piston slap force for noise reduction–investigation of piston slap force by numerical simulation ", JSAE Review,Vol.20,no.2,pp.211–216 .
[22] Dolatabadi et al,2015, "On identification of piston slap events in internal combustion engines using tribo dynamic analysis", Mechanical Systems and signal processing, Vol 58-59, pp 308-324.
[23] Rahnejat, H., Balakrishnan, S., King, S., Smith.,2006, " In-cylinder friction reduction using a surface finish optimization technique ", Proceedings of the Institution of Mechanical Engineers, Part D-Journal of Automobile Engineering,Vol.220,no.9,pp.1309–1318.
[24]Richmond,J.,Parker,D.,1987,"The quantification and reduction of piston slap noise",Proceedings of Institute of Mechanical Engineers -Part D, Journal of Automobile Engineering, Vol.201,no.4,pp.235–244.
[25]Yang,P.,Cui,J.,Jin,Z., Dowson,D.,2005, " Transient elastohyro analysis of elliptical contacts ", part 2 Thermal and Newtonian lubricant solution ", proceedings of the Institution of Mechanical Engineers, Part J-Journal of Tribology,Vol.219,no.9,pp.187-200.
[26]Pruvost,L.,Leclere,Q.,Parizet,E.,2009,"Diesel engine combustion and mechanical noise separation using an improved spectrofilter",Mechanical System and Signal Processing ,Vol.23, no.7,pp.2072–2087 .

[27]Liu,X.,Randall,R.,2005,"Blind source separation of internal combustion engine piston slap from other measured vibration signals",Mechanical System and Signal Processing, Vol.19,no.6,pp.1196–1208.

[28]Chen,J.,Randall,R.,2011,"Vibration signal processing of piston slap and bearing knock in IC engines", Surveillance 6.
[29]Meng, X.,Fang, C., Xie ,Y., 2016, " Transient tribo-dynamic model of piston skirt-liner systems with variable speed effects" ,Tribology International, Vol.94, pp. 640-651.
[30]Zhao,B.,2016, "A new numerical method for piston dynamics and lubrication analysis", Tribology International, Vol.94,pp.395-408.
[31]Dolatabadi,N.,Littlefair,B.,DelaCruz,M.,Theodossiades,S.,Rothberg,S.,Rahnejat, H., 2015," A transient tribodynamic approach for the calculation of internal combustion engine piston slap noise", Journal of Sound and Vibration, Vol.352,pp.192–209.
[32] http://www.nptel.ac.in/courses/112102015/26, Last Accessed on April 8, 2016.
[33]Roelands,C.,1966," Correlational Aspects of the Viscosity-Temperature-Pressure Relationship of Lubricating Oils" ,Ph.D. Thesis, Technical University Delft.
[34]Noor,Balia,F., Ridha, M., and Wahab,A.,2011,"Investigation into piston-slap force under friction and connecting rod effects of diesel engine", Proceeding of the International Conference on Advanced Science, Engineering And Information Technology.
[35] Littlefair,B., De la Cruz,M.,Theodossiades,S.,Mills,R.,Howell,S.,Smith,S.,Rahnejat,H.and Dwyer-Joyce,R.,2014, "Transient Tribo-Dynamics of Thermo-Elastic Compliant High-Performance Piston Skirts"
[36]Perera,M.,Theodossiades,S.,Rahnejat,R.,2007,"A multi-physics multi-scale approach in engine design analysis",Proceedings of Institute of Mechanical Engineers, Part K-Journal of Multi-body Dynamics,Vol.221,no.3,pp.335–348.

[37]Ungar,E.,Ross,D.,1965,"Vibrations and noise due to piston-slap in reciprocating machinery",Journal of Sound and Vibrations,Vol.2,no.2,pp.132–146.

[38]Cho,S.,Ahn,S.,Kim,Y.,2002, "A simple model to estimate the impact force induced by piston slap", Journal of Sound and Vibrations,Vol.255,no.2,pp.229-242.

[39]He, Z., Xie,W.,Zhang,G.,Hong,Z.,Zhang,J.,2014, "Piston dynamic characteristics analyses based on FEM method Part I: Effected by piston skirt parameters", Advances in Engineering Software,Vol.75,pp.68–85.

[40]Meng,X.,Xie,Y.,2012, "A new numerical analysis for piston skirt –liner system system lubrication considering the effects of connecting rod inertia",Vol.47,pp.235-253.
[41] Mohd Ripin , Z., Chong Tan,Y.,2013, "Analysis of piston secondary motion", Journal of Sound and Vibration, Vol.332,pp.5162–5176.

Chapter 6
Conclusions and future work

6.1 Objectives and Achievements

The main aim of the presented work was to analyze various signals acquired from a diesel engine test rig in order to monitor its working. For this purpose, both theoretical as well as experimental results have been presented. Main achievements of previously discussed goals are as follows:

Objective 1-To review different sources of noise in engines.
Achievements 1-Chapter 1 provides an overview of these sources and discusses various techniques used for effective source separation. Chapter 3 focuses on various characteristic features of these sources.

Objective 2-To study the effects of variations of different engine operational conditions on various signals acquired from transducers mounted on test engine.
Achievements 2-Different tests were carried by varying engine load, speed, amount and duration of fuel injected. Location of various transducers were changed in order to investigate the effects of change in positioning as presented in Chapter 2.

Objective 3- To show the applicability of various signal processing methods for effective monitoring of engines.

Achievements 3-Chapter 2 shows application of these methods e.g. time-frequency analysis, power spectrum density, wavelet analysis and mean frequency analysis on various acquired signals. A suitable frequency range was identified in which combustion based noise was dominant.

Objective 4-To analyze combustion based noise using acquired data.
Achievements 4-Chapter 4 discusses use of pressure, noise and vibration signals for analysis of combustion based noise. Various combustion noise related indices were defined and analyzed. A transient model of this noise based on generation mechanism was presented.

Objective 5-To develop various numerical models of piston lateral motion and validate them using experimental data.
Achievements 5-Chapter 5 presents these models of lateral motion of skirt and analyses effects of various physical design parameters on it. Resulting engine block vibrations were simulated using various dynamic parameters obtained from mobility measurements and compared with actual experimental data.

Objective 6-On the background of presented work, provide a guideline for further research**.**
Achievements 6-Some of future research works that need to be undertaken are discussed in this Chapter of thesis.

6.2 Resume of state of art

Noise, vibration and harness analysis of diesel engines has been an active topic of research during past few decades. The presented work has tried to deal with some of the important aspects of this issue. There are many key areas in which further work can be done [1]. Some of these include:
1.Quantification of various noise emissions.

A) Subjective approach -Some possible indices used for this purpose may include:

- Ranking-Various subjects may be asked to rank sound emissions from the test engine according to annoyance on a scale of 1 to10. However, number of samples must be kept low to avoid complexity [2, 3,4].
- Comparison in pairs-In this method various subjects may be asked to evaluate relative judgments on the basis of pairs, however this method can be exhaustive as number of pairs can be large [5, 6].

B) Objective approach -Various psychoacoustic indices that can be used for evaluation include:

- Loudness-It is a parameter used for evaluation of noise intensity and has unit of phon or sone. Loudness level of 1 phon is SPL of a pure tone plane wave of 1kHz frequency as perceived by human ears in frontal direction [7].

- Sharpness-A 60dB sound wave of 1kHz frequency has sharpness of 1 acum. Sharpness of a soundwave can be lowered by either adding low frequency components or by decreasing high frequency components [8].
- Roughness-This parameter takes into account modulation of waves. Its standard unit is asper.1 asper is roughness of a tone of 1kHz frequency at 60dB which is modulated by 70Hz frequency with degree of modulation equal to unity [9].
- Impulsiveness- It represents the amplitude and frequency of occurrence of peaks in SPL. Its unit is Kurt and is most significant during ideal running of engines [8].

2. Motion of gudgeon pin inside pin hole

Piston pin is held inside hole either by a full floating system or a semi floating one. For case of full floating system, both pin and connecting rod may be made of same material, whereas in case of semi floating system, piston may be made of aluminum alloy and pin of steel. Hence a semi floating system is subjected to more noise due to differences in thermal expansion coefficients of different materials used. It has been observed that pin rotates counter clockwise inside its hole before striking the wall of piston vertically in crank angle duration 20º- 30ºBTDC [10].

3. Use of gap sensor device to study piston secondary motion using different skirt profiles.

Frictional power losses for various skirt profiles can be evaluated using suitable motion gap sensors. Skirt profile having recess at top and bottom part has shown minimum frictional forces as it has better lubrication load bearing surface [11,12].

4. Use of AVL EXITE for modelling of piston motion.

This approach takes into account thermal distortions of liner using GUID (piston-liner guidance) and EPIL (elastic piston liner contact) approaches [13]. Lateral surface velocities can be analyzed both in time and frequency domains. At higher speeds, in conjunction with higher inertial forces, piston secondary motion was found to decrease. Hence both above mentioned approaches have shown almost same results [14].

5. Investigation into effects of bubble formations, mist and cavitation of lubrication oil during secondary motion of piston.

Formation of bubbles takes place in lubrication oil film as local pressure drops below ambient pressure particularly in convergent-divergent interfaces like contacts between rings and liner [15]. It has been proved that under these conditions, Reynolds equation may yield different pressure profiles [16].

6. Use of post injections or exhaust gas recirculation (EGR) and turbocharging.

a) Effects of post injection-soot emissions can be controlled by use of post injection methodology. However, noise emissions were found to remains unaffected [17].

b) Effects of EGR-EGR has been found to reduce combustion noise above 300Hz range, however excessive use of EGR may lower the thermal efficiency [18].

c)Effects of turbocharging -Noise emission during transient conditions from a turbocharged diesel engine have been found to be up to 3 dBA higher as compared to steady state conditions. This has been attributed to turbocharger lag [19].

7.Use of Blind Source Separation (BSS) and Independent Component Analysis (ICA)methods for effective noise source separation.

A BSS algorithm based on least mean square method has been applied to separate piston slapping noise from other noise emissions [20]. ICA has also been used to effectively analyze fuel injection pulses which would otherwise get suppressed by various high energy events [21].

6.3 Overall Conclusions

The presented work establishes benefits of using various intrusive as well as non-intrusive methods to analyze pressure, noise and vibrations signals from a dual cylinder diesel engine. Amongst various NVH sources in engines, the contributions due to combustion based noise and piston lateral motion are of prime importance. Hence a major portion of this work discusses these two aspects.

In Chapter 2, Time–frequency analysis has shown locations onset of various events associated with operation of test engine. High frequency components were found in frequency range 500Hz -2kHz a few degrees before TDC position, due to rapid increase in cylinder pressure after pre-injection period. PSD plots have shown that major changes due to firing of fuel occurred at around frequency of 300Hz. Hence analysis of combustion related events must be done above this frequency. In higher ranges, a sudden increase in amplitude of spectrum was seen which may be attributed to phenomenon of resonance.

Further a gird was built around the test engine to see the effects of change in locations of various transducers on acquired signals. Three such positions were marked as A, B and C. Position C was seen as being most sensitive towards combustion process, whereas position B was seen as sensitive towards intake flow process. Coherence analysis of signals showed that noise emissions in frequency range of 50Hz-400Hz were sensitive towards gas exchange process. Engine block vibrations acquired at vertical orientations were found to be more coherent towards combustion pressure development in frequency range of 0.5kHz-3.8kHz. Crank angles corresponding to minimum values (that followed the maximum values) of band filtered vertical accelerometer signals in this range were compared with crank angles at which maximum in cylinder pressure development occurred. High coefficients of proportionality were observed between the two defined positions.

It was seen that the vibration traces allowed to detect the crank angles corresponding to different phases of combustion process observed in diesel engine. End of negative values in vibration curves along with a sudden rise of in-cylinder pressure marks start of pre-mixed phase. The diffusive phase of combustion begins with vibration curves crossing the next zero markings.

Further, various regions of pressure spectrum were defined and analyzed by changing various fuel injection parameters for a test case of 3600 RPM speed under full load condition. Region 1 corresponding to lower frequencies was found to be in 10Hz-215Hz range. Medium range showing a logarithmic decrement was found to be in 215Hz-2800Hz, whereas region 3 of higher range was above 2800Hz. Various combustion noise related indices were defined and developed which showed a close correlation with in cylinder pressure development as compared to maximum pressure rise rate (MPRR). A transient model of combustion noise generation was also presented and Cepstrum analysis was used effectively for source separation.

Various mathematical models of lateral motion of piston skirt were analyzed in Chapter 5. Methods to locate possible instances of skirt-liner lateral contact were discussed and validated by using filtered block vibration signals. The dynamic equations of piston secondary motion were solved and effects of various design parameters on lateral motion of piston were analyzed.

Further a lumped mass system approach of lateral motion was also discussed in which various dynamic parameters of system were calculated using concept of mechanical mobility. The values of first resonant frequencies of skirt-liner system were found to be in 40Hz-70Hz range and it remained unaffected by variations in various engine operational conditions. Simulation of lateral motion of skirt and resulting block vibrations was also performed. The duration of sliding motion of skirt along liner was seen to fall with an increase in increase engine speed as bouncing nature dominated piston lateral motion.

6.4 Innovation Introduced

- Locations of different transducers was changed in order to investigate the effects of positioning on various acquired signals. For this purpose, a grid was built that encircled the engine, thus allowing the repetitiveness of various measurements.
- Engine block vibration data was used for analysis of various phases of combustion observed in course of a diesel engine cycle.
- The frequency ranges mainly related to combustion process were extracted using coherence function.
- Various regions of cylinder pressure spectrum were analyzed by changing various fuel injection conditions.
- New indices were developed which define relationships between injection process and resulting in pressure, noise and vibration signals.
- A Transient model of combustion noise generation was defined and various rates related to it were analyzed.
- Cepstrum analysis was used to obtain transfer function of combustion based noise and hence achieve effective source separation.
- Various methods to locate the instances of lateral contacts of skirt and liner walls were defined and validated by actual engine block vibration measurements.
- A Tribological model was used for solving the equations of lateral motion of skit and effects of various design parameters like its length, skirt-liner gap and offset distance on various parameters of lateral motion were analyzed.

References

[1] Monelletta,L.,2010, "Contribution to the study of combustion noise of automotive diesel engines", Ph.D. Thesis, University polytechnic Velencia.
[2]Otto,N.C.,Amman,S.,Eaton,C.,and Lake,S.,1999,"Guidelines for jury evaluations of automotive sounds", SAE Technical paper 1999-01-1822.
[3]Guski,R.,1997, "Psychosocial methods for evaluating sound quality and assessing acoustic information", Acta Acustica,Vol.83,no.5,pp.765-774.
[4] Bisping, R., Giehl, S., and Vogt, M.,2008, "A standardized scale for the assessment of car interior sound quality," SAE Technical Paper 971976.
[5]Hussain,M.,Golles,J.,Ronacher,A.,and Schiffbanker,H.,1991, "Statistical evaluation of an annoyance index for engine noise recordings" ,SAE Technical Paper 911080.
[6]Kahn,M.,Johansson,O.,Lindberg,W.,and Sundback,U.,1997, "Development of an annoyance index for heavy duty diesel engine noise using multivariate analysis", NCEJ,Vol.45,pp.157-167.
[7] Fastl, H., and Zwicker, E.,2007, "Psychoacoustics: Facts and Models", Springer, Berlin, ISBN 978-3-540-68888-4.
[8]Schiffbanket,H.,Brandl,F.,and Thien,G.,1991, "Development and application of an evaluation technique to assess the subjective character of engine noise", SAE Technical Paper 911081.
[9] Peluger,M.,Holdrich,R,Brandl,F.,and Biermayer,W.,1999, "Subjective assessment of roughness as a basis for objective vehicle interior noise quality evaluation",SAE Technical Paper 1999-01-1850.
[10]Kondo, T., and Ohbayashi,H.,2011, "Visualization of Oil behavior when piston pin noise occurs", Honda R&D Technical Review,Vol.23,no.2,pp.76-79.
[11] Kim, K., Shah, P., Takiguchi, M., and Aoki, S.,2009, "Part 3: A study of friction and lubrication behavior for gasoline piston skirt profile concepts," SAE Technical Paper 2009-01-0193.
[12]Kobayashi,T.,Takahashi,Y., Bell,D.,2007, " How to predict piston slap noise using 3D piston motion simulation", SAE Technical Paper 2007-04-16.
[13]Kocaoglu,C.,Tabak,M., 2014,"Comparison of two modeling techniques for piston-liner interaction in terms of piston secondary motion using AVL exite",14th OTEKON 2014, Bursa ,Turkey.
[14] AVL EXITE Power unit users guide,2009, Vol 3, pp.404.
[15]Dhuput,A.,2009, " Oil transport in piston ring assembly ", Ph.D. thesis, City university of London.
[16]Ohta,K.,Wang,X., and Saeki,A.,2016, "Piston slap induced pressure fluctuation in the water coolant passage of an internal combustion engine", Journal of Sound and Vibrations ,Vol.363,pp.329-344.

[17] Park,Y.,and Bae,C .,2013,"Effects of single and double post injection on Diesel PCCI combustion", SAE Technical Paper 2013-03-25.

[18] Shibata, G., Ushijima, H., Ogawa, H., and Shibaike, Y., 2014,"Combustion noise analysis of premixed diesel engine by engine tests and simulations," SAE Technical Paper 2014-01-1293.

[19]Rakopoulos.,and Giakoumis.,2011, "Experimental study of combustion noise radiation during transient turbocharged diesel engine operation",Vol.36,no.8, pp.4983-4995.

[20]Liu,X.,and Randall,R.,2005, " Blind source separation of internal combustion engine piston slap from other measured vibration sources ",Measurement Systems and Signal Processing ,Vol.19,no.6,pp.1196-1208.

[21]Albarbar,A.,Gu,F.,and Ball,A.,2010 , " Diesel engine fuel injection monitoring using acoustic measurements and independent component analysis ",Measurement,Vol.43,no.10,pp.1376-1386.

List of publications

1. Chiatti G., Chiavola O., Narayan S.,2016,"Modelling of Piston secondary motion in Diesel engines ", Advances in Mechanical Engineering, Sage Publications (Under Review).
2. Narayan, S.,2014, " A Review of Diesel Engine Acoustics", FME Transactions, Vol 42, no2, pp.150-154, DOI: 10.5937/fmet1402150N.
3. Narayan, S.,2014, "Analysis of Noise Radiated from Common Rail Diesel Engine", Tehnicki glasnik, ISSN 1846-6168, Vol.8 No.3, pp 210-213, UDK 621.436:534.831.
4. Narayan, S,2014, " Time frequency analysis of Diesel Engine Noise", Acta Technica Corviniensis, Bulletin of Engineering, ISSN: 2067-3809, Facsicule 3-July-September.
5. Narayan S.,2015, " Correlation between in cylinder pressure and noise emissions from engines", Journal of Kones powertrain and Transport, Vol 22, no1, pp.243-254, DOI: 10.5604/12314005.1161775.
6. Narayan Sunny,2014, "Modelling of Piston Slapping motion", Mechanical Testing and Diagnosis, ISSN 2247 – 9635, Volume 4, pp.17-24.
7. Narayan, S.,2015, " Modeling of Noise Radiated from Engines ", SAE Technical Paper ,2015-01-0107.
8. Narayan S.,2015, " Effects of Various Parameters on Piston Secondary Motion ", SAE Technical Paper 2015-01-0079.

APPENDIX

A) Anechoic chamber
B) Test Engine
C) Pressure measurements
D) Accelerometer
E) Microphone

A. Chamber description

The test engine was located in a semi-anechoic Chamber having no echoes. In order to acquire various signals under far field conditions according to SAE-J1074 and to contain engine setup, the test chamber was made with adequate dimensions. To isolate any possible vibrations from external environment, the walls of chamber were made up of dense cement. The bottom of chamber was also made of wedges and floor was formed of iron meshes. Efficient ventilations systems were provided to avoid any acoustic interference.

B. Test Engine

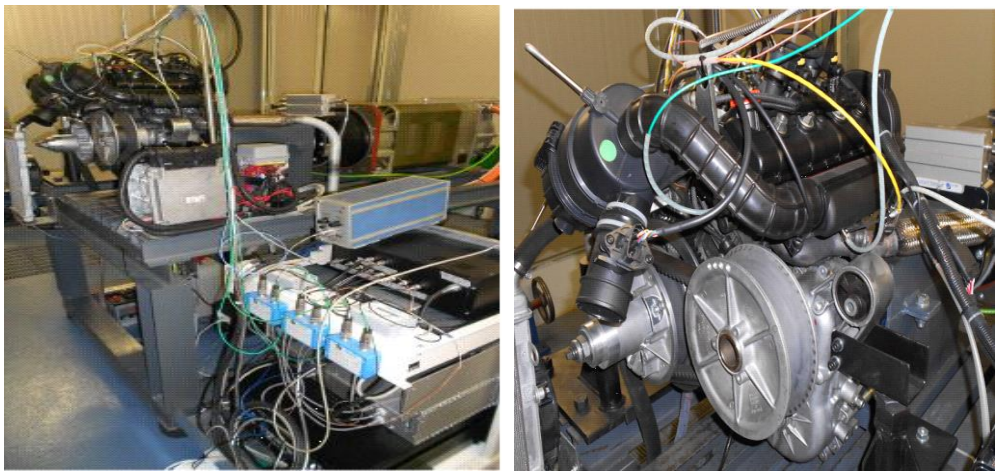

Figure no I- Test rig

Various tests were done on a water cooled LDW442CRS type Lombardini make engine having a common rail injection system as seen in figure no I. The engine has specifications which have been presented in Table no A. This engine has K type thermocouple for various temperature measurements.

Number of cylinders	2
Displaced Volume	440 cm^3
Bore	60.6mm
Stroke Length	68mm
Compression Ratio	20:1
Maximum Rated Power	8.5kW@4400RPM
Maximum Rated Torque	25N-m@2000RPM

Table no A-Engine Specifications

An electronic control unit (ECU) connected to computer was used to manage various injection parameters. This system can do maximum of 2 injections per cycle. The engine was coupled with a SIEMENS 1PH7 MAKE synchronous motor (nominal torque 360 N-m and maximum rated power 70 kW), thus allowing control over speed and load values. Locations of TDC positions were recorded by an AVL 364C type optical encoder. All signals were acquired at the same time by NI boards of 6110 type (for analog type) & 6533 type (for optical encoder signals) under LabVIEW 10 environment.

The sampling rate was varied in order to guarantee a fixed crank angle resolution. All signals were filtered using B&K Nexus device. A HBM T12 digital transducer was used for torque measurements as shown in figure no II. Locations of instances of various cyclic events of engine have been enlisted in table no B. Engine also has a provision to record nonvolatile particle numbers as well as soot emissions present in exhaust gas respectively by means of AVL particle counter and micro soot sensor.

Figure no II- HBM T12 digital torque transducer

Inlet Valve opening (IVO)	10° before TDC
Inlet Valve closure (ICV)	42° After BDC
Exhaust valve opening (EVO)	58° Before BDC
Exhaust valve closure (EVC)	10° after TDC

Table no B-Valve Operation Specifications

C. Pressure measurements

An AVL GU13P type piezoelectric transducer shown in figure no III(a) was used to acquire the instantaneous in-cylinder pressure data. Main features of this transducer is presented in table no C.

Figure no III(a)- AVL GU13P pressure transducer

Figure no III(b)- Inlet and exhaust pressure transducer

Range	0-200Bar
Sensitivity	15.8pC/Bar
Resonance frequency	130kHz

Table no C- AVL GU13P Specifications

Intake pressures were measured by means of piezo resistive Kistler 4007BS5F transducers. The exhaust pressures were measured by water cooled piezoelectric AVL QC43D. These transducers have been shown in figure no III(b). Injection pressures were measured by means of Kistler 4067A2009 transducers. An AVL 733S gravimetric fuel meter was used to monitor the fuel consumption rate.

D. Accelerometer

Various engine block vibrations were recorded by Endveco7240C make Mono axial accelerometers which were mounted by means of threaded pins in vertical as well as horizontal orientations on the engine block as seen in figure no IV. Main features of this accelerometer have been presented in table no D.

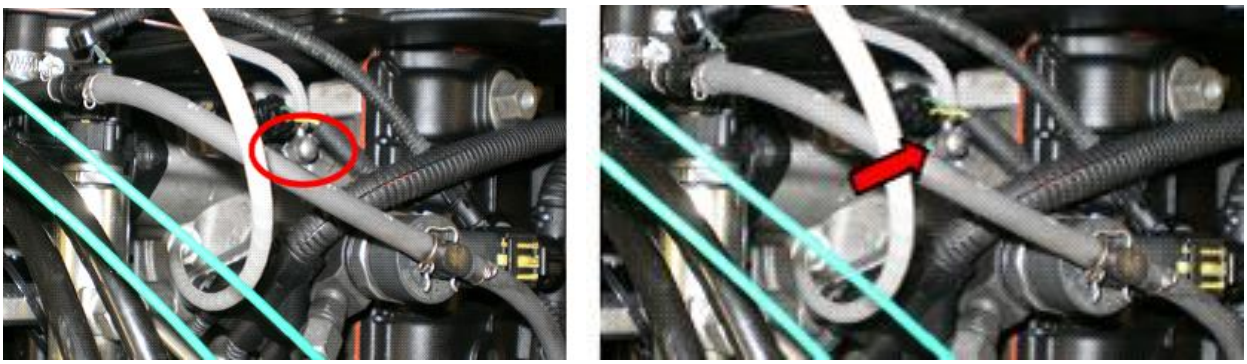

Figure no IV Accelerometer transducer location

Range	0-1000g
Sensitivity	3pC/g
Resonance frequency	90kHz

Table no D-Accelerometer Specifications

E. Microphone

A 4939 type Bruel and Kjaer free-field ¼″ make microphone having a preamplifier (type 2670) was used to acquire various noise emission signals. Figure no V shows the highlighted position of this transducer with its major specifications listed in table no E.

Figure no V- Microphone location

Frequency Range	4-100KHz
Sensitivity	4mV/Pa
Dynamic range	28-164dB

Table no E-Microphone Specification

SAE classification	$a*10^8$	b	c
10W and 10W10	0.0850	820.723	93.625
10W/20	0.1031	773.810	93.153
10W/30	0.2020	737.690	89.9
10W/40	0.1165	1033.340	120.800
10W/50	0.0952	1304.170	15.220
20W and 20W/20	0.1350	737.810	77.7
20W/30	0.4141	811.962	93.458
20W/40	0.1671	793.329	93.931
20W/50	0.0948	1146.250	124.7
30W	0.1531	720.015	71.123

Table no F-Values of viscosity coefficients for various grades of oil